UNCLASSIFIED

AD NUMBER
AD805717

LIMITATION CHANGES

TO:

Approved for public release; distribution is unlimited.

FROM:

Distribution authorized to U.S. Gov't. agencies and their contractors; Administrative/Operational Use; NOV 1966. Other requests shall be referred to Air Force Weapons Lab., Kirtland AFB, NM.

AUTHORITY

AFWL ltr 30 Nov 1971

THIS PAGE IS UNCLASSIFIED

805717

DEVELOPMENT OF LONG-DURATION EXPLOSIVE LOADING TECHNIQUES AND RESPONSE OF SIMPLE STRUCTURES TO PULSE LOADS

A. L. Florence

Poulter Laboratories
Stanford Research Institute
Menlo Park, California
Contract AF29(601)-6364

TECHNICAL REPORT NO. AFWL-TR-65-81

November 1966

AIR FORCE WEAPONS LABORATORY
Research and Technology Division
Air Force Systems Command
Kirtland Air Force Base
New Mexico

Research and Technology Division
AIR FORCE WEAPONS LABORATORY
Air Force Systems Command
Kirtland Air Force Base
New Mexico

BLANK PAGE

DEVELOPMENT OF LONG-DURATION EXPLOSIVE LOADING TECHNIQUES
AND RESPONSE OF SIMPLE STRUCTURES TO PULSE LOADS

A. L. Florence

Poulter Laboratories
Stanford Research Institute
Menlo Park, California
Contract AF29(601)-6364

TECHNICAL REPORT NO. AFWL-TR-65-81

This document is subject
to special export controls and
each transmittal to foreign
governments or foreign
nationals may be made only
with prior approval of AFWL
(WLRP), Kirtland AFB, N.M.
Distribution of this document
is limited because of the
technology discussed.

FOREWORD

This report has been reviewed and is approved.

WALTER D. DITTMER
Lt, USAF
Project Officer

EDGAR A. MUNYON
Colonel, USAF
Chief, Physics Branch

CLAUDE K. STAMBAUGH
Colonel, USAF
Chief, Research Division

ABSTRACT

Described is an experimental technique for providing long-duration pulses which can be applied to a part or all of a simple structure such as a beam, plate or cylinder. The technique employs essentially the familiar shock tube except that the detonation front of a gaseous explosive provides the shock wave. Many pulse shapes can be produced by placing in the tube and against the target, layers of different materials such as styrofoam, polyurethane, and Mylar, and by sending the explosively-induced shock wave through them to the target. The search for pulse shapes was mainly confined to those of the blast type but the generation of other types is equally feasible.

Outlines of the theoretical treatments of four problems are given. They concern the responses of (a) a clamped beam to a blast pulse uniformly distributed over a central length, (b) a simply supported circular plate to a blast pulse uniformly distributed over a central circular area, (c) a clamped circular plate to a rectangular pulse uniformly distributed over the whole plate, and (d) a clamped circular plate to a rectangular pulse uniformly distributed over a central circular area. Analytical treatments employ the rigid-plastic theory because of interest in moderately large permanent deformations and relative simplicity of analysis.

Long-duration pulses were applied to clamped beams and clamped circular plates, and the permanent central displacements are correlated with theoretical predictions.

A preliminary study is made of the modification of the applied pulse due to the mobility of the target.

This page intentionally left blank.

CONTENTS

CONTENTS (Continued)

ILLUSTRATIONS

ILLUSTRATIONS (Continued)

ILLUSTRATIONS (Continued)

ILLUSTRATIONS (Continued)

TABLES

SECTION I

INTRODUCTION

Re-entry vehicles are liable to be subjected to loads ranging from sharp pulses, which for structural response may be considered as ideal impulses, to pulses with durations comparable to the fundamental elastic response times. Short-duration loads have been applied in tests on actual ICBM structures [1.1 - 1.4]* and in experimental and theoretical studies of simplified ICBM structural components such as cylinders, plates, and beams [1.5 - 1.25]. As a result much is known about response to short pulses. Less is known about the effects of long-duration pulses [1.26 - 1.29] especially when these act only on parts of a structure. One reason for this deficiency is the dearth of meaningful experimental results and this in turn is due to the need for controlled long-duration loading techniques.

In Section II is described such a technique suitable for applying loads to part of the surface of a structure. The development was guided by the following pulse requirements:

(1)   low peak pressures,

(2)   durations comparable with fundamental elastic response times,

(3)   rise time much smaller than duration,

(4)   sharp edges to the pressure distribution whenever appropriate,

(5)   pulse shape control, and

(6)   adaptability for use over larger areas.

The long-duration loading technique meets these requirements, partly chosen so that pulses of the blast type (sudden pressure rise and gradual decay) are included, but in addition it provides medium and high peak pressures, medium-duration pulses, and shapes other than those associated with blast pulses. Section II also includes a preliminary

---

*Numbers in brackets indicate references listed at the end of this report.

1

study of the effect on the pulse of the mobility of the target and it is concluded that the effect can definitely be first order.

Section III is a theoretical study of the response of a clamped beam subjected to a blast pulse uniformly dist buted over a central part of the span. On the basis of interest in moderately large permanent deformations the rigid-plastic theory is employed. This theory neglects elastic deformations and provides a relatively simple approach. The clamped beam problem was chosen primarily because of its simplicity and because it gives much insight into the response or deformation mechanisms. Some structural experiments were performed on clamped beams but since the reproducibility required some improvement the results are regarded as preliminary. They indicate that the predicted damage is from 2 to 4 times the actual damage.

Section IV is a theoretical sutdy of the response of a simply supported plate subjected to a blast pulse uniformly distributed over a central circular area. The solution, which again uses the rigid-plastic theory, is for low peak pressures only, or rather for low values of the ratio of the peak pressure to the static collapse pressure acting on the same area.

Section V is a theoretical and experimental study of the response of a clamped circular plate subjected to a blast pulse over the whole area of the plate. Using rigid-plastic theory a solution is presented for the special case of a rectangular pulse. In the experiments, the plates were subjected to blast pulses having an exponential decay. Hence true correlation of theoretical and experimental damage is not achieved. It is believed that the rectangular pulse among all blast pulses with the same pressure and impulse causes the greatest damage and the correlation showed that the predicted damage is from 3 to 7 times the actual damage, so with true correlation these values should be reduced. This problem was chosen as a preliminary to that in Section VI, where the plate is partially loaded, because of the complexity of these kinds of problems.

Section VI is a theoretical and experimental study of the response of a clamped circular plate subjected to a blast pulse over a central circular area of plate. Using rigid-plastic theory a solution is presented for the special case of a rectangular pulse. In the experiments, the plates were subjected to pulses which may be considered approximately rectangular but having an exponential decay. Correlation of the theoretical and experimental central deflections shows that the predicted damage overestimates over the wide range of factors from 2 1/2 to 24. The large factors are attributed partly to the fact that the experimental pulse is not rectangular and partly to the use of thin plates which, due to their mobility, do not receive the full impulse.

Section VII is a description of a simple mathematical model of the experimental configuration of the long-duration loading technique. The model successfully describes the mechanics of the operation and forms a good basis for further refinement. It is a valuable aid to experimental design towards achieving the pulses desired.

Section VIII is a study of the effect of pulse shape on simple rigid-plastic structures. It is proved that for a certain class of structures the rectangular pulse, among all pulses of equal peak pressure and impulse, causes the greatest damage. It is also indicated that the theorem is true for a wider class of rigid-plastic structures. The importance of this study lies in the fact that it is much easier to analyze structures when the pulse is rectangular and the result serves as an upper bound on the damage acquired.

This page intentionally left blank.

SECTION II

EXPERIMENTS

1. Long-Pulse Technique

In developing a technique for providing and applying long-duration pulses the following properties are being sought:

(a)   pulse duration about 1/2 msec,

(b)   short rise time to peak pressure,

(c)   monotonic decay following peak pressure,

(d)   uniform pressure distribution on loaded surface,

(e)   each load unit applicable to small area of structure, and

(f)   units capable of being combined for larger surface loading.

An experimental arrangement which provides pulses meeting the above requirements when they are applied to fixed targets is shown in Figs. 2.1 and 2.2. It essentially consists of a shock tube in which the shock is the detonation front of a 50/50 gaseous mixture of oxygen and acetylene. One end of the tube is placed against a fixed target plate, the junction being made air-tight by means of a rubber gasket. In the fixed endplate is mounted a pressure transducer. The open end of the tube is sealed with a sheet of Mylar. Inlet and outlet hoses for the gas mixture pass through this Mylar sheet. The gas is detonated at the opposite end of the tube to the pressure transducer [2.1], so that the detonation front travels towards the endplate producing an instantaneous rise of pressure there and a pulse duration depending on the tube length. Figure 2.3 shows a typical pulse obtained with this experimental arrangement.

One limitation of this arrangement is that the peak pressure is always a constant for a given gas mixture although this can be relaxed somewhat by varying the ratio of oxygen to acetylene. Also the form of the decay in pressure remains the same, its rapidity depending on the tube length. Another and more important limitation for spot

5
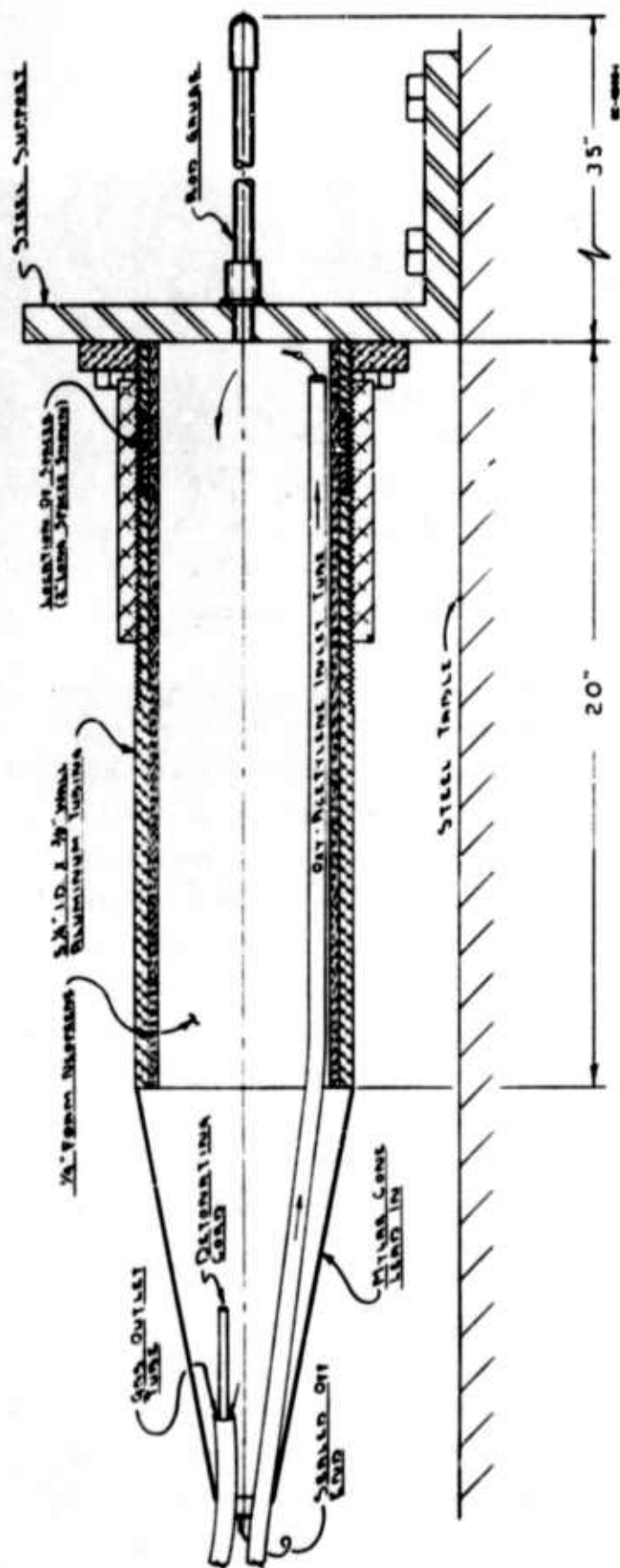
FIG. 2.1 OXYACETYLENE SHOCK TUBE

6
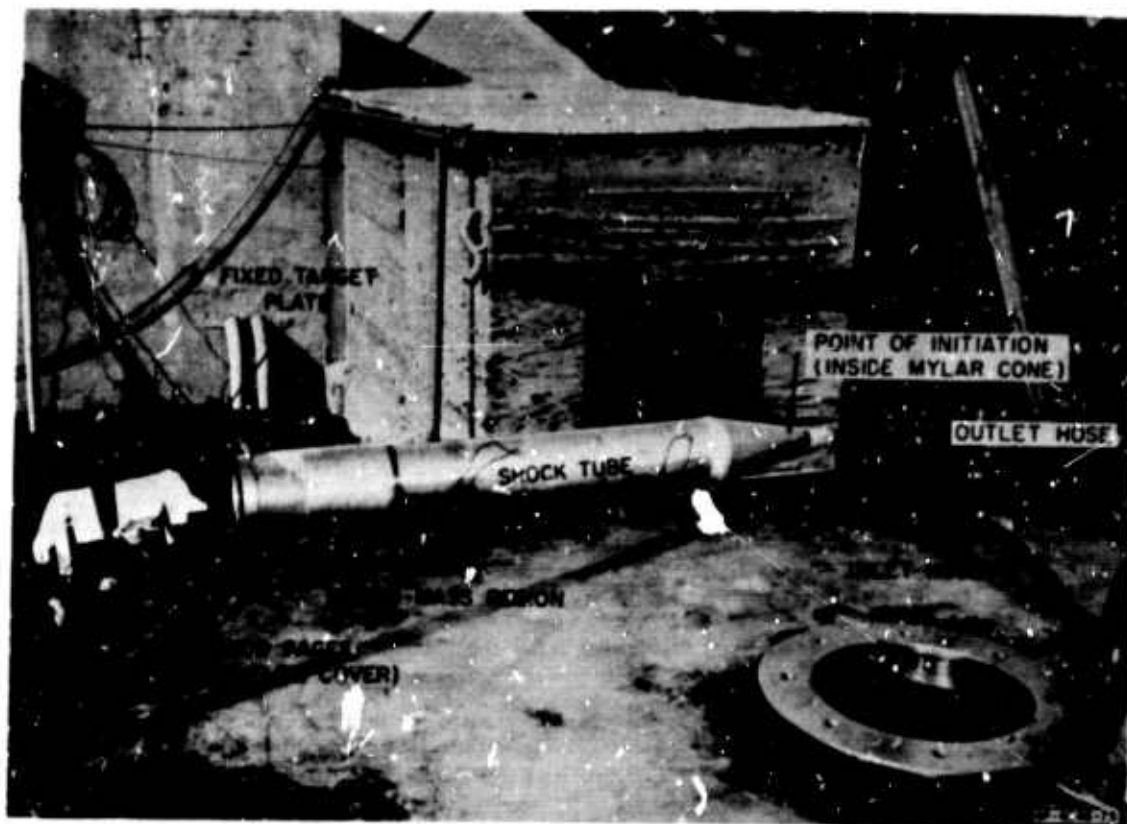
FIG. 2.2 OXYACETYLENE SHOCK TUBE

applications is that separation of the target and tube allows rarefaction waves to travel over the target surface and rapidly curtail the pulse duration. The arrangement is, however, suitable for clamped plates where the plate support is an extension of the shock tube (see Section V).

An arrangement which does not have these limitations and provides innumerable pulse shapes consists of filling the end of the tube next to the target with various materials on which the shock wave from the detonated gas must act. One such arrangement is shown schematically in Fig. 2.4 where alternate layers of polyurethane foam and Mylar form a spring-mass system. Between the gas and the foam-Mylar combination is a layer of styrofoam which acts as a light piston

7
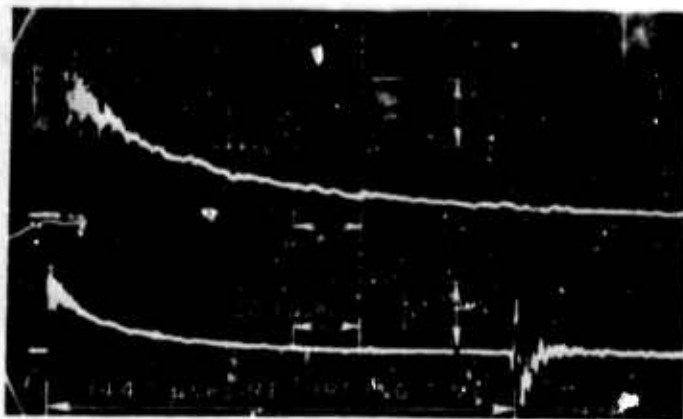
FIG. 2.3 ROD-GAGE RECORD — OXYACETYLENE GAS PULSE

and helps to spread the pressure uniformly over the face of the target.
By changing this system of masses and nonlinear springs various pulse
shapes can be obtained.

It is desirable that the compressed spring-mass system should
be much more flexible than the target to minimize the disturbance of
the uniformity of the pressure distribution as the target deforms.
This property influenced the choice of the spring material and mass
geometry.

In Figs. 2.5 to 2.9 are displayed sequences of pulses that have
been obtained by varying certain parameters of the spring-mass
system of Fig. 2.4. Attention has been focussed on obtaining pulses
which can be approximated by rectangles, triangles, exponential
curves or simple combinations of these. Many of the pressure records
display the oscillations of the systems but they are of such high fre-
quency that a structure will respond only to the mean pressure.
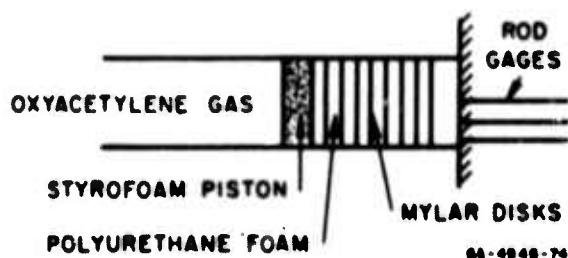
FIG. 2.4 TYPICAL SPRING—MASS SYSTEM

Details of the pulses and config-urations are shown in Tables 2.1 to 2.5 on the pages opposite the pulse records. The main observation to be made is that a fairly high degree of control of the pulse shaping can be obtained with the spring-mass system. Furthermore, the pulse shaping experiments are reproducible and provide a reasonably uniform pressure distribution over the target face. This last point was established by using three rod gages, located at the center, a half-radius point, and close to the edge of the target area.

In addition to the cylindrical tube experiments, spring-mass systems were tried in a tube of rectangular cross section. Similar pulse shapes were obtained but both the reproducibility and uniformity of pressure distribution were found to be unsatisfactory (for example, peak pressure variation was ± 10%). These deficiencies are attributed to the cross-sectional dimensions of the tube used in the experiments. A rather narrow rectangle, 5 inches by 1 inch, was used resulting in the intrusion of the edge effects (friction, slight lack of fit of spring-mass system, etc). Should a rectangular tube with the same aspect ratio for the cross section be required for an experiment it is suggested that the scale be increased to provide 10 inches by 2 inches, say. Also, it would be desirable to provide finer tolerances by using machined parts. Figure 2.10 shows the experimental arrangement using a tube of rectangular cross section located vertically over three 3-foot rod gages.

9

Spring-Mass System for Pulses of Figs. 2.5(a) to (d)

Configuration Diagram
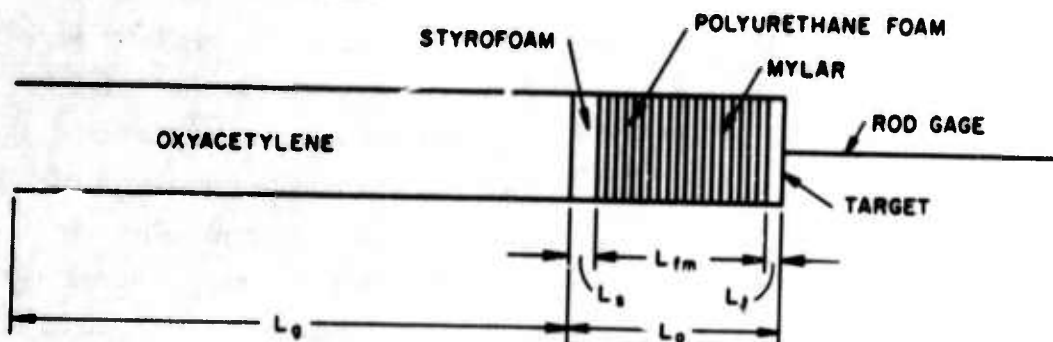
Table 2.1 — Experimental Data

P u l s e	DIMENSIONS (Inches)					SCALES (sides of square grid)				Peak Pressure P_m (lb/in^2)	Impulse $(lb\text{-}sec/in^2)$
						Upper Trace		Lower Trace			
	L_g	L_o	L_s	L_{fm}	L_t	Vert. (lb/in^2)	Horiz. (μsec)	Vert. (lb/in^2)	Horiz. (μsec)		
a	32	12	2	9	1	655	100	1310	100	1015	0.324
b	"	"	4	7	"	"	"	"	"	114	0.352
c	"	"	6	5	"	"	"	"	"	1409	0.236
d	"	"	8	3	"	"	"	"	"	1836	0.277

The Mylar disks are 10-mils thick and are located at 1/2-inch centers.
Impulse values are obtained by crude curve fitting.

Material	Density	
	lb/ft^3	gm/cm^3
Styrofoam	4	0.064
Polyurethane	5	0.080
Mylar	87.4	1.4

Observations

1. Trend of the sequence is from an exponential curve to a triangle.

2. Peak pressures increase monotonically from about 1000 lb/in^2 to 1800 lb/in^2.

3. Impulses tend to decrease.
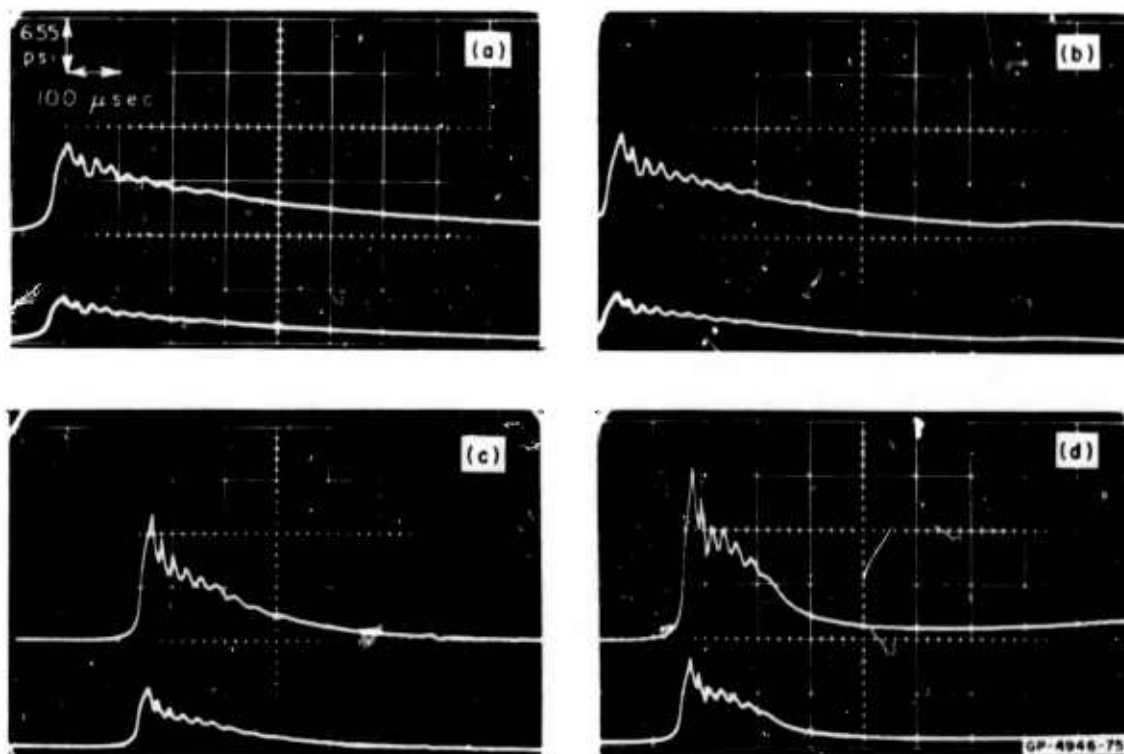
FIG. 2.5 ROD-GAGE RECORDS

Spring-Mass System for Pulses of Figs. 2.6(a) to (f)

Configuration Diagram

STYROFOAM   POLYURETHANE FOAM   MYLAR   ROD GAGE

OXYACETYLENE   TARGET

L_{fm} L_s L_t L_o L_g
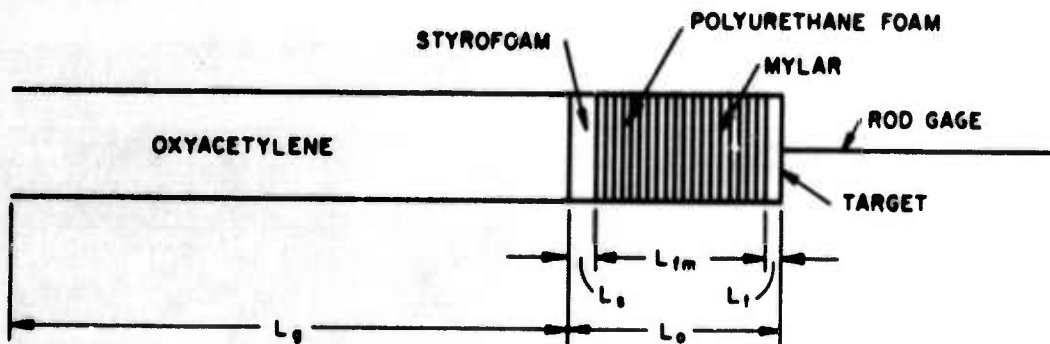
Table 2.2 — Experimental Data

Pulse	DIMENSIONS (inches)					SCALES (sides of square grid)				Peak Pressure P_{m_2} (lb/in^2)	Impulse (lb-sec/in^2)
						Upper Trace		Lower Trace			
	L_g	L_o	L_s	L_{fm}	L_t	Vert. (lb/in^2)	Horiz. (μsec)	Vert. (lb/in^2)	Horiz. (μsec)		
a	32	12	1½	9½	1	655	100	1310	100	1080	0.346
b	"	11	"	8½	"	"	"	"	"	1440	0.389
c	"	10	"	7½	"	"	"	"	"	1570	0.521
d	"	9	"	6½	"	"	"	"	"	1830	0.347
e	"	7	"	4½	"	"	50	"	50	2620	0.534
f	"	6	"	3½	"	"	"	"	"	3140	0.518

The Mylar disks are 10-mils thick and are located at 1/2-inch centers.
Impulse values are obtained by crude curve fitting.

Material	Density	
	lb/ft^3	gm/cm^3
Styrofoam	4	0.064
Polyurethane	5	0.080
Mylar	87.4	1.4

Observations

1. Trend of the sequence is from a slowly decaying exponential curve toward a rectangle followed by a rapidly decaying exponential curve.

2. Peak pressures increase monotonically from about 1000 lb/in^2 to 3200 lb/in^2.

3. Impulses, generally higher than those of Fig. 2.5, tend to increase.

12
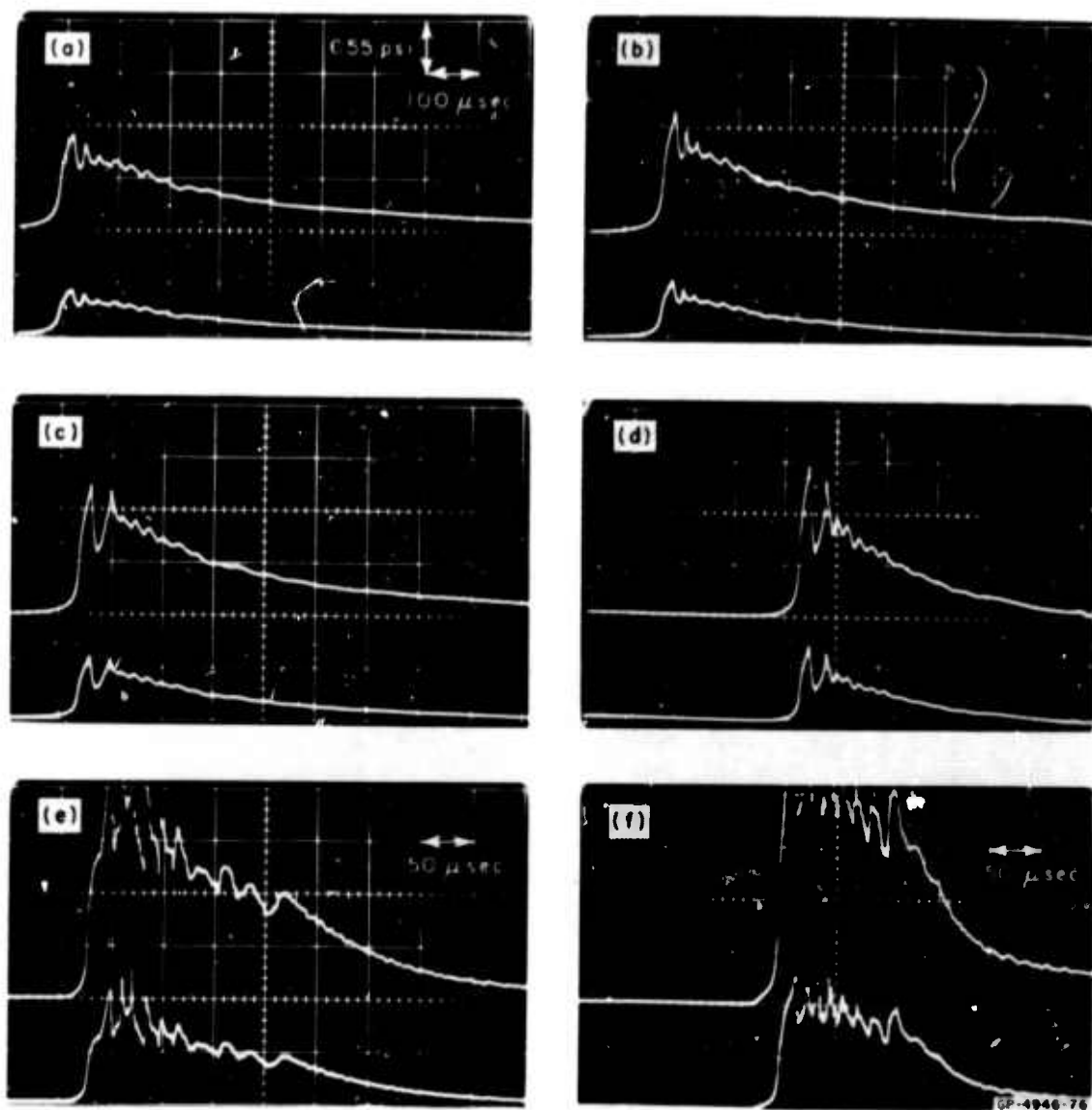
FIG. 2.6 ROD-GAGE RECORDS

13

Spring-Mass System for Pulses of Figs. 2.7(a) to (d)

Configuration Diagram
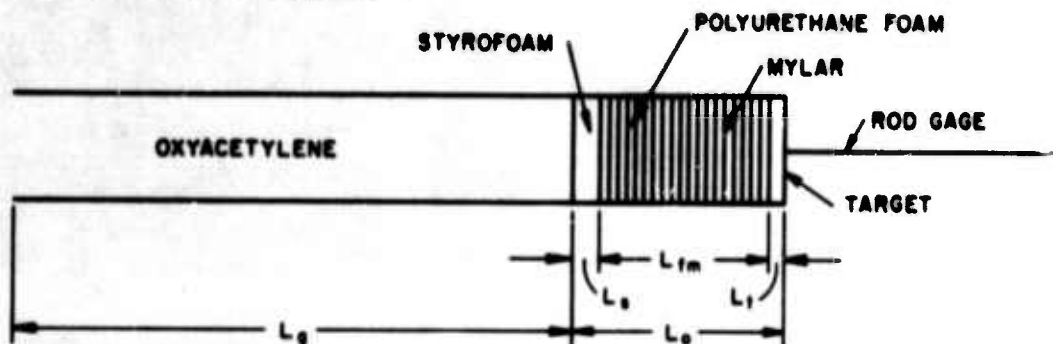
Table 2.3 — Experimental Data

Pulse	DIMENSIONS (inches)					SCALES (sides of square grid)				Peak Pressure P_m (lb/in²)	Impulse (lb-sec/in²)
						Upper Trace		Lower Trace			
	L_g	L_o	L_s	L_{fm}	L_t	Vert. (lb/in²)	Horis. (μsec)	Vert. (lb/in²)	Horis. (μsec)		
a	32	10	2	0	8	680	100	1360	100	1630	0.495
b	"	"	"	2	6	"	"	"	"	1360	0.414
c	"	"	"	4	4	"	"	"	"	1290	0.504
d	"	"	"	6	2	"	"	"	"	1230	0.566

The Mylar disks are 10-mils thick and are located at 1/2-inch centers.
Impulse values are obtained by crude curve fitting.

Material	Density	
	lb/ft³	gm/cm³
Styrofoam	4	0.064
Polyurethane	5	0.080
Mylar	87.4	1.4

Observations

1. Trend of the sequence is from a triangle to a rectangle followed by a triangle or exponential curve.

2. Peak pressures decrease monotonically from about 1600 lb/in² to 1200 lb/in².

3. Impulses in the same range as those of Fig. 2.6 and tend to increase.

14
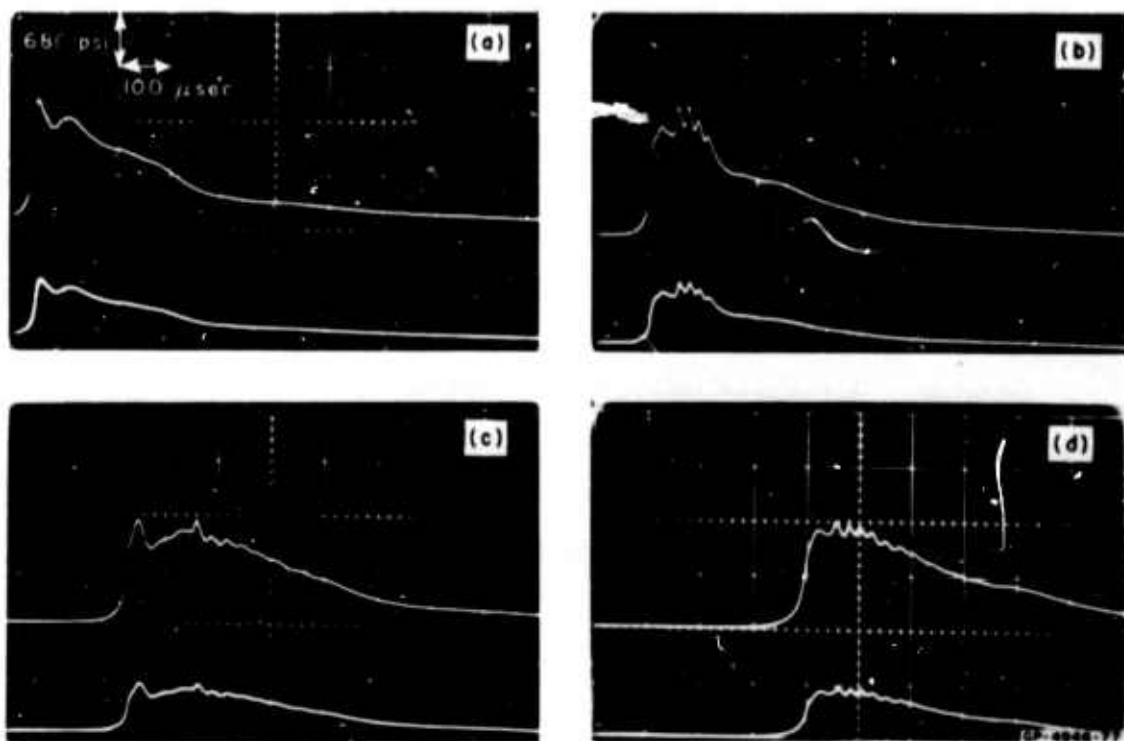
FIG. 2.7 ROD-GAGE RECORDS

Spring-Mass System for Pulses of Figs. 2.8(a) to (f)

Configuration Diagram
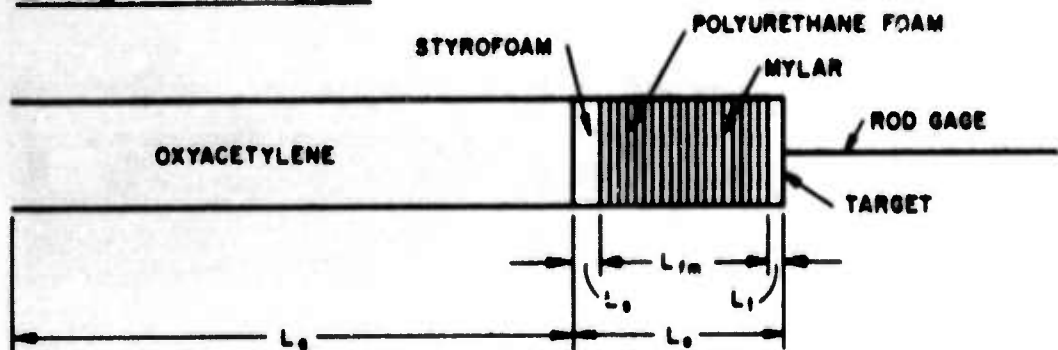
Table 2.4 — Experimental Data

Pulse	DIMENSIONS (inches)					No. of 10-mil Mylar Disks at 1/2-inch Spacing Ordered from Styrofoam	s_{um}	SCALES (sides of square grid)				Peak Pressure P_m (lb/in²)	Impulse (lb-sec/in²)
								Upper Trace		Lower Trace			
	L_g	L_o	L_s	L_{fm}	L_t			Vert. (lb/in²)	Horiz. (μsec)	Vert. (lb/in²)	Horiz. (μsec)		
a	32	10	2	4	4	2 2 2 2 2 1 1 1	14	680	100	1360	100	952	0.475
b	"	"	"	5	3	2 2 2 2 2 1 1 1 1	16	"	"	"	"	985	0.542
c	"	"	"	6	2	2 2 2 2 2 1 1 1 1 1 1 1	18	"	"	"	"	1054	0.493
d	"	"	"	4	4	3 3 2 2 2 1 1 1	16	262	"	680	"	865	0.445
e	"	"	"	4½	3½	4 3 3 2 2 2 1 1 1	20	"	"	"	"	760	0.516
f	"	"	"	4½	3½	4 4 3 3 2 2 2 1 1 1	23	"	"	"	"	642	0.426

Material	Density	
	lb/ft³	gm/cm³
Styrofoam	4	0.064
Polyurethane	5	0.080
Mylar	87.4	1.4

Observations

1. Pulse shapes do not change radically.

2. Peak pressures increase monotonically in subsequence (a), (b), (c) from about 950 lb/in² to 1050 lb/in² and decrease monotonically in subsequence (d), (e), (f) from about 850 lb/in² to 650 lb/in².

3. Impulses remain fairly steady and are in the same range as those of Figs. 2.5, 2.6 and 2.7.

16
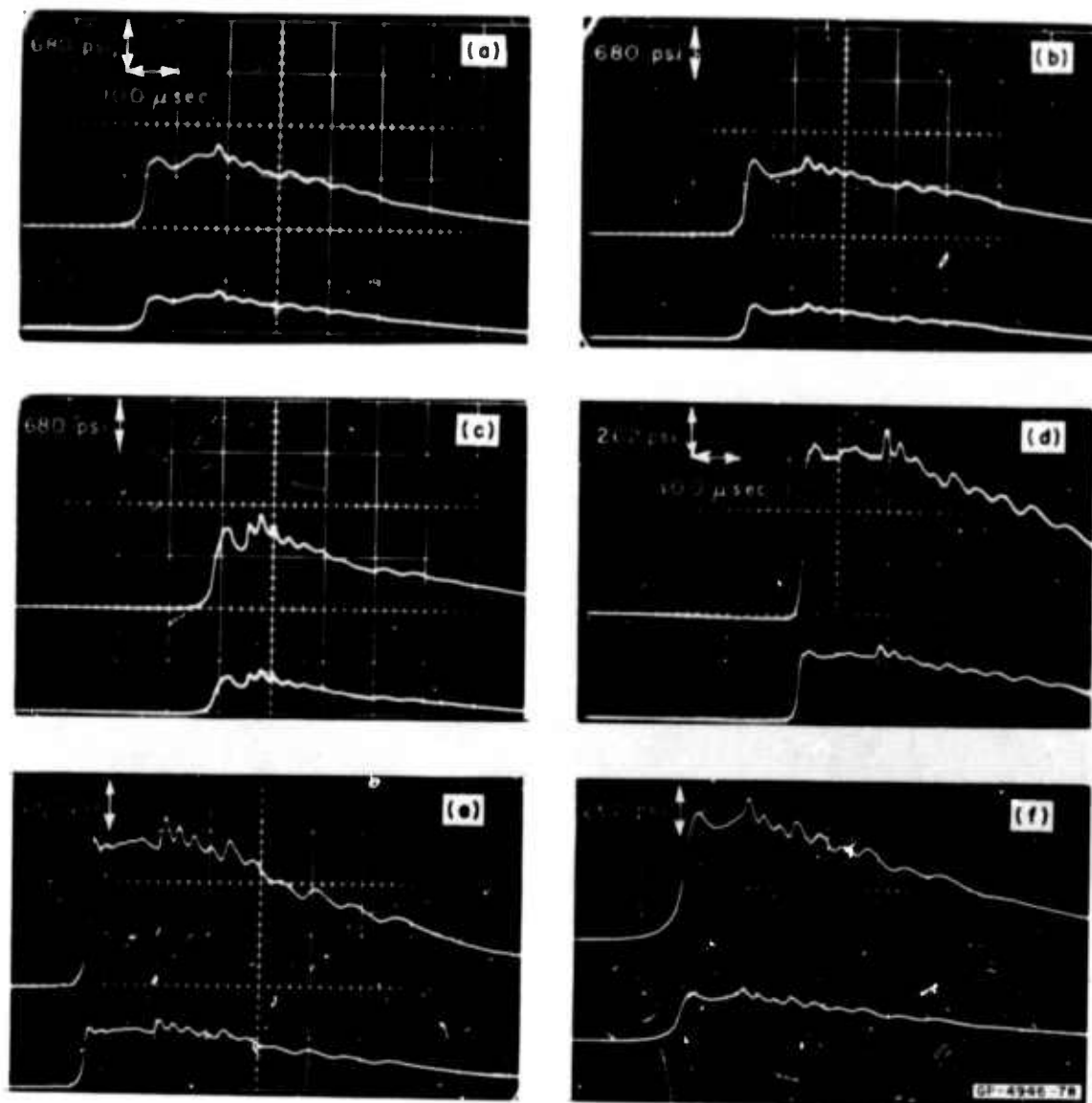
FIG. 2.8 ROD-GAGE RECORDS

17

Spring-Mass System for Pulses of Figs. 2.9(a) to (d)

Configuration Diagram
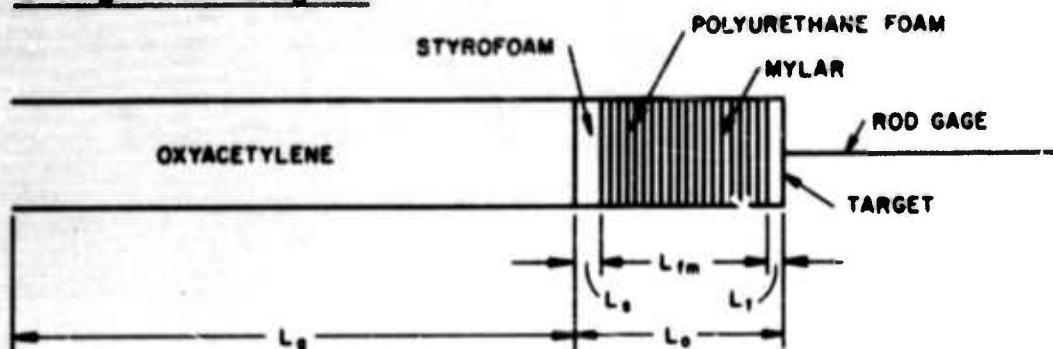
Table 2.5 — Experimental Data

Pulse	DIMENSIONS (inches)					No. of 10-mil Mylar Disks at 1/2-inch Spacing Ordered from Styrofoam	Sum	SCALES (sides of square grid)				Peak Pressure P_m (lb/in²)	Impulse (lb-sec/in²)
								Upper Trace		Lower Trace			
	L_g	L_o	L_s	L_{fm}	L_t			Vert. (lb/in²)	Horiz. (µsec)	Vert. (lb/in²)	Horiz. (µsec)		
a	14	7	2	0	5	1 1 1 1 1	5	262	100	680	100	760	0.206
b	"	"	"	2	3	2 2 1 1 1	7	"	"	"	"	695	0.220
c	"	"	"	2	3	3 2 2 1 1 1	10	"	"	"	"	590	0.243
d	"	"	"	2½	2½	3 3 2 2 1 1 1	13	"	"	"	"	524	0.229
e	"	"	"	3	2			"	"	"	"	485	0.218

Material	Density	
	lb/ft³	gm/cm³
Styrofoam	4	0.064
Polyurethane	5	0.080
Mylar	87.4	1.4

Observations

1. Trend of the sequence is from a triangle to a rectangle followed by an exponential curve.

2. Peak pressures decrease monotonically from about 750 lb/in² to 500 lb/in².

3. Impulses remain fairly steady and are about one-half of the impulses in Figs. 2.5 to 2.8 (only about half the length of gas used).
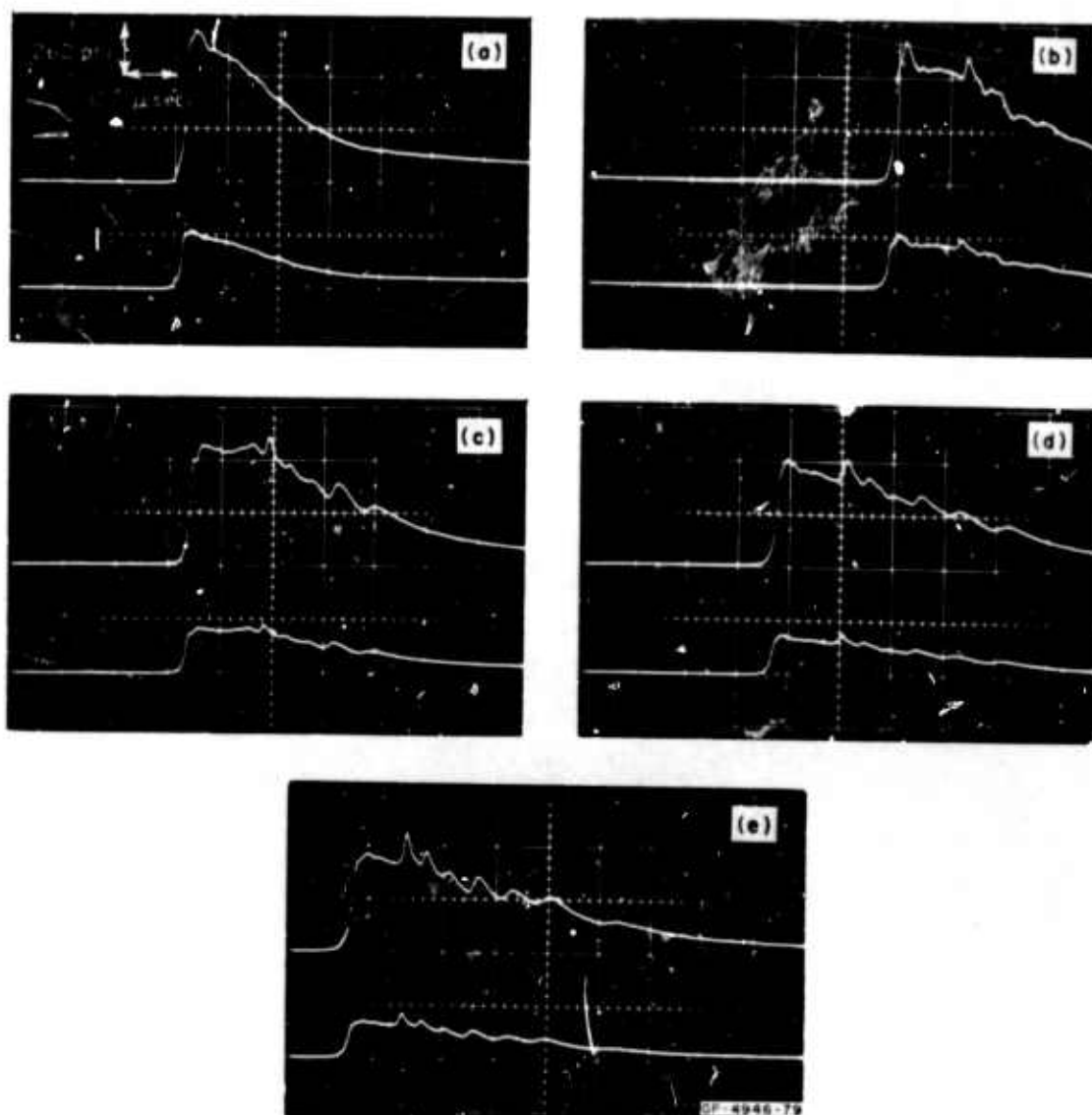
FIG. 2.9   ROD-GAGE RECORDS

FIG. 2.10 EXPERIMENTAL ARRANGEMENT — SHOCK TUBE
OF RECTANGULAR CROSS SECTION

2. Photodiode Experiments

In order to assess the effect on the pulses of the mobility of the
target, pulses from the fixed target configurations associated with
Figs. 2.8(d) and 2.9(e) were applied to free disks placed against the
end on the shock tube (Fig. 2.11). It is reasonable to suppose that,
at least in the early stages of the application of the pressure, the
fixed target pressure will be modified most if the plate is completely
free to move away.

20
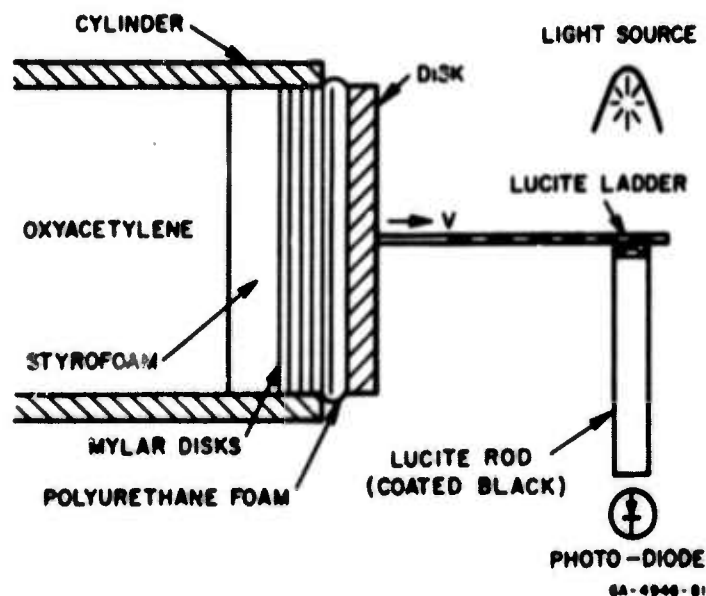
FIG. 2.11 DIAGRAM OF PHOTODIODE SETUP (during motion)

The technique consists of obtaining an x, t plot for the disk of sufficient accuracy to allow the second derivative $\ddot{x}$, or the acceleration, to be computed accurately. Then, by Newton's law $p(t) = m\ddot{x}$ it is possible to construct the pressure-time relation. Also, for a pulse of duration T , it is possible to find the impulse since $I(T) = m\dot{x}(T)$.

A diagram of the experimental setup to provide an accurate x, t plot for the disk is shown in Fig. 2.11. A lucite "ladder" in a light magnesium frame is attached to the center of the disk by means of a ball joint (Fig. 2.12) and, as the disk moves, the ladder holder is guided along teflon-lined tracks (Figs. 2.12, 2.13 and 2.14). The strip of lucite has 50 or 100 lines per inch equally spaced on one surface, the lines being perpendicular to the direction of motion and having a thickness equal to the space between them. On one side of the ladder is located a powerful light source while on the opposite side, perpendicular to the ladder, is a lucite rod. The curved surface of the rod is coated black to exclude light and on the end next to the ladder is an array of lines with the same spacing and parallel to those on the ladder.

21
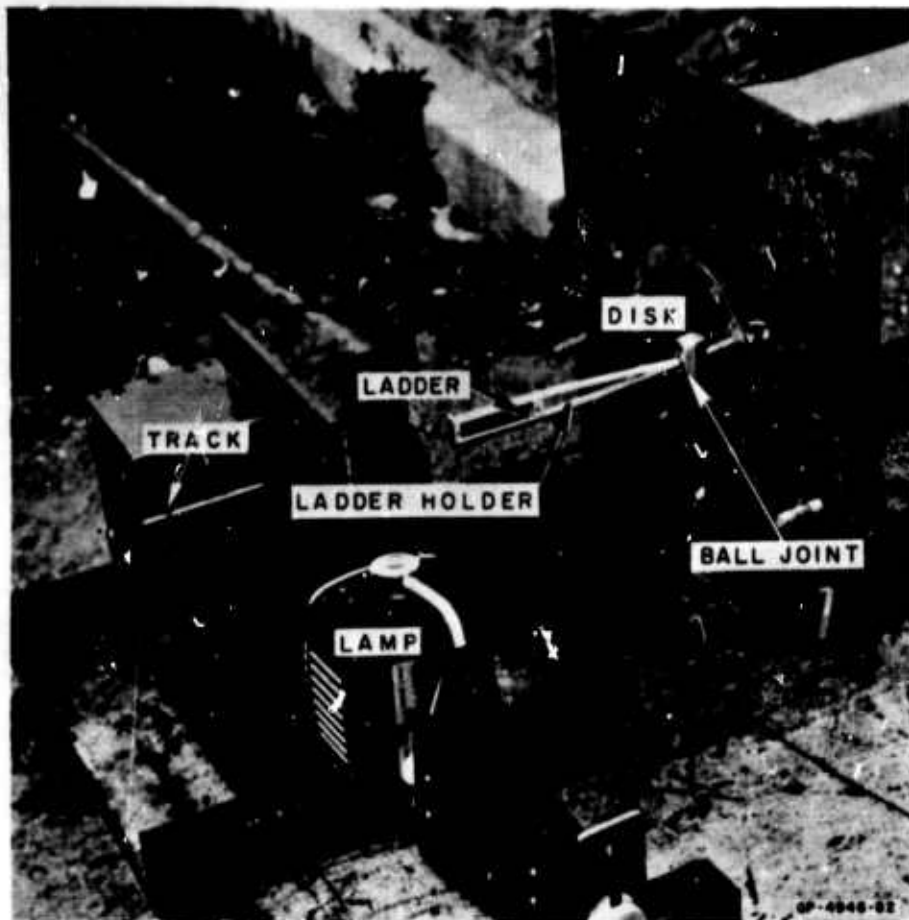
FIG. 2.12 EXPERIMENTAL ARRANGEMENT FOR PHOTODIODE MEASUREMENTS
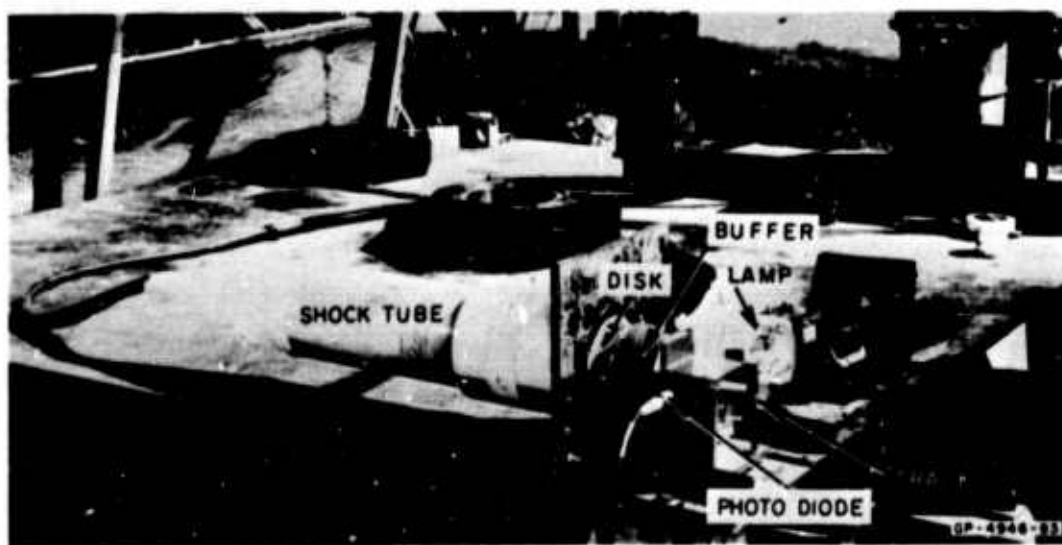
FIG. 2.13 EXPERIMENTAL ARRANGEMENT FOR PHOTODIODE MEASUREMENTS
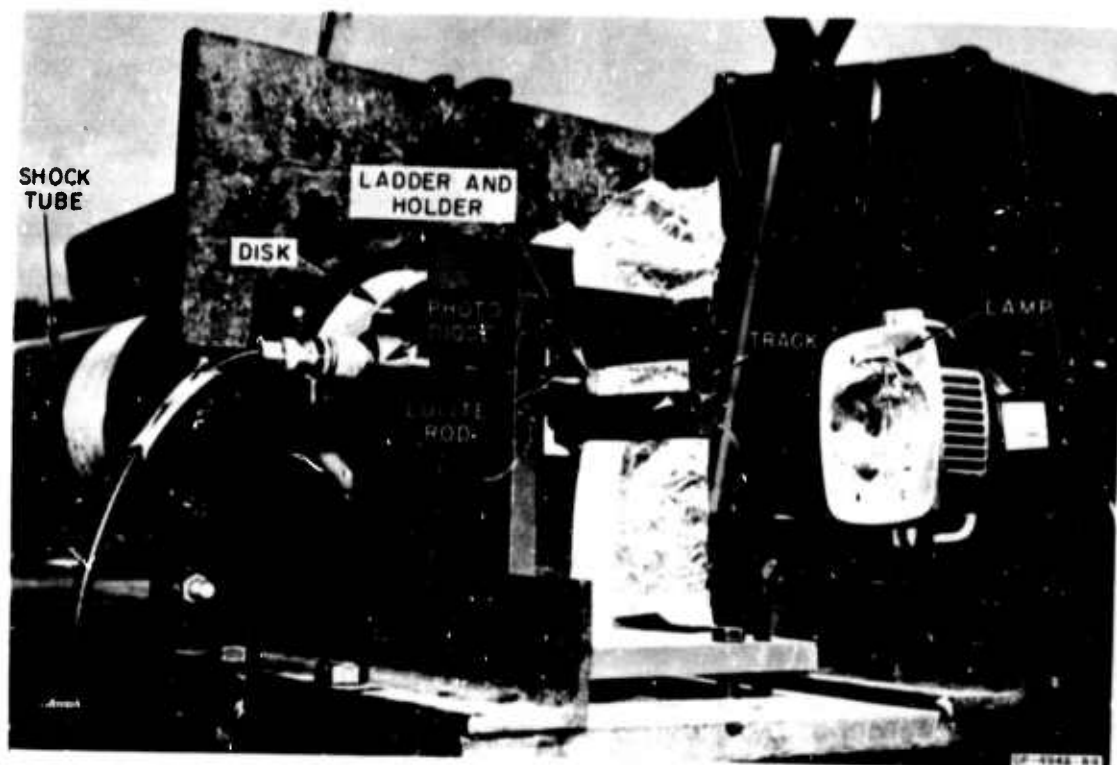
FIG. 2.14 EXPERIMENTAL ARRANGEMENT FOR PHOTODIODE MEASUREMENTS

Each line is completely opaque so that when they are exactly opposite each other the maximum amount of light is transmitted along the lucite rod; almost complete interference or darkness prevails when the lines are exactly opposite the spaces. As the ladder moves across the end of the rod, the intensity of light traveling down the rod varies and is converted into a voltage variation by means of a photodiode located at the other end. The voltage variation is recorded on oscilloscopes.

Figures 2. 15(a) and (b) are oscillograms showing the voltage variation when a ladder having 50 lines per inch is attached to a 1/2-inch-thick aluminum disk which receives a pulse from the configuration associated with the record in Fig. 2. 9(e). The sweep rate is 20 μsec per cm and by using appropriate delays in two dual beam oscilloscopes a total time coverage of 800 μsec is achieved. The distance traveled by the disk during the time interval between crests
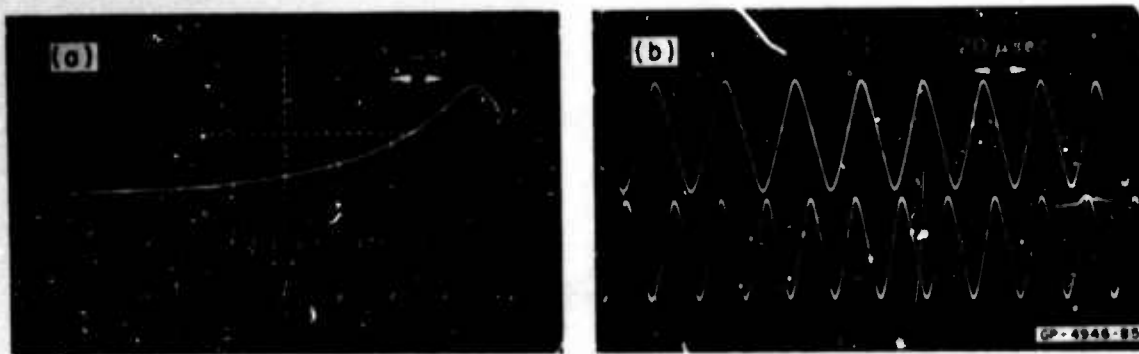
FIG. 2.15 PHOTODIODE RECORDS EXPERIMENTAL CONFIGURATION ASSOCIATED
WITH FIG. 2.9(e) (Ladder has 50 lines/inch)

or troughs is 0.02 inch. Thus an (x, t) plot for the disk is obtained
and is shown in Fig. 2.16 as the curve labelled "experiment."
Additional points can be obtained by using the trace between the crests
and troughs. In particular, the upper trace in Fig. 2.15(a) gives the
initial motion of the disk.

As stated earlier the second derivative of the (x, t) plot gives
the pressure. It was found that the method gave the initial part of
the pressure-time diagram satisfactorily, but around the peak pressure
and at later times it appears that the pressure is varying quite rapidly
and this demands greater accuracy. However, the ultimate accuracy
of the method has not been reached.

As an inverse method one can take the pressure pulse acting
on the fixed target (rod-gage record), idealize it, and modify it so that
its (x, t) plot falls on top of the experimental (x, t) curve. In Fig. 2.16,
curves A and B are (x, t) plots from idealized pulses having the shapes
shown in the figure, impulses and peak pressures equal to those of the
fixed target pulse, and a ramp pressure rise taking 100 μsec to reach
peak pressure. Such pulse shapes could form a reasonable starting
point, especially for early times where the mobility of the target has
least effect.

24
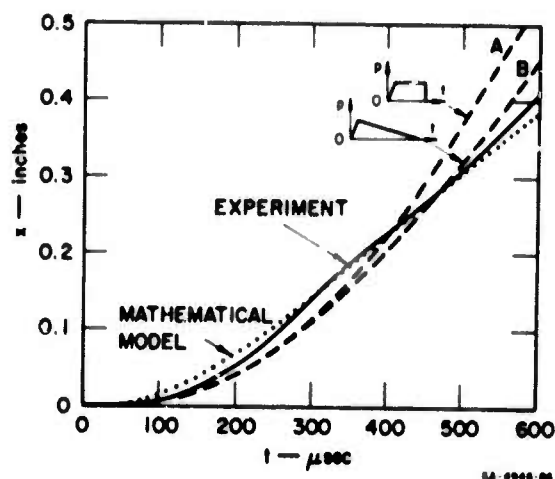
FIG. 2.16 (x,t) PLOTS FOR FREE DISK—
CONFIGURATION OF FIG. 2.9(e)

One point worthy of notice is that the impulse imparted to the
free disk is considerably less than that on a fixed target. This can be
seen in Fig. 2.16 by comparing the final slope of the curves A and B
with the final average slope of the experimental curve. From two
photodiode experiments with the configuration of Fig. 2.8(d) the final
velocities corresponded to impulses of 0.208 and 0.219 lb-sec/in^2 for
a fixed target impulse of 0.363 lb-sec/in^2. From three photodiode
experiments with the configuration of Fig. 2.9(e) the impulses were
0.117 0.119, and 0.120 lb-sec/in^2 corresponding to the fixed-target
impulse of 0.209 lb-sec/in^2. The average ratios of free-target to
fixed-target impulses are respectively 0.59 and 0.57 which represents
a considerable reduction of impulse due to full mobility of the target.

3.   Mathematical Model

Each assemblage of layered media used to sha   pulses has been
regarded as and is called a spring-mass system, whereas it is actu. 'y
a somewhat more complicated system. However, a mathematical model
was constructed consisting of masses and linear or cubic springs which
gives a reasonable account of the behavior of the layered media, at least
for the few cases studied. The description of and results from the
mathematical model are contained in Section VII. The (x, t) plot of a
freely supported disk used in the photodiode experiment with the con-
figuration of Fig. 2.9(e) is shown in Fig. 2.16.

25

4.   Structural Experiments

Some experiments were performed in each of which a central
length of a clamped beam was subjected to loading by placing the beam
against the target end of the shock tube of rectangular cross section.
The pulse applied to each beam was taken as that measured against a
fixed target (rod-gage record) for the same experimental configuration.
As was mentioned above at the end of Subsection 1, the pulses obtained
were neither sufficiently reproducible nor uniform. In spite of this a
few beams of 6061-T6 aluminum were loaded to demonstrate the
feasibility of the structural experiments. The results, which can only
be regarded as preliminary, indicate that the ratio of the theoretical
to experimental final central deflections range from about 3 to 4 for
λ values (ratio of peak pressure to static collapse pressure) ranging
from about 3 to 12, the theoretical deflection being that from a rec-
tangular pulse. In conclusion it should be stated that these experiments
could almost certainly be improved by using wider beams and hence a
wider shock tube. This remark is based on the good reproducibility
and uniformity of pressure distribution obtained when the shock tube is
cylindrical. Experiments on plates are described at the ends of Sections
V and VI.

5.   Large Surface Loading

For the loading of larger structural surfaces the shock-tube units,
which can have any reasonable cross section, can be placed side by
side to cover the loading area. A number of units are especially re-
quired when the loading surface is curved to ensure that the wave
strikes the surface at right angles and to ensure that the layers are
not buckled or crumpled by being forced to occupy a smaller area.
Figure 2.17 shows a section through a suggested two-unit assembly of
shock tubes for applying a load to a cylindrical surface. Unlike the single
units the assembly shown would involve a detonation wave striking the
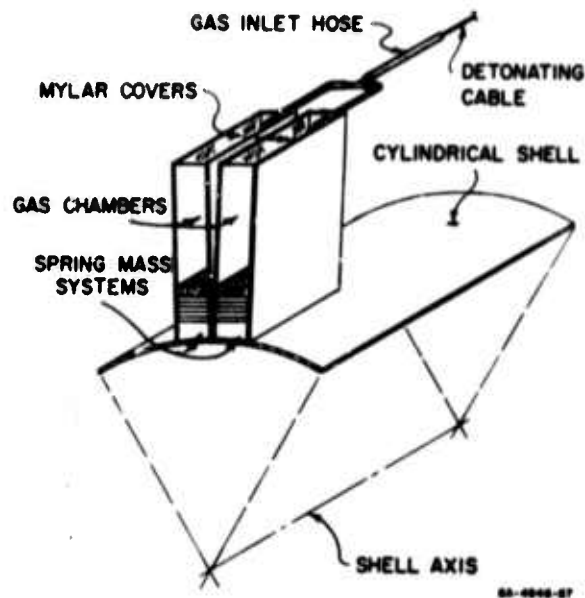
FIG. 2.17   SECTION OF A TWO UNIT
ASSEMBLY OF SHOCK TUBES

styrofoam piston obliquely, the front traveling along the top of the
styrofoam at a velocity higher than the detonation velocity. The
pressure pulse for this setup would first be obtained from rod gages
and possibly photodiode experiments before being applied to the
structure.

It should be possible to approximate a loading which varies not
only with time but with position on the loaded surface by using an
assemblage of shock tubes each with its own spring-mass configuration.
A cosine distribution of loading around one-half of a cylinder appears
quite feasible.

This page intentionally left blank.

SECTION III

CLAMPED BEAM

1.   Introduction

The problem treated here is the response of a clamped beam of
rigid-plastic material subjected along a central portion of its span to
a pressure which is constant along the beam but varying with time in
the form of a blast pulse. Figure 3.1 illustrates the problem. A
blast pulse is here defined as a pulse with a time-dependent pressure
satisfying

$$t\,p(t) \leq \int_0^t p(\tau)d\tau \tag{3.1}$$
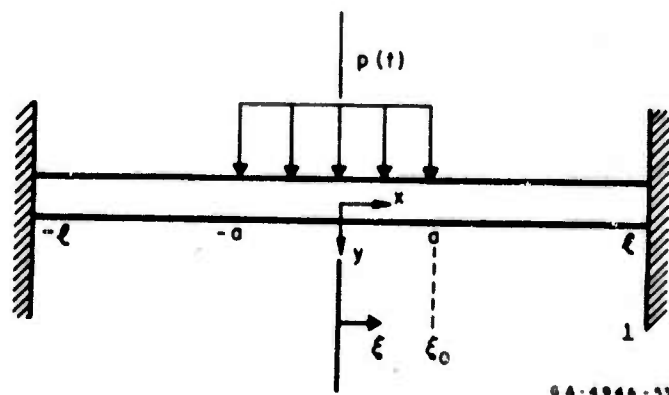
FIG. 3.1 CLAMPED BEAM PROBLEM

The main characteristics of such a pulse are the instantaneous
rise to peak pressure and a decay in accordance with condition (3.1).

When the moment-curvature relation for a beam is approximated
by that corresponding to a beam made of a rigid-ideally plastic material,

29

no deformations and hence no curvature is possible until the bending moment at a cross section is equal to the fully plastic moment, whereupon the curvature becomes unbounded. This property determines failure in rigid-plastic structures by means of mechanisms.

In the Semiannual Technical Report No. 1 it was shown that the clamped beam can fail in one of four types of mechanisms. The parameters determining the initial mechanism are the peak pressure of the pulse and the loaded length of the beam. In the following section the equations of motion and their solutions are presented for each mechanism. Two of these mechanisms are the subject of a paper by M. Conroy [3.1]. Although the work primarily concerns beams of infinite length, its application for a clamped beam can easily be made.

Section III considers the deformations caused by three types of blast pulses: rectangular, triangular and exponential. A derivation of formulas for the deformed shape of the beam is presented only for the case of a rectangular pulse. Formulas for the midspan deflections are contained in Appendix A. For the rectangular pulse only, formulas for the deformed shape are contained in Appendix B. The variation of the midspan deflection with peak pressure, impulse and loaded length for all three pulses are shown in Figs. 3.3 to 3.11.

2.   Mechanisms of Deformation

   (a)   Mechanism 1

Peak pressures, p_m , which are slightly above the static collapse pressure p_s , cause small inertia forces and the beam deforms in the static collapse mechanism. The cross sections of the beam at the supports and at midspan carry a fully plastic moment, M_o , and the resulting motion of each half-beam is a rotation as a rigid body about the supports. The corresponding velocity distribution along a half-beam , $0 \le x \le \ell$, is

$$\dot{y}(x, t) = w(t)(\ell - x) \qquad (3.2)$$

30

where $\omega(t)$ is the angular velocity about the ends. The equation of motion can readily be written in the form

$$\dot{\omega} = \frac{6M_o p_s}{m\ell^2} \left(\frac{p}{p_s} - 1 \right) \qquad (3.3)$$

where p_s is the static collapse pressure given by

$$p_s = \frac{4M_o}{\ell^2 \xi_o (2 - \xi_o)} \qquad (3.4)$$

and m is the mass per unit length of beam.

The equilibrium equation for a length x of the half-beam $(0 \leq x \leq \ell)$ is

$$M = M_o - \int_o^x \int_o^{x_1} (p - m\ddot{y}) dx' \, dx \qquad (3.5)$$

When $\ddot{y}$, found by differentiating (3.2) and using the result (3.3) for $\dot{\omega}$, is substituted in (3.5) and the integration performed, (3.5) provides the following relations for the bending moment

$$\frac{M}{M_o} = 1 + \frac{p}{p_s} (3\xi^2 - \xi^3) - \frac{p}{p_s} \left(\frac{2\xi^2}{2\xi_o - \xi_o^2} \right) \qquad 0 \leq \xi \leq \xi_o$$

$$\qquad (3.6)$$

$$\frac{M}{M_o} = 1 + \frac{p}{p_s} (3\xi^2 - \xi^3) - \frac{2p}{p_s} \left(\frac{2\xi - \xi_o}{2 - \xi_o} \right) \qquad \xi_o \leq \xi \leq 1$$

The conditions which ensure no violation of the yield condition, $|M| \leq M_o$, are now stated.

From expressions (3.6) it can be shown that a necessary and sufficient condition for a maximum moment at midspan is

$$\frac{p}{p_s} \leq \frac{3\xi_o (2 - \xi_o)}{2 - 3\xi_o (2 - \xi_o)} \qquad \xi_o \leq 1 - 1/\sqrt{3} = .433$$

$$\qquad (3.7)$$

$$\frac{p}{p_s} \leq \frac{3\xi_o (2 - \xi_o)}{3\xi_o (2 - \xi_o) - 2} \qquad \xi_o \geq 1 - 1/\sqrt{3}$$

31

Similarly a minimum moment will occur at the support, that is at $\xi = x/\ell = 1$, if

$$\frac{p}{p_s} \leq 3\left(\frac{2-\xi_0}{2-3\xi_0}\right) \qquad \xi_0 \leq 2/3$$

$$\tag{3.8}$$

$$\frac{p}{p_s} \leq 3\left(\frac{2-\xi_0}{3\xi_0-2}\right) \qquad \xi_0 \geq 2/3$$

The conditions (3.7) and (3.8) are also sufficient for the moment to decrease monotonically for $0 \leq \xi \leq \xi_0$ and $\xi_0 \leq \xi \leq 1$ respectively.

The loading range for this mechanism represented by $\lambda = p_m/p_s$ can then be written as

$$1 \leq \lambda \leq \lambda_1$$

where

$$\lambda_1 = \begin{cases} 3\left(\frac{2-\xi_0}{2-3\xi_0}\right) & \xi_0 \leq 1/2 \\[4mm] \frac{3\xi_0(2-\xi_0)}{3\xi_0(2-\xi_0)-2} & \xi_0 \geq 1/2 \end{cases} \tag{3.9}$$

Mechanism 1 applies to any type of loading whereas the other three mechanisms require the restriction (3.1) of a blast load.

(b)   <u>Mechanism 2a</u> $\xi_0 \geq 1/2$

For the case where the loading acts over more than half the span and $\lambda > \lambda_1$, the yield condition is violated in the neighborhood of $\xi = 0$. This suggests a mechanism of deformation which retains the plastic hinges at the supports but has two plastic hinges which travel towards the center. The decreasing central section of the beam will translate downward while the outer portions rotate as rigid bodies

about the supports. After the moving hinges meet at the center the beam will deform according to mechanism 1.

Denoting the position of the moving hinge by $x_o(t)$, the velocity distribution meeting the above description is

$$\dot{y}(x, t) = \begin{cases} \dot{y}_o(t) & 0 \leq x \leq x_o \\[2em] \dot{y}_o(t) \left(\frac{x - \ell}{x_o - \ell}\right) & x_o \leq x \leq \ell \end{cases} \tag{3.10}$$

The equations of motion for the half beam are

$$m\ddot{y}_o = p \tag{3.11}$$

$$\frac{m}{3}(\ell - x_o)^2 \dot{\omega} = \frac{p}{2}(a - x_o)(2\ell - a - x_o) - 2M_o \tag{3.12}$$

where $\omega = \dot{y}_o/(\ell - x_o)$ is the angular velocity of the outer portions of the beam.

Integrating (3.11) and (3.12), using the initial conditions $y(x, 0) = \dot{y}(x, 0) = 0$ yields the following two equations for y_o and x_o:

$$y_o = \int_o^t I(t)dt \tag{3.13}$$

$$(\ell - x_o)^2 = \frac{12M_o t}{I(t)} + 3(a - \ell)^2 \tag{3.14}$$

where

$$I(t) = \int_o^t p(\tau)d\tau$$

By substituting the velocity field (3.10) in the moment expression (3.5) and carrying out the integration the moment distribution is found to be

$$M = \begin{cases} M_o & 0 \le x \le x_o \\[2mm] M_o - \dfrac{p}{2}(x-x_o)^2 - \dfrac{m\dot{w}}{6}\varphi & x_o \le x \le a \qquad (3.15) \\[2mm] M_o - \dfrac{p}{2}(a-x_o)(2x-a-x_o) - \dfrac{m\dot{w}}{6}\varphi & a \le x \le \ell \end{cases}$$

where

$$\varphi = x^3 - 3x^2\ell - 3xx_o + 6xx_o\ell + 2x_o^3 - 3x_o^2\ell$$

Using (3.15) it can be shown that the yield condition will not be violated so long as the pulse obeys the condition (3.1) and $\lambda = p_m/p_s$ is bounded by the values λ_1 and λ_2 ; that is

$$\lambda_1 \le \lambda \le \lambda_2$$

where

$$\lambda_2 = \frac{3\xi_o(2-\xi_o)}{(1-\xi_o)^2} \qquad \xi_o \ge 1/2$$

and λ_1 is given by (3.9).

(c) <u>Mechanism 2b</u> $\xi_o \le 1/2$

When the loaded length is less than the half span and $\lambda > \lambda_1$ the yield condition is violated at the supports. A mechanism of deformation is thus considered which has a plastic hinge at mid-span and two hinges which travel towards the supports. The only motion is that of the inner portion of the half beam, $0 \le x \le x_1$, which rotates as a rigid body about the moving hinge at $x = x_1(t)$. After the moving hinges reach the supports the structure will deform according to mechanism 1.

34

In accordance with the above motion, the velocity distribution is

$$
\dot{y}(x, t) = \begin{cases} \dot{y}_o(t) \left(1 - \dfrac{x}{x_1}\right) & 0 \le x \le x_1 \\[2ex] 0 & x_1 \le x \le \ell \end{cases} \tag{3.17}
$$

where $\dot{y}_o$ is the velocity at the center of the beam.

The momentum equations for the half-beam are

$$
m \frac{d}{dt}(x_1 \dot{y}_o) = 2ap \tag{3.18}
$$

$$
m \frac{d}{dt}(x_1^2 \dot{y}_o) = 3a^2 p + 12 M_o \tag{3.19}
$$

With the initial conditions of zero displacement and velocity the solution of (3.18) and (3.19) is

$$
\dot{y} = \frac{4a^2 I^2(t)}{12 M_o m t + 3a^2 m I(t)} \tag{3.20}
$$

$$
x_1 = \frac{3a}{2} + \frac{6 M_o t}{a\, I(t)} \tag{3.21}
$$

This mechanism was investigated in [3.1] and it was found that the yield condition will not be violated so long as (3.1) is satisfied and

$$
\frac{I(t)}{t} \le \frac{12 M_o}{a^2} \tag{3.22}
$$

In (3.22), $I(t)/t \longrightarrow p_m$ as $t \longrightarrow 0$, so that $p_m \le 12 M_o / a^2$. Hence

$$
\lambda_1 \le \lambda \le \lambda_2
$$

35

where

$$\lambda_2 = 3 \left(\frac{2 - \zeta_o}{\zeta_o} \right) \qquad \zeta_o \leq 1/2 \qquad (3.23)$$

and λ_1 is given by (3.9).

(d) Mechanism 3

For sufficiently high pressures such that $\lambda > \lambda_2$, mechanism 2 violates the yield condition either at the supports (if $\zeta_o \leq 1/2$) or at mid-span (if $\zeta_o \geq 1/2$). This suggests a mechanism of deformation in which moving plastic hinges are formed on both sides of the loading boundary, $x = a$. The hinge at $x = x_o$ and under the loaded segment of the beam moves towards midspan while the other at $x = x_1$ moves towards the support. If the support receives the approaching hinge first, the structure enters mechanism 2a, whereas if the mid-span receives the other approaching hinge first, the structure enters mechanism 2b.

The motion of the half beam is as follows: the inner segment, $0 \leq x \leq x_o$ translates downward while the midsection, $x_o \leq x \leq x_1$, rotates about the outer hinge, x_1 . The velocity field can therefore be written as

$$\dot{y}(x, t) = \begin{cases} \dot{y}_o & 0 \leq x \leq x_o \\ \dot{y}_o \left(\frac{x_1 - x}{x_1 - x_o} \right) & x_o \leq x \leq x_1 \\ 0 & x_1 \leq x \leq \ell \end{cases} \qquad (3.24)$$

The momentum equations for the half-beam are

$$\int_o^t a p(\tau) d\tau = \int_o^\ell m \dot{y} \, dx$$

and

$$\int_o^t \left(2M_{o_s} + p \frac{a^2}{2} \right) d\tau = \int_o^\ell m x \dot{y} \, dx$$

36

with the solution

$$m y_o = \int_0^t I(\tau)d\tau \tag{3.25}$$

$$x_o = a - (\frac{12M_o t}{I})^{1/2} \tag{3.26}$$

$$x_1 = a + (\frac{12M_o t}{I})^{1/2} \tag{3.27}$$

In [3.1] it is shown that the yield condition will not be
violated if the loading is a blast pulse satisfying (3.1) and

$$\lambda \geq 3(\frac{2-\xi_o}{\xi_o}) \qquad \xi_o \leq 1/2$$

$$\tag{3.28}$$

$$\lambda \geq \frac{3\xi_o(2-\xi_o)}{(1-\xi_o)^2} \qquad \xi_o \geq 1/2$$

To find the initial locations of x_1 and x_2 set $I = p_m t$
in (3.26) and (3.27) which is approximately true for small t. Then

$$x_2(0) = x_o + (12M_o/p_m)^{1/2}$$

$$x_1(0) = x_o - (12M_o/p_m)^{1/2}$$

Hence as λ_m or p_m increases indefinitely the initial
positions of x_1 and x_2 move closer to x_o, coinciding with x_o
for an ideal impulse.

(e) Summary of Mechanisms

The results obtained for the modes of failure giving
dependence upon dimensionless peak pressure and loaded length are

37

shown in Fig. 3.2. For convenience, λ_1 and λ_2 are given below.

$$\lambda_1 = \begin{cases} 3\zeta_0(2-\zeta_0)/[3\zeta_0(2-\zeta_0)-2] & 1/2 \le \zeta_0 \le 1 \\ \\ 3(2-\zeta_0)/[3(2-\zeta_0)-4] & 0 < \zeta_0 \le 1/2 \end{cases}$$

$$\lambda_2 = \begin{cases} 3\zeta_0(2-\zeta_0)/1-\zeta_0)^2 & 1/2 \le \zeta_0 \le 1 \\ \\ 3(2-\zeta_0)\zeta_0 & 0 < \zeta_0 \le 1/2 \end{cases}$$

Once a blast pulse is known its peak pressure and the loaded
length of beam can be plotted on Fig. 3.2 to give the initial mechanism.
Knowing this, the analysis can proceed directly towards obtaining
permanent deformations.

3.   **Permanent Deformations**

(a)   **Introduction**

In this Section the permanent deformations are considered
for three blast pulses: rectangular, triangular and exponential. These
particular pulses need only two parameters for their complete
description. The parameters chosen are the peak pressure, p_m,
and the total impulse per unit beam length, I_1, defined as

$$I_1 = \int_0^\infty p(t)dt$$

Since the method of solution is identical for all three
loadings, expressions are derived for the final deformed shape due to
a rectangular pulse causing initial deformation by mechanism 2a. For
the other initial mechanisms only the results are given and they may be
found in Appendix B. The central deflection formulas for all three
pulses are contained in Appendix A.

38
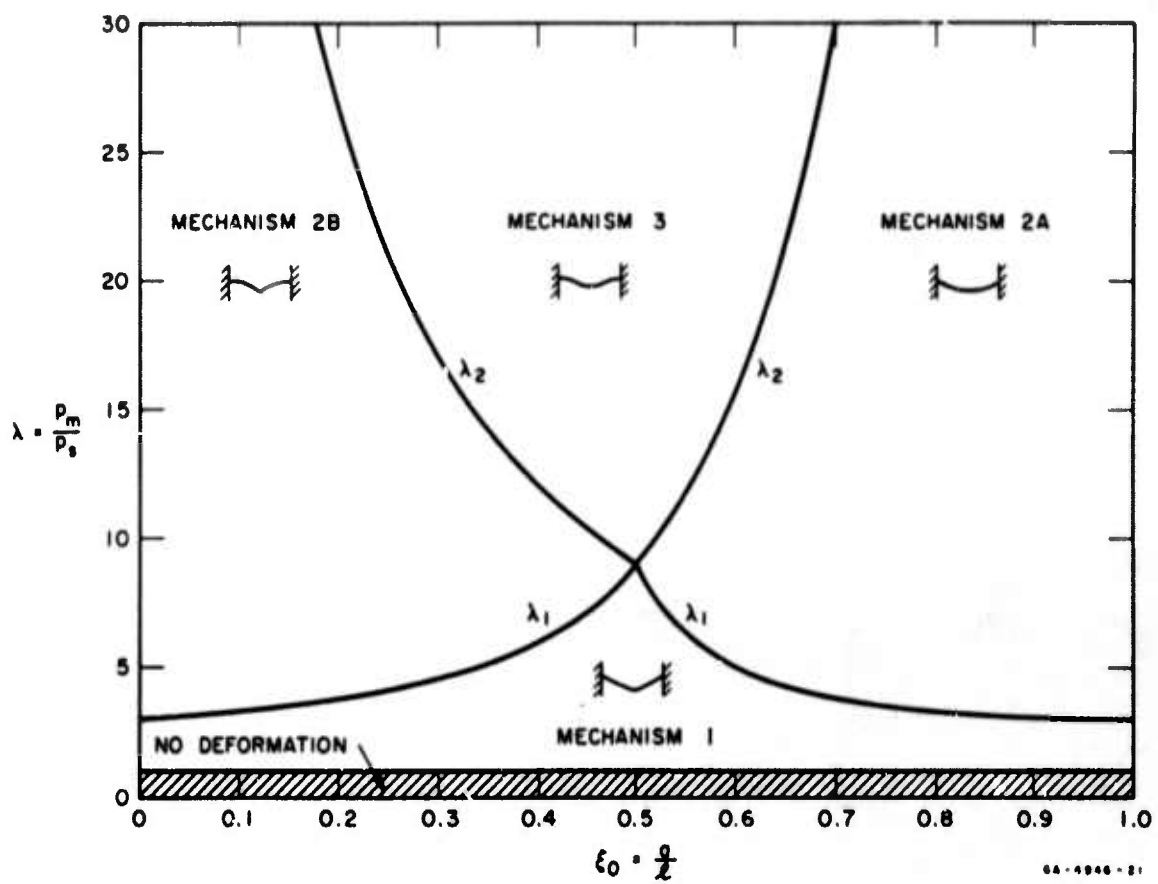
FIG. 3.2(a)   DEFORMATION MECHANISM DIAGRAM

39
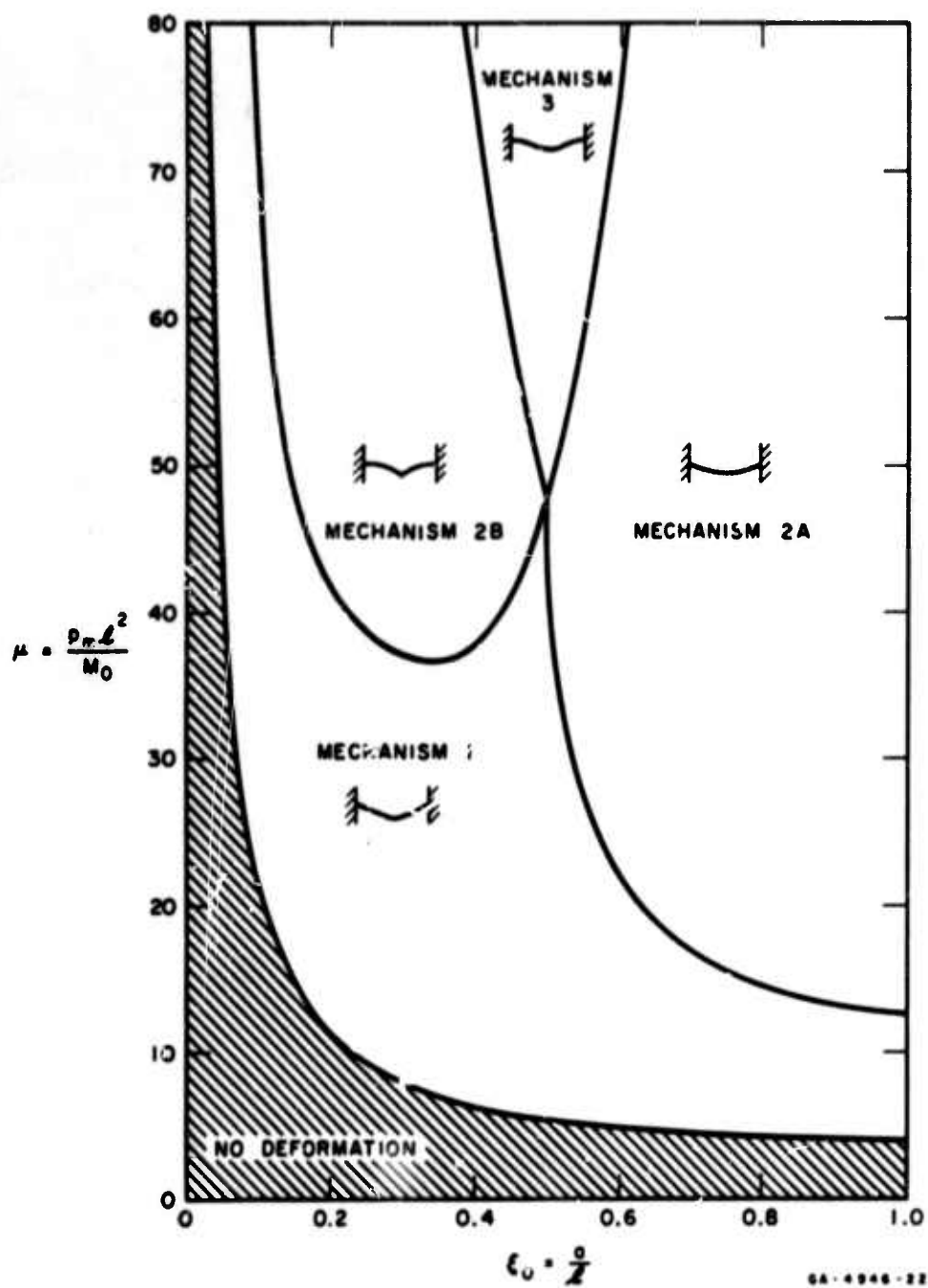
FIG. 3.2(b)   DEFORMATION MECHANISM DIAGRAM

(b)   Rectangular Pulse

The loading under consideration is given by

$$p = \begin{cases} P_m & 0 \le t \le t_o \\ 0 & t > t_o \end{cases}$$

where

$$t_o = I_1/P_m$$

A special feature associated with a rectangular pulse is that all plastic hinges are stationary while it is acting on the beam. This simplifies the analysis since the quantity $I(t)$, appearing in the equations of Section III-2, can be replaced by the constant I_1.

The derivation of expressions for the final deformed shape is confined, for simplicity, to the initial mechanism 2a. For the remaining initial mechanisms the expressions are listed in Appendix B.

Mechanism 2a : $\lambda_1 < \lambda \le \lambda_2$ $1/2 \le \xi_o \le 1$

The expressions for the final shape of the half beam will be quite different on either side of the initial hinge position $x = x_o(0)$ for two reasons. Firstly, a discontinuity of slope at $x = x_o(0)$ is created during phase 1 because a rectangular pulse causes the hinge to remain stationary. Secondly, during phase 2 the hinge initially at $x = x_o(0)$ travels through the region $0 \le x \le x_o(0)$ toward the center of the beam.

During phase 1, the equation of motion in the region $0 \le x \le x_o(0)$ is $m\ddot{y} = P_m$ which upon integrating twice between $t = 0$ and $t = t_o = I/P_m$ yields

$$y(x, t_o) = I_1^2/2mP_m \qquad 0 \le x \le x_o(0) \qquad (3.29)$$

The portion of beam $x_o(0) \leq x \leq \ell$ rotates about the support as a rigid body. Hence

$$y(x, t_o) = (I_1^2 / 2mp_m)(\ell - x)/[\ell - x_o(0)] \quad x_o(0) \leq x \leq \ell \quad (3.30)$$

During phase 2 let the time be τ when the moving hinge reaches a point in the segment $0 \leq x \leq x_o(0)$. The point moves at a constant velocity I/m during the time $\tau - t_o$ after which it moves as part of the rigid portion rotating about the support and for a time $t_1 - \tau$, t_1 denoting the end of phase 2. Now the equations of motion for the parts on either side of $x = x_o$ are $\dot{y}_o = I/m$ and $m(\ell - x_o)^3 \dot{\omega}/3 = -2M_o$ from which $\dot{x}_o = -6M_o/I(\ell - x_o)$ and $(\ell - x)^2 - [\ell - x_o(0)]^2 = 6M_o(\tau - t_o)/I$. The velocity of points on the rigid rotating portion is $\dot{y} = I(\ell - x)/m(\ell - x_o)$. Hence the deflections which occur during phase 2 are, by integration of velocities,

$$y(x, t_1) - y(x, t_o) = \frac{I_1}{m}(\tau - t_o) + \frac{I_1}{m}(\ell - x) \int_\tau^{t_1} \frac{dt}{\ell - x_o}$$

$$= \frac{I_1}{m}[\tau - t_o) + (\ell - x) \int_x^0 \frac{dx_o}{\dot{x}_o(\ell - x_o)}]$$

$$= I_1^2 [(\ell - x)^2 - \ell - x_o(0)^2 + x(\ell - x)]/6mM_o$$

$$0 \leq x \leq x_o(0) \quad (3.31)$$

and

$$y(x, t_1) - y(x, t_o) = \frac{I_1}{m}(\ell - x) \int_{t_o}^{t_1} \frac{dt}{\ell - x_o} = \frac{I_1}{m}(\ell - x) \int_{x_o(0)}^0 \frac{dx_o}{\dot{x}_o(\ell - x_o)}$$

$$= I_1^2 x_o(0) \cdot (\ell - x)/6mM_o \quad x_o(0) \leq x \leq \ell \quad (3.32)$$

42

Figures 3.4(a) to (d) show the same curves as those of Figs. 3.3(a) to (c) only they have been regrouped. For a given loaded length the λ versus ν curve for each of the three types of pulse are shown side by side. Again regarding the impulse as the same for each type of pulse, Figs. 3.4(a) to (d) show that for a given value of λ the central deflections are greatest when the pulse shape is rectangular and least when it is exponential. For low values of λ the spread of δ is quite large whereas, as expected, for high values of λ the spread is small. The latter observation is of course due to each pulse tending toward an ideal impulse.

Figures 3.5(a) to (c) give the same information as that in Figs. 3.3(a) to (c) but in a form convenient for studying the variation of λ with the impulse I_1. They are essentially pressure-impulse diagrams (p-I diagrams),each curve showing how the pressure and impulse must vary to achieve a given central deflection δ. It can be seen that above certain values of λ the peak pressure can be varied significantly with very little change of impulse required to maintain δ (see Conclusion 4).

Figures 3.6(a) to (c) show the same curves as those of Figs. 3.5(a) to (b) only they are regrouped according to loaded length so that the effect of the pulse shape may be seen more clearly. For any fixed peak pressure, or λ value, the impulse required to produce a given δ is least when the pulse is rectangular and greatest when it is exponential. The differences are most pronounced when λ is low, especially in the range $1 < \lambda < 2$.

Figures 3.7(a) to (c) are essentially another form of pressure-impulse diagram (p-I diagram). The impulse I_1 has been rendered dimensionless by dividing by I_i, which is the ideal impulse required to give the same central deflection as I_1. Consequently all the curves have a vertical asymptote through $I_1/I_i = 1$. For any given central deflection δ the curves show the relationship between λ and I_1/I_i. The curves are of course, similar to those of Figs. 3.5(a) to (c).

45

Figures 3.8(a) to (c) show the same curves as those in Figs. 3.7(a) to (c) but they are regrouped according to loaded length to bring out the effect of the pulse shapes. They are similar to those of Figs. 3.6(a) to (c).

Figure 3.9 shows the relationship between the peak pressure and the central deflection by means of the parameters μ and ν. This is an alternate way of representing the information in Figs. 3.3(a) to (c) to give the peak pressure directly instead of from $\lambda = p_m/p_s$.

Figures 3.10(a) to (c) show the relationship between the central deflection δ and the loaded length a by means of the parameters ν and ζ_o with each curve representing a constant peak pressure characterized by the parameter μ. A vertical line drawn through some chosen value of ζ_o intersects the μ curve for the peak pressure of interest. Then, for the impulse of interest the central deflection can be calculated from the ordinate value of ν. Figures 3.10 can therefore be regarded as design curves for clamped beams of rigid-plastic material. Where the μ curves intersect the horizontal axis $\nu = 0$ gives an idea of the loaded length below which no deflection occurs. For example, if $\mu = 10$ more than one-fifth of the span must be loaded to give a permanent central deflection. Now in this region elastic effects become important and so it is probable that one-fifth is a lower bound of the fraction of span that must be loaded to give a permanent deflection. If a beam is subjected to a pulse with a shape that can be approximated by a rectangular, triangular or exponential shape of the same impulse and peak pressure then, for each impulse and central deflection, ν is determined. A horizontal line through this value of ν cuts μ curves which give the relationship between the peak pressure and loaded length to maintain the central deflection (regard μ curves as contours). The loaded length must always be greater than the value at the intersection of the horizontal line through ν with the curve $\mu = \infty$ which represents the ideal impulse case.

46

Figure 3.11 shows the curves $\mu = 20$ for each type of pulse plotted in the ν, ζ_o plane and shows, for a given ζ_o , how the shape effects the final deflection when the peak pressure and impulse remain fixed.

5.   Conclusions

From the information given in Figs. 3.3 to 3.11 the following conclusions can be drawn.

(1)   For a given impulse I_1 and loaded length ζ_o , the central deflection increases monotonically with pressure p_m (or λ), and becomes a maximum when the pressure is infinite, that is, when the given impulse is applied as an ideal impulse. This can be seen best in Figs. 3.5 to 3.8.

(2)   For a given impulse I_1 , Table 3.1 shows approximate values of λ , corresponding to pulse shape and loaded length ζ_o , above which over 80 percent of the maximum central deflection (the deflection δ_i when I_1 is ideal, i.e., $I_1 = I_i$) is obtained. Below the listed values of λ the decrease of δ with λ is quite pronounced. This behavior can be observed best in Figs. 3.3 and 3.4. In Table 3.1 some lower bound values of μ are also listed.

Table 3.1

LOWER BOUNDS FOR λ AND μ GIVING $\delta > 0.8\ \delta_i$

ζ_o	Rectangle		Triangle		Exponential	
	λ	μ	λ	μ	λ	μ
1/4	9	85	11	100	15	140
1/2	5	26	6	32	9	48
3/4	4	17	5	21	8	34
1	4	16	5	20	8	32

(3)   The effect of pulse shapes on the midspan deflection δ when the peak pressure p_m , impulse I_1 and the loaded

47

length ratio ζ_o are given can be seen in Figs. 3.4 and 3.9. Rectangular pulses cause the greatest midspan deflection and the exponential pulses cause the least.

(4)   For a given midspan deflection δ, as the pressure ratio λ decreases from infinity of some value λ_L, the deflection δ is maintained with less than a 10 percent increase in impulse over the ideal impulse ($1 < I_i < 1.1$ for $\lambda_L < \lambda < \infty$). Values of λ_L obtainable from Fig. 3.7 or 3.8 are shown in Table 3.2 for the three types of pulses and for $\zeta_o = 1/4$, 1/2, and 1 . For values of λ below λ_L a significant increase in impulse is required to maintain δ, especially in the range $1 < \lambda < 2$.

Table 3.2

LOWER BOUNDS OF λ REQUIRING
$I_1/I_i < 1.1$ TO MAINTAIN δ

ζ_o	λ		
	Rectangle	Triangle	Exponential
1/4	8	11	18
1/2	1	7	10
1	4	6	9
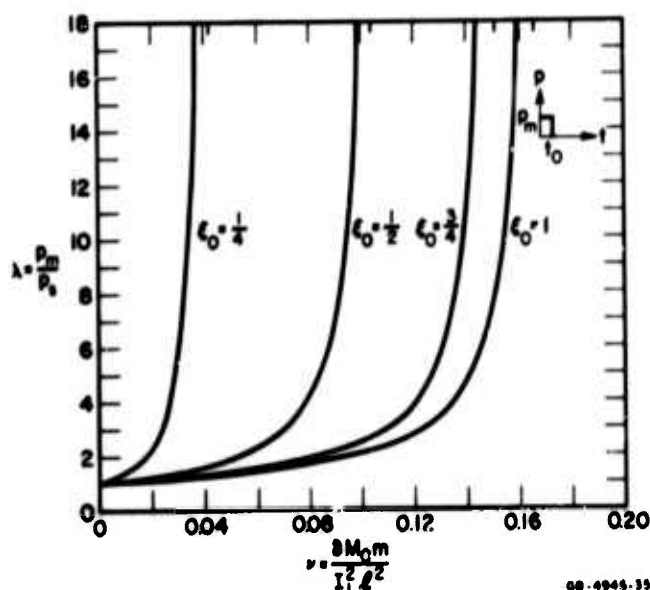
FIG. 3.3(a)   PRESSURE RATIO vs. MIDSPAN DEFORMATIONS: RECTANGULAR PULSE

48
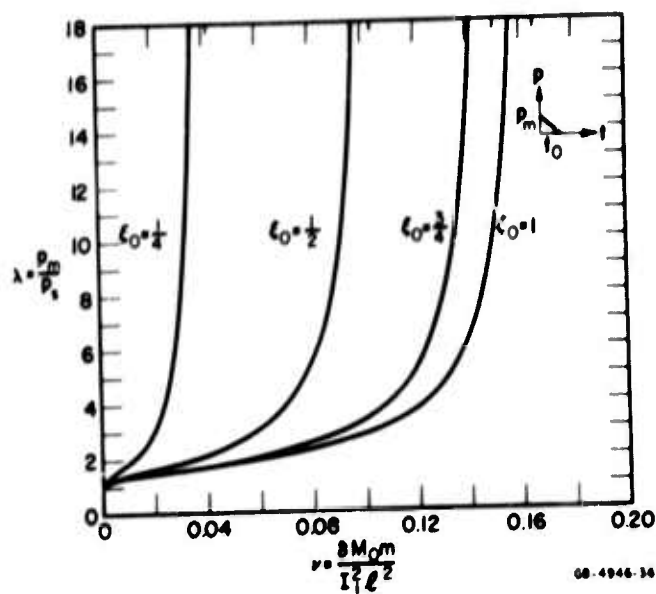
FIG. 3.3(b) PRESSURE RATIO vs. MIDSPAN DEFORMATIONS: TRIANGULAR PULSE
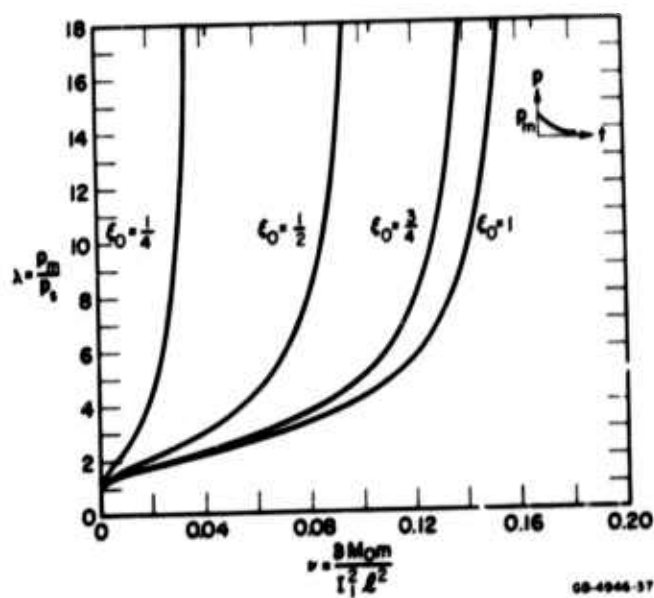
FIG. 3.3(c) PRESSURE RATIO vs. MIDSPAN DEFORMATIONS: EXPONENTIAL PULSE
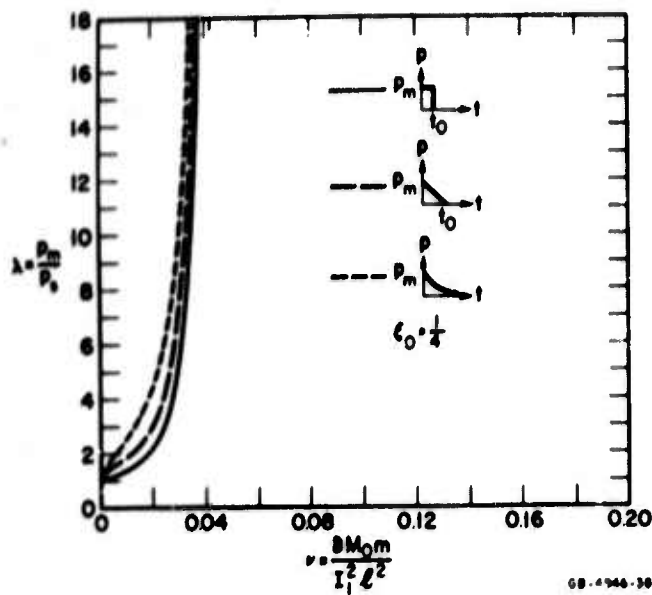
FIG. 3.4(a) COMPARISON OF PRESSURE RATIO vs. MIDSPAN DEFORMATIONS
FOR RECTANGULAR, TRIANGULAR, AND EXPONENTIAL PULSES
Loading length ratio: one quarter
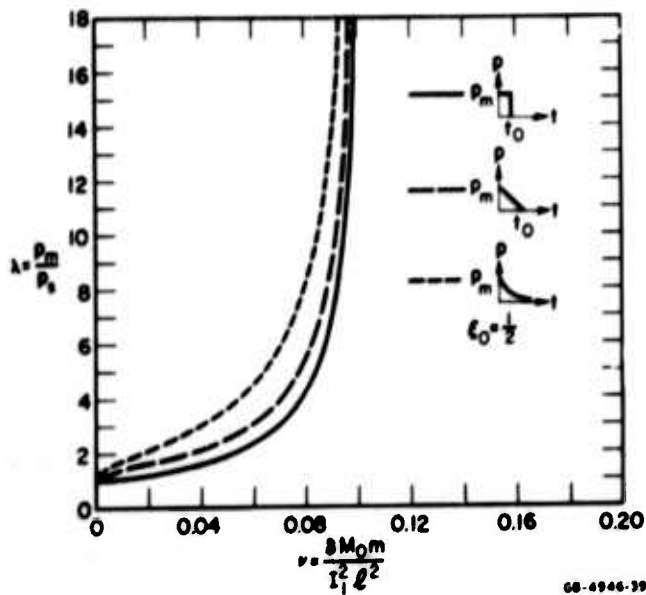
FIG. 3.4(b) COMPARISON OF PRESSURE RATIO vs. MIDSPAN DEFORMATIONS
FOR RECTANGULAR, TRIANGULAR, AND EXPONENTIAL PULSES
Loading length ratio: one half
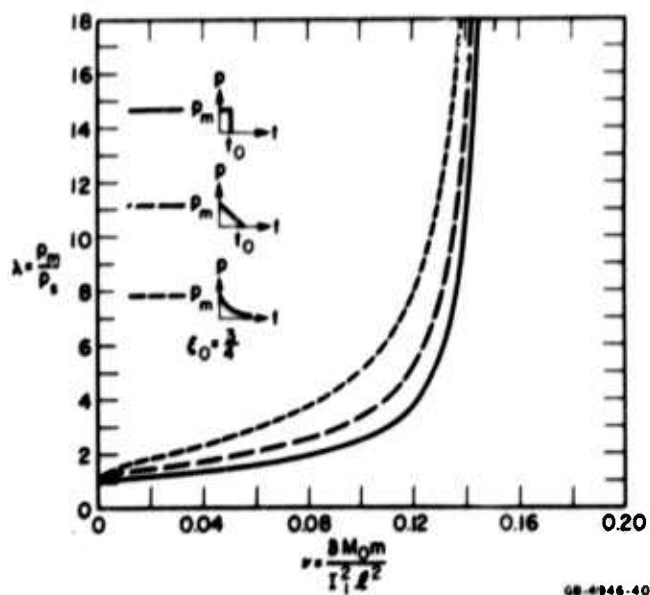
FIG. 3.4(c) COMPARISON FOR PRESSURE RATIO vs. MIDSPAN DEFORMATIONS
FOR RECTANGULAR, TRIANGULAR, AND EXPONENTIAL PULSES
Loading length ratio: three quarters
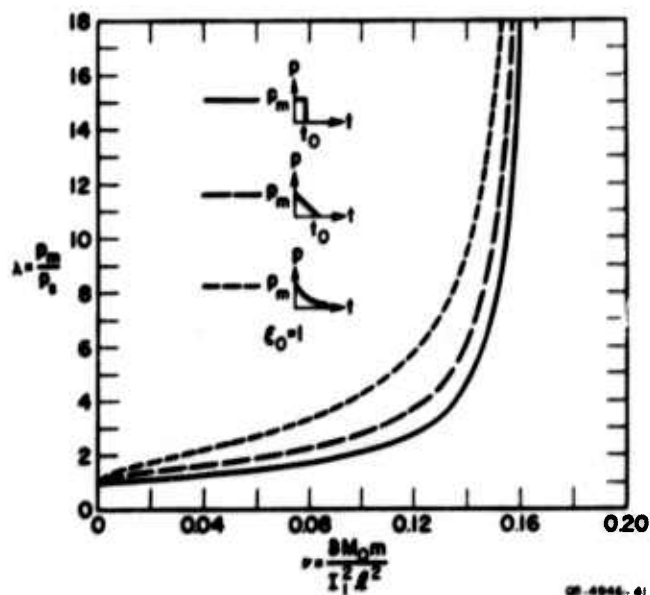
FIG. 3.4(d) COMPARISON FOR PRESSURE RATIO vs. MIDSPAN DEFORMATIONS
FOR RECTANGULAR, TRIANGULAR, AND EXPONENTIAL PULSES
Loading length ratio: total span

51
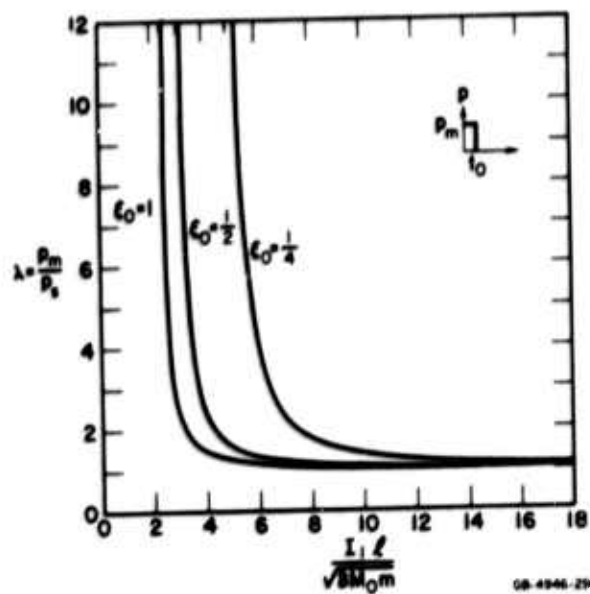
FIG. 3.5(a)   PRESSURE RATIO vs. IMPULSE: RECTANGULAR PULSE
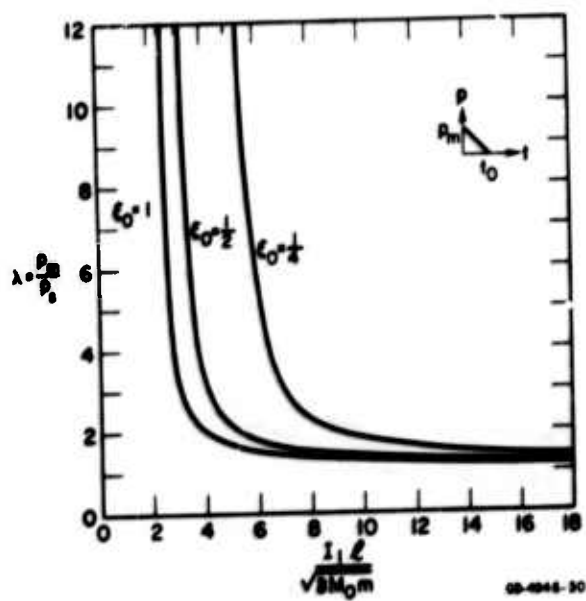
FIG. 3.5(b)   PRESSURE RATIO vs. IMPULSE: TRIANGULAR PULSE

52
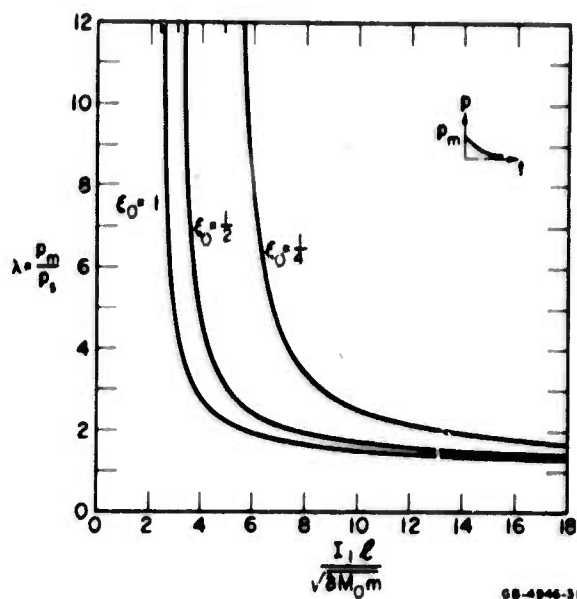
FIG. 3.5(c)   PRESSURE RATIO vs. IMPULSE: EXPONENTIAL PULSE
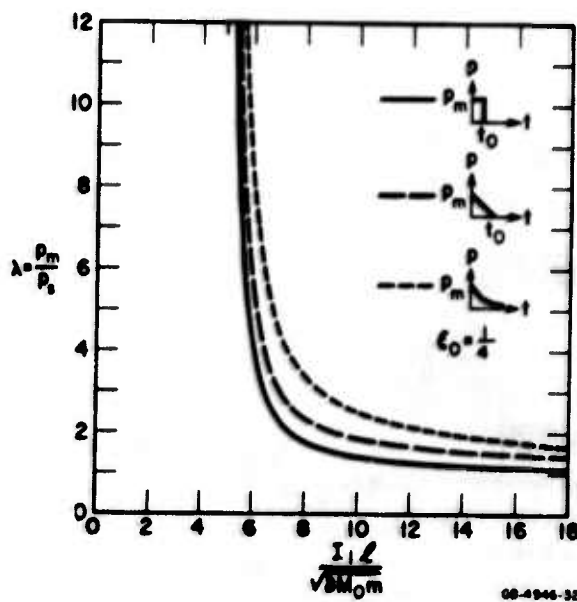
FIG. 3.6(a)   PRESSURE RATIO vs. IMPULSE: ALL PULSES $\xi_0 = \frac{1}{4}$

53
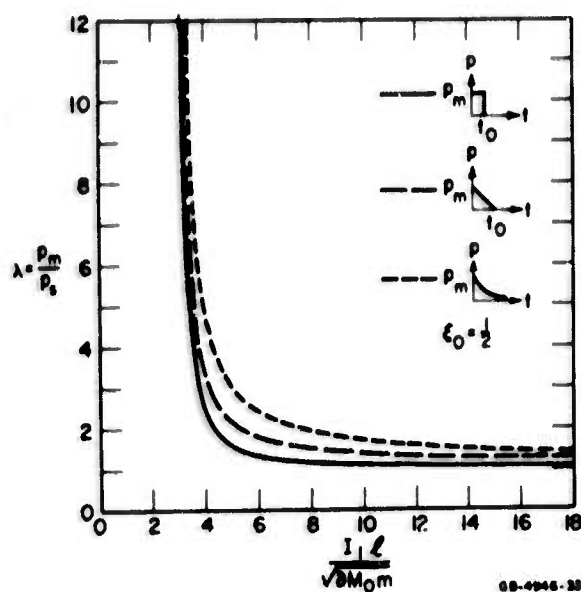
FIG. 3.6(b)   PRESSURE RATIO vs. IMPULSE: ALL PULSES $\xi_0 - \frac{1}{2}$
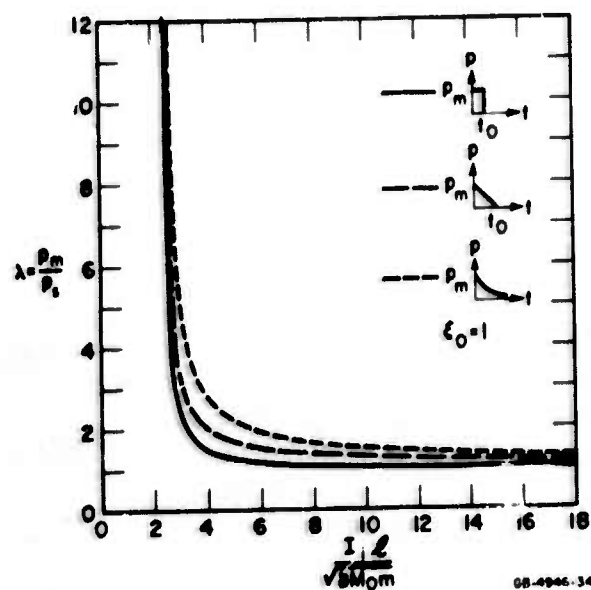
FIG. 3.6(c)   PRESSURE RATIO vs. IMPULSE: ALL PULSES $\xi_0 - 1$

54
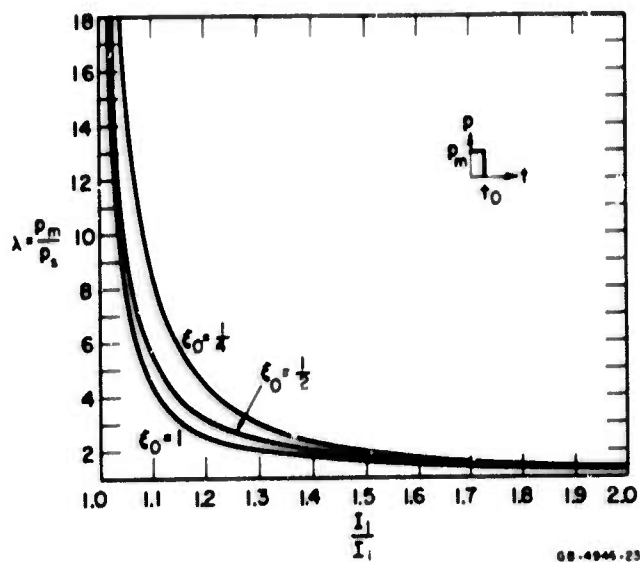
FIG. 3.7(a)   PRESSURE-IMPULSE DIAGRAM: RECTANGULAR PULSE
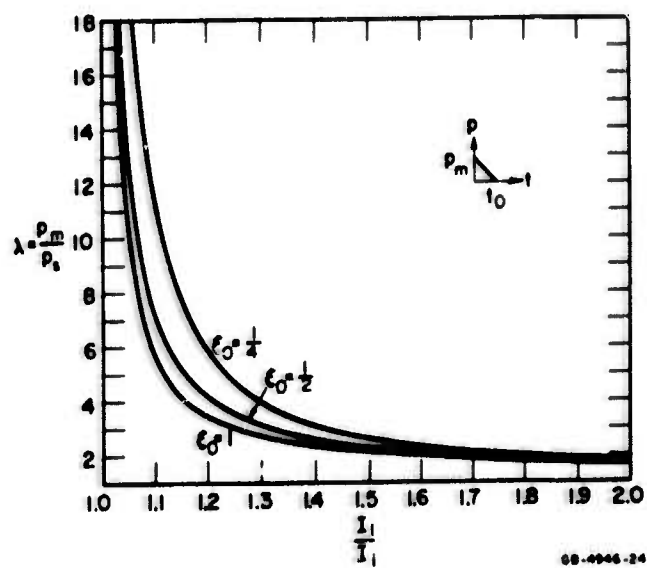
FIG. 3.7(b)   PRESSURE-IMPULSE DIAGRAM: TRIANGULAR PULSE

55
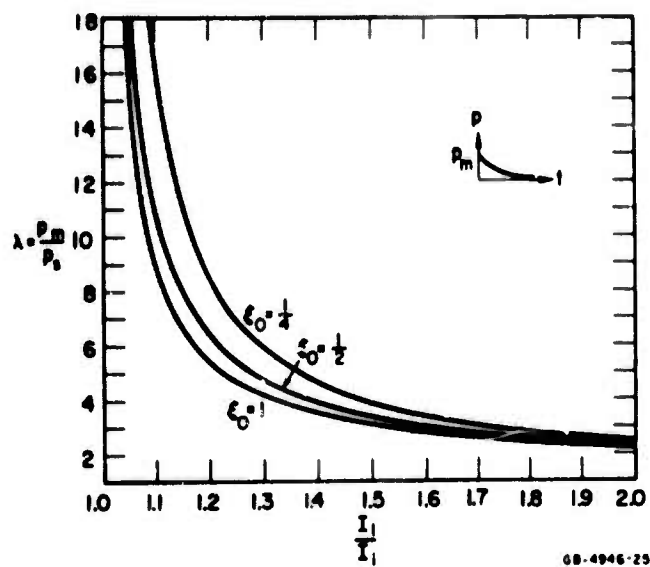
FIG. 3.7(c) PRESSURE-IMPULSE DIAGRAM: EXPONENTIAL PULSE
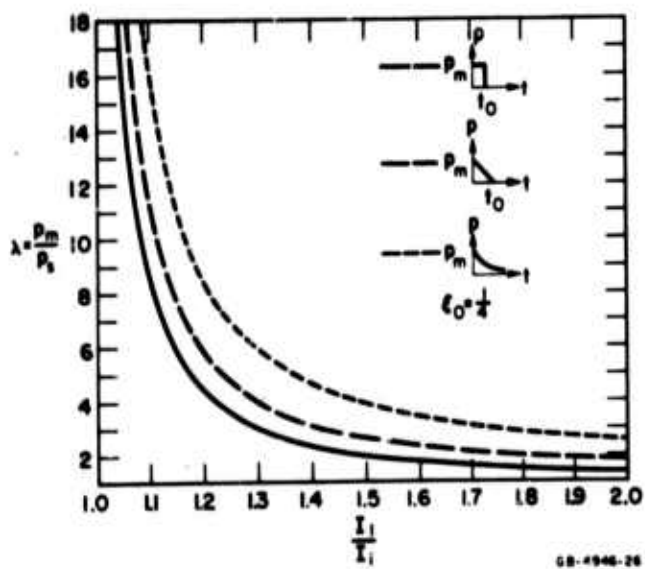
FIG. 3.8(a) PRESSURE-IMPULSE DIAGRAM: ALL PULSES $\xi_0 = \frac{1}{4}$
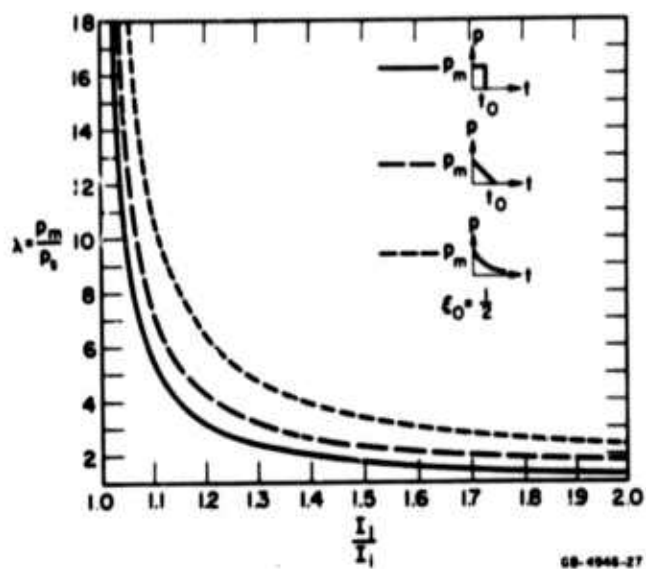
FIG. 3.8(b)   PRESSURE–IMPULSE DIAGRAM: ALL PULSES $\xi_0 = \tfrac{1}{2}$
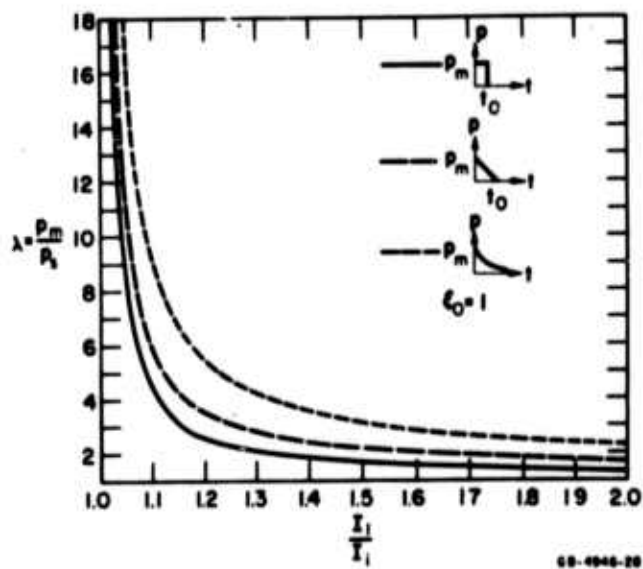
FIG. 3.8(c)   PRESSURE–IMPULSE DIAGRAM: ALL PULSES $\xi_0 = 1$
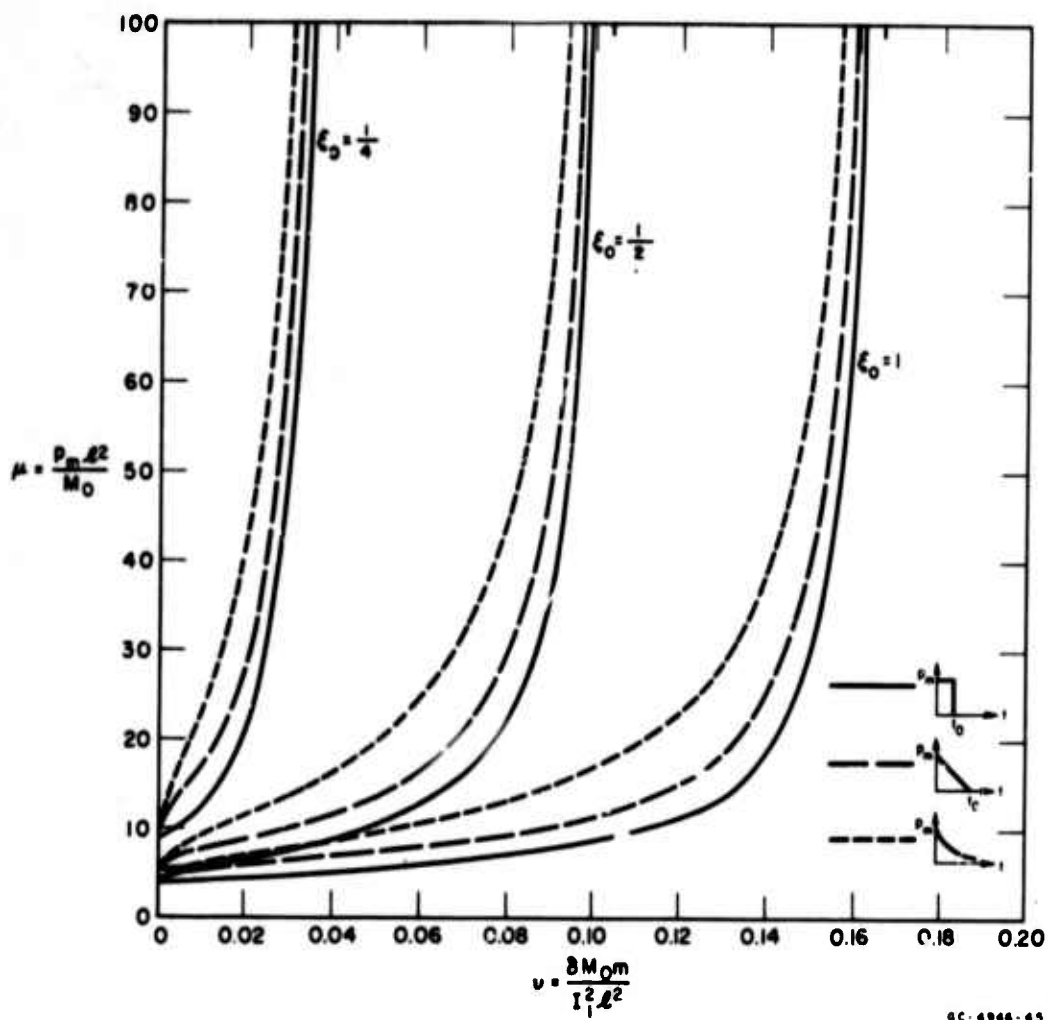
FIG. 3.9 PRESSURE vs. DEFLECTION: ALL PULSES $\xi_0 = \frac{1}{4}, \frac{1}{2}$, AND, 1

58
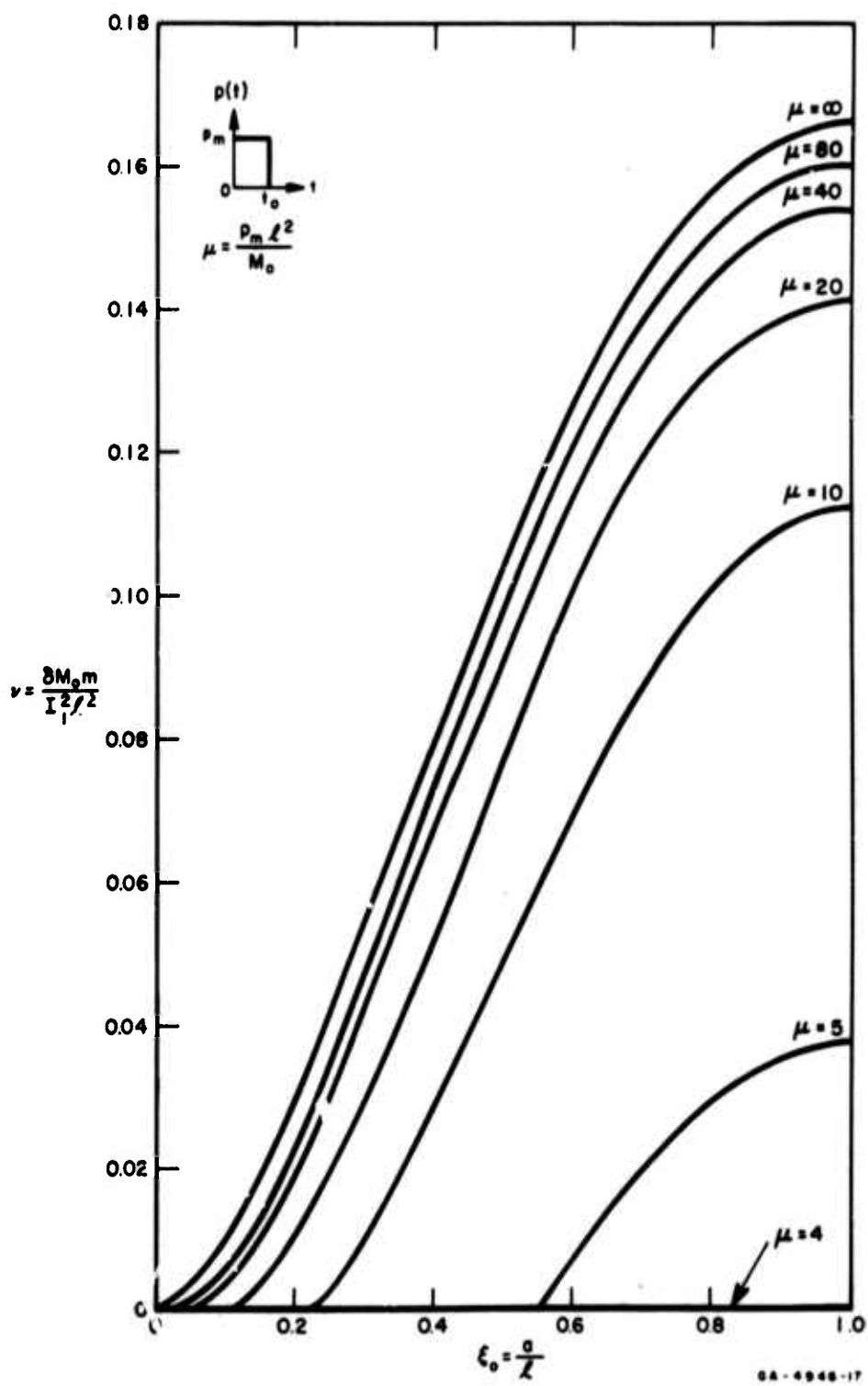
FIG. 3.10(a) DEFLECTION, LOADED LENGTH, PRESSURE RELATIONSHIP:
RECTANGULAR PULSE

59
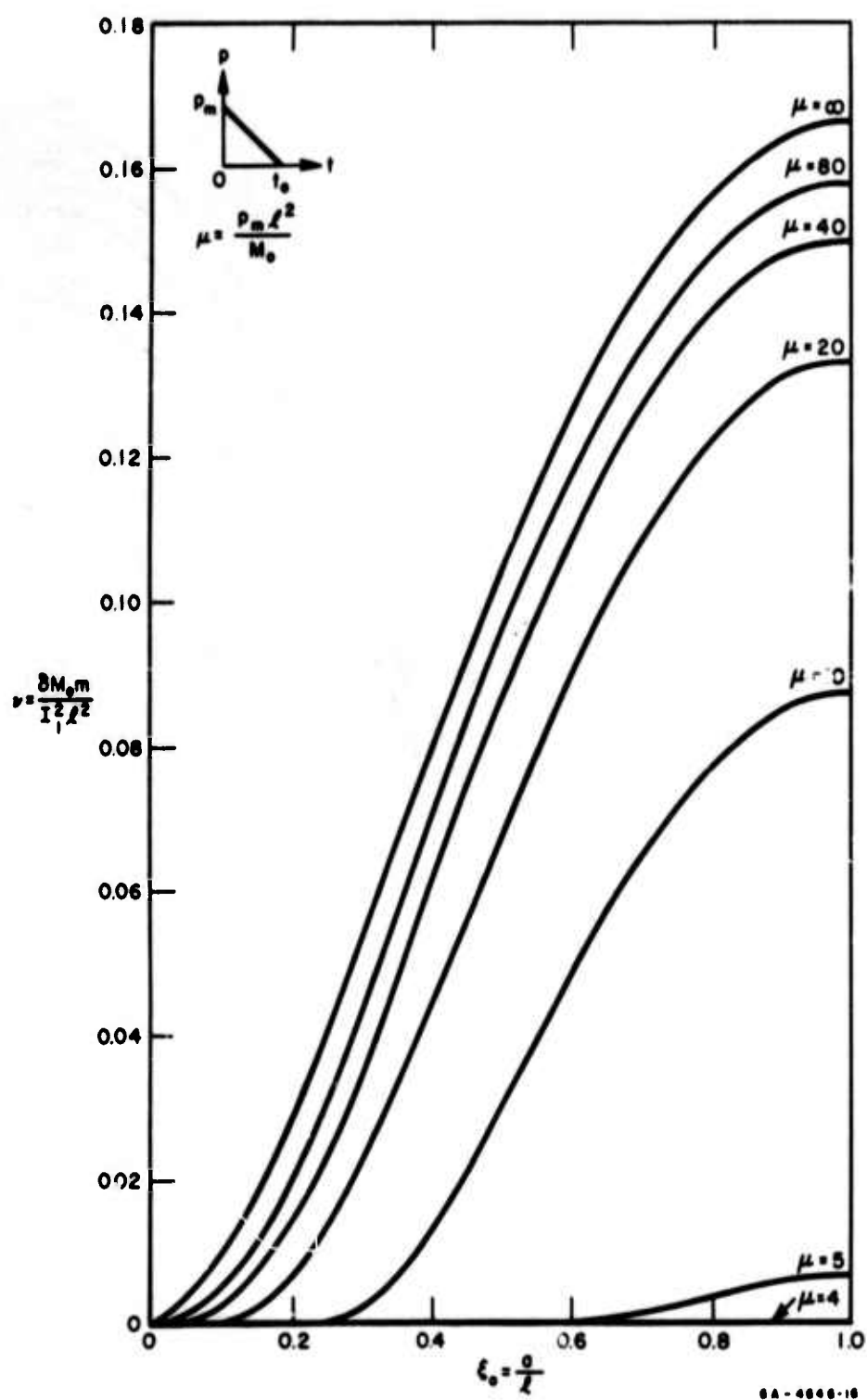
FIG. 3.10(b) DEFLECTION, LOADED LENGTH, PRESSURE RELATIONSHIP:
TRIANGULAR PULSE

60
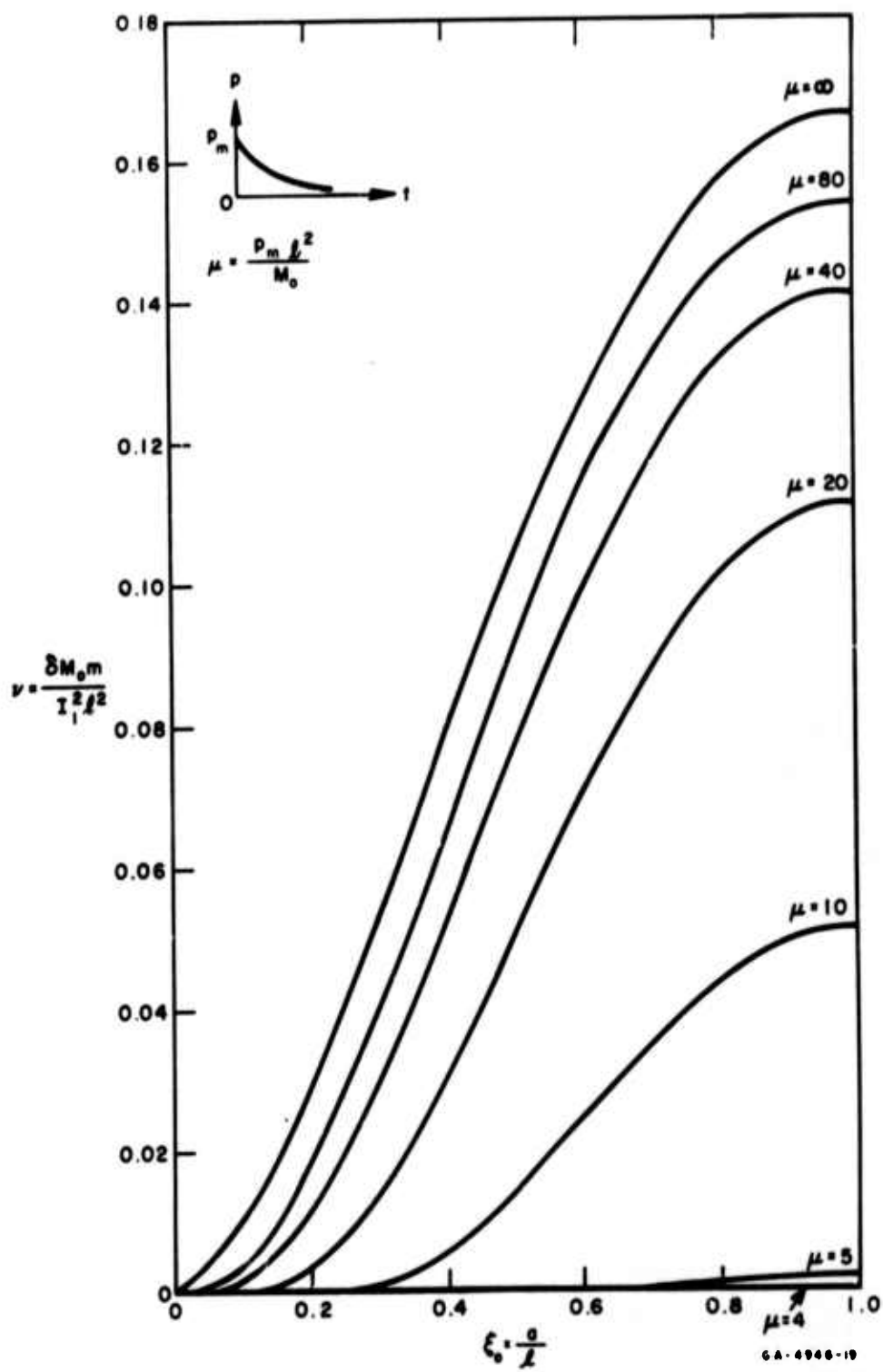
FIG. 3.10(c) DEFLECTION, LOADED LENGTH, PRESSURE RELATIONSHIP:
EXPONENTIAL PULSE

61
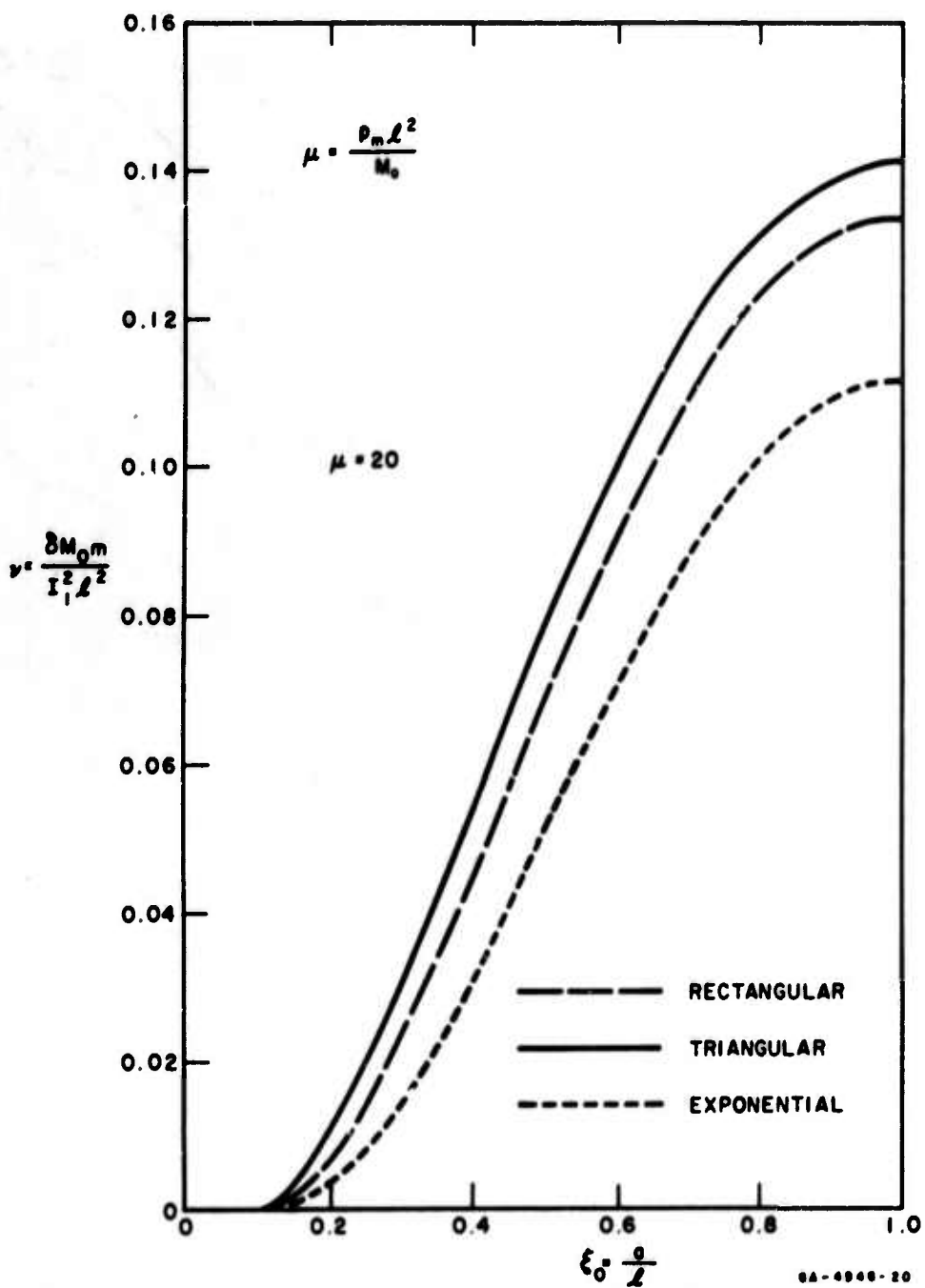
FIG. 3.11 DEFLECTION, LOADED LENGTH, PRESSURE RELATIONSHIP:
ALL PULSES $\mu = 20$

62

NOMENCLATURE

a	load half length
I	impulse at time $t < t_o$
I_1	total impulse
I_i	ideal impulse
ℓ	half span
m	mass per unit length
M	bending moment
M_o	fully plastic moment
p	pressure
P_m	peak pressure of pulse
P_g	static collapse pressure
s	P_m/I_1
t	time
t_o	I_1/P_m, pulse duration
t_1, t_2	phase change times
x	distance coordinate
x_o, x_1	positions of plastic hinges
y	deflection
y_o	central deflection
δ	final central deflection
δ_i	final central deflection due to I_i
λ	P_m/P_s
λ_1, λ_2	mechanism bounds on λ
μ	$P_m \ell^2/M_o$
ν	$\delta M_o m/I_1^2 \ell^2$
ξ	x/ℓ
ξ_o	a/ℓ
τ	time variable
ω	angular velocity

This page intentionally left blank.

SECTION IV

SIMPLY SUPPORTED RIGID-PLASTIC PLATES
UNDER BLAST LOADING

1.   Introduction

A simply supported circular plate of rigid-plastic material
subjected to a blast load of low peak pressure acting on a central
circular area is analyzed in this section (Fig. 4.1). The pressure
is assumed to rise instantaneously to its peak pressure p_m and there-
after to decay monotonically. Only one deformation mechanism is
investigated, namely, that corresponding to static collapse. Conse-
quently, only the response of the plate to low peak pressures is
presented below.

Yielding is assumed to occur in bending according to the Tresca
yield condition and the associated flow rule (Fig. 4.2) [4.1], membrane
action being neglected. In Fig. 4.2, M_r and M_θ are the radial and
circumferential components of bending moment. $\dot{x}_r$ and $\dot{x}_\theta$ are the
corresponding components of rate of curvature. Positive bending
moments and shear force Q are shown in Fig. 4.3.
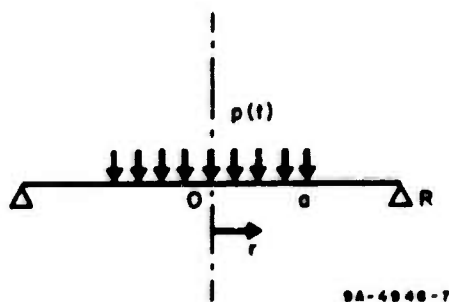
FIG. 4.1 CIRCULAR PLATE
          PROBLEM
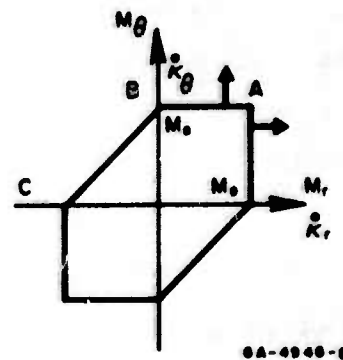
FIG. 4.2 TRESCA YIELD
          HEXAGON
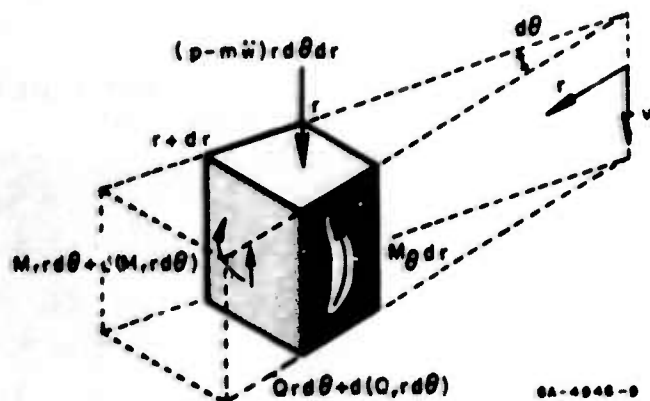
FIG. 4.3 PLATE ELEMENT

2.   Deformation Under Low Peak Pressures

The deformation mechanism is assumed that of static collapse, namely,

$$w(r, t) = W(t)(1-r/R) \qquad (4.1)$$

where R is the plate radius. Deflection formula (4.1) describes a deformation in which, at any instant, the plate is a shallow cone. According to (4.1) the rates of curvature are

$$\dot{\kappa}_r = -\ddot{w}_{rr} = 0 \qquad \text{and} \qquad \dot{\kappa}_\theta = -\dot{w}_r/r = \dot{W}/Rr \qquad (4.2)$$

The flow rule as described by Fig. 4.2 and results (4.2) dictate that the plate is in the plastic regime AB. In fact, at the plate center $M_\theta = M_r = M_o$ which corresponds to the regime A; at the support $M_r = 0$ which corresponds to regime B. Thus the bending moments corresponding to Eq. (4.2) are

$$M_\theta = M_o \quad \text{and} \quad 0 \le M_r \le M_o \qquad (4.3)$$

where M_o is the fully plastic moment per unit length of cross section.

With the aid of Fig. 4.1 the equation of motion can be derived in the form

$$M_o - \frac{\partial}{\partial r}(rM_r) = \int_o^r (p - mw)r \, dr \qquad (4.4)$$

where m is the mass per unit area of plate.

66

Integrating Eq. (4.4) using formulas (4.1) and (4.3) yields

$$\ddot{W} = 12 M_o (\lambda - 1)/mR^2 \qquad (4.5)$$

In Eq. (4.5), $\lambda = p/p_s$ where p_s is the pressure required to cause static collapse and is [4.2]

$$p_s = 6 M_o / R^2 \alpha^2 (3 - 2\alpha) \qquad (4.6)$$

α being the ratio a/R.

Now Eq. (4.5) is analogous to Eq. (3.3) for the clamped beam subjected to low pressures. Thus, Section III-2(1) can be taken over to complete the discussion on the simply supported plate.

By successive integrations of (4.5), the velocity and displacement of the plate center are

$$\dot{W} = 12 M_o (I - I_s)/p_s mR^2 \qquad (4.7)$$

$$W = 12 M_o (A - A_s)/p_s mR^2 \qquad (4.8)$$

where

$$I(t) = \int_0^t p(\tau)d\tau \quad , \quad I_s(t) = p_s t$$

$$A = \int_0^t I(\tau)d\tau \quad , \quad A_s = p_s t^2/2$$

Motion ceases when $W(t) = 0$, at time $t = t_f$, say. Then from (4.7) t_f is determined by $I(t_f) = p_s t_f$. Consequently the maximum deflection is $W(t_f)$, found by substituting $t = t_f$ in (4.8).

For each α, the peak load (represented nondimensionally as $\lambda_m = p_m/p_s$) has an upper bound λ_1 such that when it is exceeded, the mechanism (4.1) does not apply because the yield condition is violated. Determining λ_1 so that (4.3) is satisfied leads to the following range for λ_m corresponding to mechanism (4.1)

$$1 \leq \lambda_m \leq \lambda_1 = 2\alpha^2(3-2\alpha)/[2\alpha^2(3-2\alpha)-1] \qquad 1/2 \leq \alpha \leq 1$$

$$\qquad\qquad\qquad\qquad\qquad\qquad\qquad\qquad\qquad\qquad\qquad (4.9)$$

$$1 \leq \lambda_m \leq \lambda_1 = (3-2\alpha)/(3-4\alpha) \qquad\qquad 0 \leq \alpha \leq 1/2$$

The curves (4.9) are plotted in Fig. 4.4.
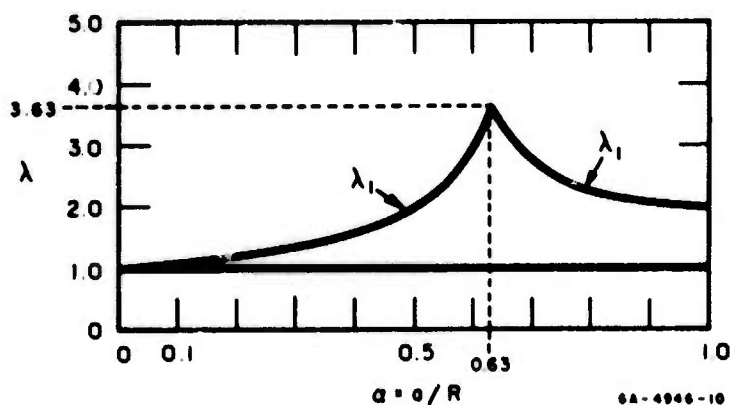
FIG. 4.4 DEFORMATION MECHANISM DIAGRAM

For peak pressures of blast pulses such that the value of λ lies in the range $1 < \lambda \leq \lambda_1$ the permanent central deflection is given by

$$W_f = 12M_o(A_f-A_s)/p_s mR^2 \qquad\qquad (4.10)$$

where $W_f = W(t_f)$, $A_f = A(t_f)$, and $t_f = I(t_f)/p_s = I_f/p_s$. This result is exactly analogous to entire deformation by mechanism 1 for clamped beams (Section III).

68

NOMENCLATURE

a	radius of loading
A	$\int_{0}^{t} I(\tau)d\tau$
A_f	$A(t_f)$
A_s	$p_s t^2/2$
I	impulse
I_f	$I(t_f)$
I_s	$p_s t$
m	mass per unit area
M_r , M_θ	components of moment
M_o	fully plastic moment
p	pressure
P_m	peak pressure
P_s	static collapse pressure
r	radial component
R	radius of plate
t	time
t_f	time when motion ceases
w	deflection
W	central deflection
W_f	final central deflection
α	a/R
θ	circumferential coordinate
$\varkappa_r$, $\varkappa_\theta$	components of curvature
λ	p/P_s
λ_1	an upper bound of λ
λ_m	P_m/P_s

This page intentionally left blank.

SECTION V

CLAMPED RIGID-PLASTIC PLATES UNDER BLAST LOADING

A theoretical study is made of clamped circular plates of rigid-plastic material subjected to blast loading uniformly distributed over the surface. The dependence of the permanent central deflection on pressure and impulse is obtained when the blast pulse is taken as a rectangular pulse. Experiments are described and the permanent central deflections obtained are correlated with the theoretical predictions.

1. Introduction

The problem treated is the response of a clamped circular plate subjected to a suddenly applied pressure uniformly distributed over the whole of one side of the plate. The pressure is assumed high enough or held on the plate long enough to produce moderately large plastic deformations. Although the governing equations are derived for a general pressure-time relationship they are solved for the simplest case; that of a pressure which is held constant for a time and then suddenly released (a rectangular pulse). It is the variation of the permanent central deflection with pressure and impulse (area under pressure-time curve) that constitutes the principal result of interest. To simplify the analysis the plate material is assumed to be rigid-perfectly plastic in behavior obeying the Tresca yield condition and the associated flow rule. Only the bending action of the plate is taken into account.

The response of a clamped circular rigid-plastic plate to a uniformly distributed ideal impulse was found by Wang and Hopkins [5.1]. Their method of solution, established continuity and jump conditions, and nomenclature are employed here. Wang [5.2] obtained the response to an ideal impulse for simply supported plates. Hopkins and Prager. [5.3] solved the problem similar to one presented here but for simply supported plates and their results are used later to assess the effect of the boundary conditions.

71

2. Mechanisms of Deformation

A blast pulse may be idealized to that shown in Fig. 5.1 with an instantaneous rise to the peak pressure p_m followed by a continuous monotonic decay. This property will be used later. If the peak pressure is only slightly greater than the static collapse pressure p_s it is reasonable to expect the dynamic mode of collapse to be similar because the inertia forces are still small. In [5.4] it is shown that the static collapse pressure is

$$p_s = 6M_o / r_s^2 \tag{5.1}$$

where M_o is the fully plastic moment per unit length and r_s is a certain radius determined by the equation

$$5 + \ln(R/r_s)^2 = 3(R/r_s)^2 \tag{5.2}$$

where R is the radius of the plate. In fact, the solution of (5.2) is $r_s/R = 0.73$.

Figure 5.2 shows the mechanism of deformation called mechanism 1, corresponding to peak pressures in excess of p_s but below a pressure p_1 to be determined. The radius $r_1(t)$ replaces r_s. At the plate center the plastic regime is A in Fig. 5.3 where $M = N = M_o$, M and N being the radial and circumferential components of bending moment (positive moments causing tension on the underside of the plate).
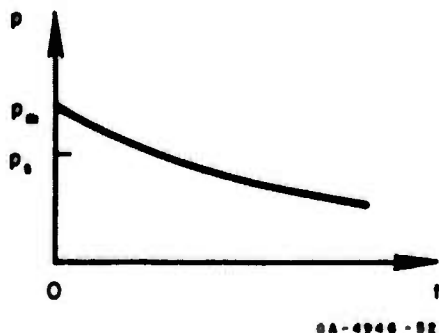
FIG. 5.1 IDEALIZED BLAST PULSE

FIG. 5.2 MECHANISM 1

72
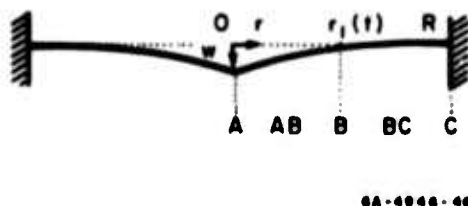
At $r = r_1(t)$ and $r = R$ the regimes are B and C while in the regions $0 \leq r \leq r_1(t)$ and $r_1(t) \leq r \leq R$ they are AB and BC. A velocity field which satisfies the flow rule, boundary conditions and the appropriate continuity and discontinuity conditions [5.1] is

$$w_t = \begin{cases} V(1-\sigma r/r_1) & 0 \leq r \leq r_1(t) \\ V\sigma \ln R/r & r_1(t) \leq r \leq R \end{cases} \tag{5.3}$$

with

$$1/\sigma = \ln R/r_1 + 1 \tag{5.4}$$

In (5.3), w is the plate deflection, V is the velocity of the plate center and the subscript t denotes partial differentiation. The initial condition of the plate at rest may be expressed by $V(0) = 0$.

The upper bound p_1 of the peak pressure p_m is that pressure which causes at the plate center an inflection point in the bending moment diagram for the radial component, that is $\partial^2 M/\partial r^2 = 0$ at $r = 0$. The inequality $p_m < p_1$ prevents violation of the yield condition at the plate center. This suggests that whenever the peak pressure exceeds p_1 a central region $0 \leq r \leq r_0(t) < r_1(t)$ of the plate acquires a uniform velocity. This mechanism, called mechanism 2, is shown in Fig. 5.4 with the plastic regimes indicated and has the following velocity field [5.1]

$$w_t = \begin{cases} V & 0 \leq r \leq r_0(t) \\ V(1-\sigma(r-r_0)/r_1) & r_0(t) \leq r \leq r_1(t) \\ V\sigma \ln(R/r) & r_1(t) \leq r \leq R \end{cases} \tag{5.5}$$
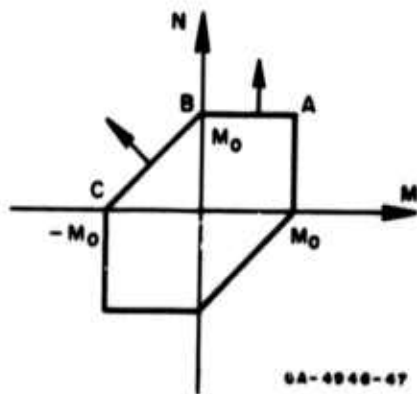
FIG. 5.3 TRESCA YIELD HEXAGON
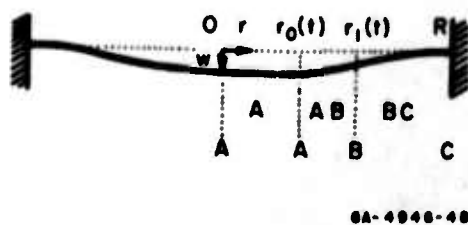
FIG. 5.4 MECHANISM 2

where

$$1/\sigma = \ell nR/r_1 + (1 - r_0/r_1) \tag{5.6}$$

By taking the blast pulse in the form of Fig. 5 1 the value of $r_0(t)$ is a maximum at time $t = 0$ and thereafter decreases to zero. During the remaining time the plate deforms in accordance with mechanism 1.

3. Governing Equations

Independent of mechanisms the equation of motion is

$$N - (rM)_r = \int_0^r (p - mw_{tt})rdr \tag{5.7}$$

A subscript r indicates partial differentiation with respect to r .

(1) Mechanism 2

When the peak pressure is large enough to cause deformation by mechanism 2 ($p_m > p_1$) the acceleration to be substituted in (5.7) is obtained by differentiating (5.5) with respect to time. The circumferential component of the bending moment N is eliminated by using the yield condition (Fig. 5.3). Due to the three properties $M = N = 0$ in $0 \le r \le r_0$, $M(r_1, t) = 0$, and $M(R, t) = - M_0$, carrying out the integration in (5.7) provides the following three equations.

$$V' = \lambda e^{2\xi}/2 \tag{5.8}$$

$$V'(\xi+\eta)\eta[2\xi(3-3\eta+\eta^2) + \eta(6-8\eta+3\eta^2)] - V\xi'\eta^2[\xi(6-8\eta+3\eta^2)+\eta(1-\eta)(4-3\eta)]$$
$$-V\eta'\eta^2[2\xi(3-2\eta)+\eta(4-3\eta)] = [\lambda e^{2(\xi_s-\xi)}\eta(3-3\eta+\eta^2) - 1]e^{2\xi}(\xi+\eta)^2 \tag{5.9}$$

$$V'(\xi+\eta)[3e^{2\xi}-3 - 2\xi(3-3\eta+3\eta^2-\eta^3)] -V\xi'[3e^{2\xi}-3 - 2\xi\{3-\eta^2(1-\eta)(3-2\eta)\}$$
$$- 2\xi^2(3-6\eta+6\eta^2-2\eta^3)]-V\eta'[3e^{2\xi}-3 - 2\xi(3-3\eta^2+2\eta^3) - 6\xi^2(1-\eta)^2]$$
$$= [3\lambda e^{2(\xi_s-\xi)}(e^{2\xi}-1)/2 - (1+\xi)]e^{2\xi}(\xi+\eta)^2 \tag{5.10}$$

74

The new variables that have been introduced in the derivation of (5.8), (5.9) and (5.10) are defined by [5.1]

$$\xi = \ell n(1/\rho_1) \qquad \eta = 1 - \rho_0/\rho_1 \qquad \rho_1 = r_1/R$$

$$\rho_0 = r_0/R \qquad \lambda = p/p_s \qquad \xi_s = \ell n(1/\rho_s) \qquad \rho_s = r_s/R$$

Also, the primes indicate differentiation with respect to the variable τ' where

$$\tau' = 12M_0 t/mR^2$$

The value of r_s, and hence ρ_s and ξ_s, is the solution of Eq. (5.2) while the static collapse pressure p_s is given by (5.1).

(2)   Mechanism 1

When the value of $\lambda = p/p_s$ falls in the range $1 \leq \lambda \leq \lambda_1$ where $\lambda_1 = p_1/p_s$ deformation occurs by means of mechanism 1. The governing equations can be found by substituting in (5.7) the accelerations found by differentiating (5.3) with respect to time and carrying out the integration noting that $M(r_1, t) = 0$ and $M(R, t) = - M_0$. Alternatively, they can be found by setting $\eta = 1(\rho_0 = 0)$ and $\eta' = 0$ in Eqs. (5.9) and (5.10). Performing either of these operations yields

$$V'(\xi + 1)(2\xi + 1) - V\xi'\xi = [\lambda e^{2(\xi_s - \xi)} - 1]e^{2\xi}(\xi+1)^2 \qquad (5.11)$$

$$V'(\xi+1)(3e^{2\xi}-3-4\xi) - V\xi'(3e^{2\xi}-3-6\xi-2\xi^2) = [3\lambda e^{2(\xi_s - \xi)}(e^{2\xi}-1)/2$$
$$- (1+\xi)]e^{2\xi}(\xi+1)^2$$

$$(5.12)$$

Whenever $V' = \lambda e^{2\xi_s}/2$ an inflection point in the bending moment diagram for M occurs at the plate center which, for pulses of the type shown in Fig. 5.1, occurs immediately. This condition gives λ_1 where $\lambda_1 = p_m/p_s$.

4. Solution for Rectangular Pulse

(1) Mechanism 2 $\quad \lambda_1 < \lambda$

Specializing to a rectangular pulse a solution of Eqs. (5.8), (5.9) and (5.10) is obtained if it is assumed that ξ and η are constants while the load is acting. This means that while p is constant, r_o and r_1 are constants. This phase of motion will be called phase 1a. Setting $\xi' = \eta' = 0$ in (5.9) and (5.10), and substituting V' from (5.8) in (5.9) and (5.10) gives

$$2(\xi + \eta) = \lambda e^{2(\xi_s - \xi)} \eta^3 (2-\eta) \tag{5.13}$$

$$2(\xi + \eta)(1 + \xi) = \lambda e^{2(\xi_s - \xi)} [3e^{2\xi}(\xi - 1 + \eta) + \xi(3 - 6\eta + 6\eta^2 - 2\eta^3) + 3(1-\eta)] \tag{5.14}$$

The lower bound λ_1 of λ may be found by substituting $\eta = 1(\rho_0 = 0)$ in (5.13) and (5.14). Doing this gives

$$\lambda_1 e^{2\xi_s} = 2(\xi + 1)e^{2\xi} \tag{5.15}$$

where ξ is determined by the equation

$$3\xi e^{2\xi} = 1 \tag{5.16}$$

From (5.15) and (5.16), $\lambda_1 = 1.998$ and $\xi = 0.2163$ ($\rho_1 = 0.805$).

For a given value of λ such that $\lambda > \lambda_1$ Eqs. (5.13) and (5.14) give the initial values of ξ and η. Some numerical values are shown in Table 5.1.

Let the pulse end at time $t = t_o$ or when $\tau' = \tau_o'$. If the velocity of the plate center at this time be denoted by V_o, integration of Eq. (5.8) gives

$$V_o = 1/2 \, \lambda e^{2\xi_s} \tau_o' = I/m$$

where $I = pt_o$ is the impulse.

76

Table 5.1

INITIAL VALUES OF ξ AND η

Mechanism	λ	$\xi(0)$	$\eta(0)$	$\rho_1(0)$	$\rho_o(0)$
1	1.1	.302	1.0	.739	0
	1.2	.290	1.0	.748	0
	1.3	.279	1.0	.756	0
	1.4	.268	1.0	.764	0
	1.6	.248	1.0	.780	0
	1.8	.232	1.0	.793	0
	1.9	.224	1.0	.800	0
	1.998*	.2163	1.0	.805	0
2	2.0	.216	.998	.806	.001
	2.24	.2	.883	.819	.096
	3.80	.14	.569	.869	.375
	6.51	.10	.395	.905	.547
	9.48	.08	.313	.923	.634
	15.71	.06	.233	.942	.722
	32.53	.04	.156	.961	.811
	56.13	.03	.116	.970	.858

*Value of λ_1 .

Now $V = pt/m$, so by integration, the central deflection δ_o of the plate at time $t = t_o$ is

$$\delta_o = I^2/2mp = (I^2 R^2/12mM_o)/\lambda e^{2\xi_s} \qquad (5.17)$$

When $t > t_o$, no pressure acts on the plate so that $\lambda = 0$ and hence from Eq. (5.8) $V' = 0$. This means that the central region of the plate, $0 \le r \le r_o(t)$ moves at a constant velocity. It is evident from (5.9) and (5.10) that ξ and η can no longer be treated as constants. Introducing a dimensionless time $\tau = 12M_o(t-t_o)/mR^2 V_o = 12M_o(t-t_o)/IR^2$

Eqs. (5.9) and (5.10) become

$$\varsigma'[\varsigma(6-8\eta+3\eta^2)+\eta(1-\eta)(4-3\eta)] + \eta'[2\varsigma(3-2\eta)+\eta(4-3\eta)] = e^{2\varsigma}(\varsigma+\eta)^2/\eta^2 \tag{5.18}$$

$$\varsigma'[3e^{2\varsigma}-3-2\varsigma\left\{3-2\eta^2(1-\eta)(3-2\eta)\right\} -2\varsigma^2(3-6\eta+6\eta^2-2\eta^3)]$$
$$+ \eta'[3e^{2\varsigma}-3-2\varsigma(3-3\eta^2+2\eta^3) - 6\varsigma^2(1-\eta)^2] = e^{2\varsigma}(\varsigma+\eta)^2(\varsigma+1) \tag{5.19}$$

where now the primes denote differentiation with respect to τ. In (5.8), (5.9) and (5.10) derivatives are with respect to $\tau'(d\tau' = V_o d\tau)$. This phase of the motion described by Eqs. (5.18) and (5.19), called here phase 1b, is analogous to the first phase of motion in the impulse problem [5.1], except that the initial values of ς and η are $\varsigma^{(0)}$ and $\eta^{(0)}$ from Eqs. (5.13) and (5.14) instead of $\varsigma = 1$ and $\eta = 0$. Phase 1b ends when $\eta = 1(\rho_o = 0)$.

An outline of the method used to solve Eqs. (5.18) and (5.19), which is essentially the same as that used in [5.1], follows immediately. From (5.18) and (5.19)

$$d\varsigma/d\eta = -P(\varsigma,\eta)/Q(\varsigma,\eta)$$

where

$$P(\varsigma,\eta) = 3(1+2\varsigma+2\varsigma^2-e^{2\varsigma})+\eta[\eta^2(4-3\eta)(\varsigma+1) - 4\varsigma^2(\eta^2-3\eta+3)]$$

$$Q(\varsigma,\eta) = 3(1+2\varsigma+2\varsigma^2-e^{2\varsigma})+\eta[\eta^2(4-3\eta)(1-\eta) + \varsigma\eta^2(6-8\eta+3\eta^2)-3\varsigma^2(4-6\eta+4\eta^2-\eta^3)]$$

Let $d\varsigma/d\eta = -P(\varsigma^{(0)},\eta^{(0)})/Q(\varsigma^{(0)},\eta^{(0)}) = m_o$, where $\varsigma^{(0)}$ and $\eta^{(0)}$ are determined from (5.13) and (5.14) and depend only on λ. Choose a new value of ς, say $\varsigma^{(1)}$ slightly greater than $\varsigma^{(0)}$; this corresponds to the assumption that ρ_1 decreases in phase 1b. Then the new value of η, say $\eta^{(1)}$, is determined by $\eta^{(1)} = \eta^{(0)} + (\varsigma^{(1)} - \varsigma^{(0)})/m_o$. Now find a new value for the ratio $d\varsigma/d\eta$ from $-P(\varsigma^{(1)},\eta^{(1)})/Q(\varsigma^{(1)},\eta^{(1)}) = m_1$. Continue this process until $\eta = 1$, when the plastic hinge circle reaches the center and phase 1b terminates. The remaining deformation occurs

78

in mechanism 1. Figure 5.5 shows the $\xi - \eta$ trajectories obtained by this procedure for eight values of λ . To find the time at the end of phase 1b first find the function $\xi'(\xi,\eta)$ using (5.18) and (5.19). Then the numerical value of $\xi'^{(0)}$ is $\xi'(\xi^{(0)}, \eta^{(0)})$. Now find the time increment from $\tau^{(1)} - \tau^{(0)} = (\xi^{(1)} - \xi^{(0)})/\xi'^{(0)}$. Continue this process along a $\xi - \eta$ trajectory until $\eta = 1$. The sum of the time increments then gives τ_1 corresponding to the duration of phase 1b.
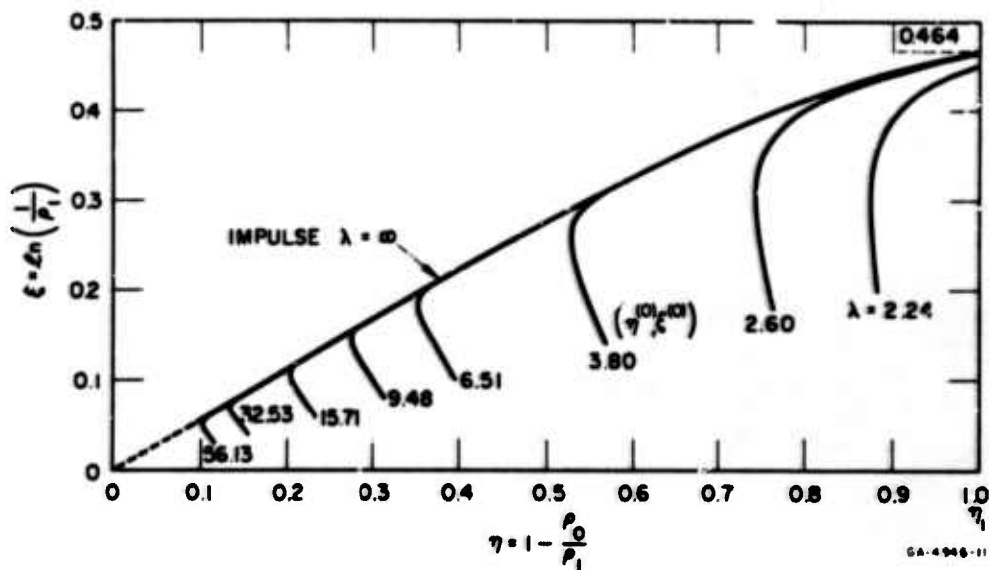
FIG. 5.5 VARIATION OF ξ WITH η DURING PHASE 1b

If δ_1 is the deflection of the plate center at the end of phase 1 it is obtained from the equation

$$\delta_1 - \delta_0 = V_0(t_1 - t_0) = r^2 R^2 \tau_1 / 12 m M_0 \qquad (5.20)$$

in which δ_0 is given by (5.17).

The final phase of the motion, called phase 2, is governed by Eqs. (5.9) and (5.10) with $\eta = 1$, $\eta' = 0$ and $\lambda = 0$. With these special values and retention of the dimensionless time variable τ used

in phase lb Eqs. (5.9) and (5.10) become

$$\zeta'(\xi + 1)(2\xi + 1) - \zeta\xi'\xi = -(\xi + 1)^2 e^{2\xi} \tag{5.21}$$

$$\zeta'(\xi + 1)(3e^{2\xi} - 3 - 4\xi) - \zeta\xi'(3e^{2\xi} - 3 - 6\xi - 2\xi^2) = -(\xi + 1)^2 e^{2\xi} \tag{5.22}$$

where $\zeta = V/V_o$. Equations (5.21) and (5.22) can be derived directly by substituting the velocity field defined by (5.3) and (5.4) in the equation of motion (5.7).

From (5.21) and (5.22)

$$\zeta = \left(\frac{\xi + 1}{\xi_1 + 1}\right) \exp\left[-\int_{\xi_1}^{\xi} \frac{(1 - \xi)d\xi}{4 + 7\xi + 2\xi^2 - 3e^{2\xi}} \right] \tag{5.23}$$

in which ξ_1 is the value of ξ at the end of phase lb.

Motion ceases when $\zeta = 0$ and this occurs when $\xi = \xi_2 \approx 0.478$ which is the solution of the equation

$$4 + 7\xi + 2\xi^2 - 3e^{2\xi} = 0$$

Figure 5.6 shows the variation of ζ with ξ.

Let τ_2 be the value of τ when motion ceases. Then

$$\tau_2 - \tau_1 = \int_{\xi_1}^{\xi_2} \frac{d\xi}{\xi'} = \int_{\xi_1}^{\xi_2} \frac{(3e^{2\xi} - 4\xi^2 - 6\xi - 3)\zeta d\xi}{e^{2\xi}(\xi + 1)(4 + 7\xi + 2\xi^2 - 3e^{2\xi})} \tag{5.24}$$

Finally, let the central deflection when $\tau = \tau_2 (t = t_2)$ be δ_2. Then

$$\delta_2 - \delta_1 = \frac{IR^2}{12M_o} \int_{\tau_1}^{\tau_2} V d\tau = \frac{I^2 R^2}{12mM_o} \int_{\xi_1}^{\xi_2} \frac{(3e^{2\xi} - 4\xi^2 - 6\xi - 3)\zeta^2 d\xi}{e^{2\xi}(\xi + 1)(4 + 7\xi + 2\xi^2 - 3e^{2\xi})} \tag{5.25}$$
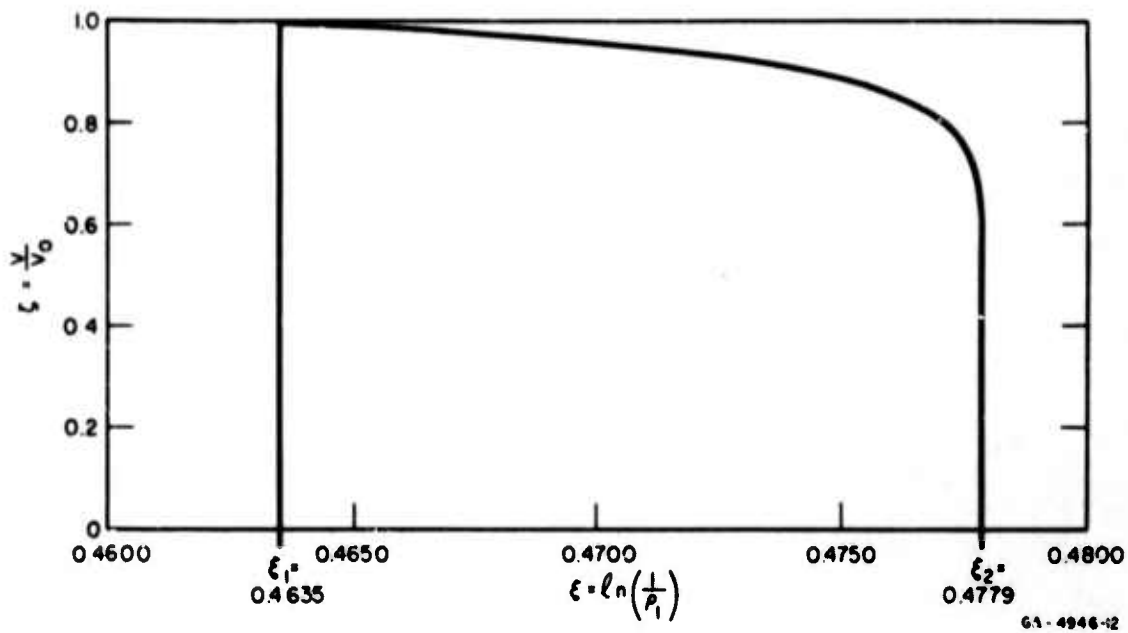
FIG. 5.6 VARIATION OF ζ WITH ξ DURING PHASE 2

Figures 5.7, 5.8 and 5.9 show the variation of ρ_0 and ρ_1 with τ for λ equal to 2.24, 6.51 and 56.13 respectively.
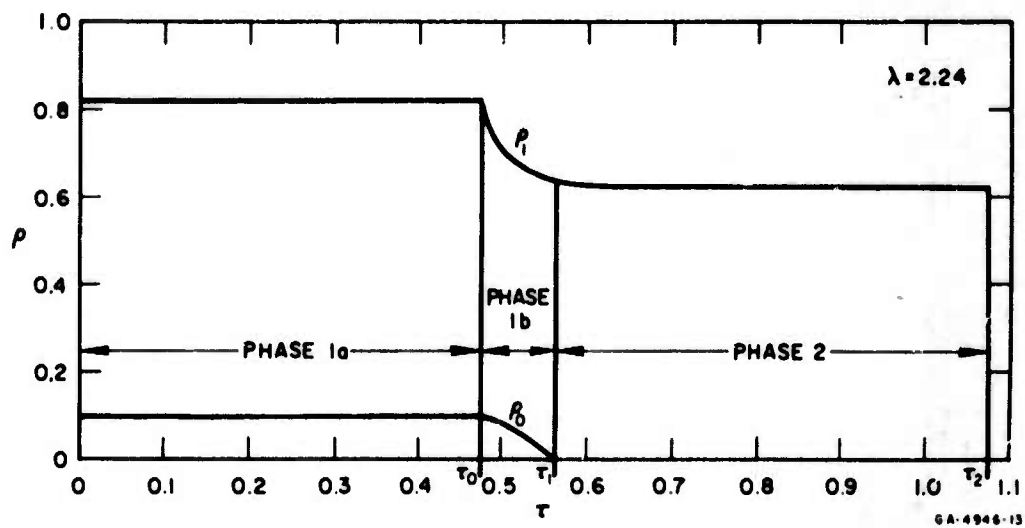
FIG. 5.7 VARIATION OF ρ_0 AND ρ_1 WITH τ. $\lambda = 2.24$

81
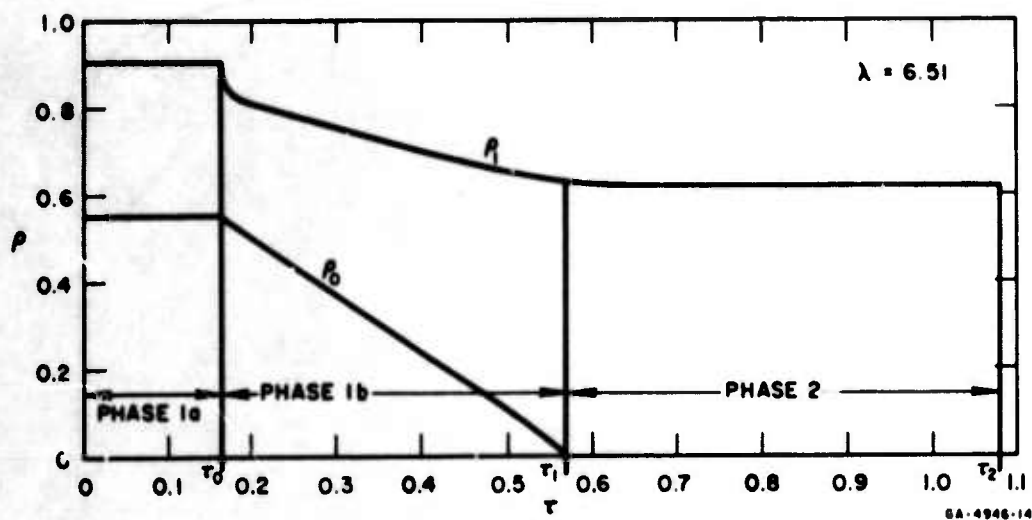
FIG. 5.8 VARIATION OF ρ_0 AND ρ_1 WITH τ. $\lambda = 6.51$

The value of ρ_1 is almost constant during phase 2. As λ increases
the diagrams become progressively stronger in resemblance to that
for an ideal impulse (see Fig. 3 of [5.1]).
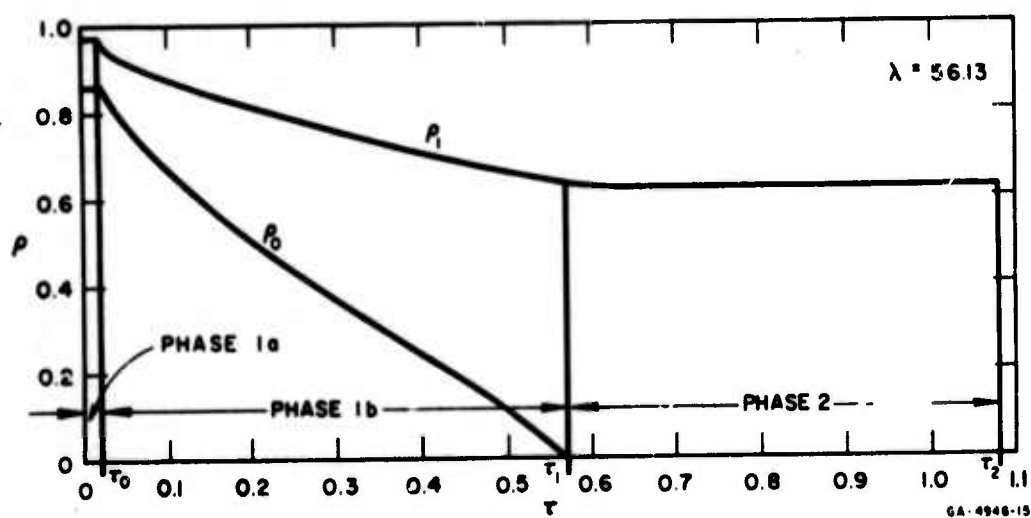
FIG. 5.9 VARIATION OF ρ_0 AND ρ_1 WITH τ. $\lambda = 56.13$

82

(2)   Mechanism 1 $1 < \lambda \leq \lambda_1$

When the constant pressure lies between p_s and p_1 the equations governing the motion during phase 1a can be obtained by substituting in (5.9) and (5.10) the special values $\eta = 1$, $\eta' = 0$ and $\xi' = 0$. These substitutions give

$$V'(2\xi + 1) = [\lambda e^{2(\xi_s - \xi)} - 1]e^{2\xi}(\xi + 1) \tag{5.26}$$

$$V'(3e^{2\xi} - 3 - 4\xi) = [3\lambda e^{2(\xi_s - \xi)}(e^{2\xi} - 1)/2 - (\xi + 1)]e^{2\xi}(\xi + 1) \tag{5.27}$$

where the prime denotes differentiation with respect to τ'. Equations (5.26) and (5.27) also result when the velocity field defined by (5.3) and (5.4) is substituted in the equation of motion (5.7) and use is made of the properties $M(r_1, t) = 0$ and $M(R, t) = -M_o$.

Combining Eqs. (5.26) and (5.27) to eliminate V' provides the following equation which determines ξ once λ is given (by choosing ξ's and finding λ's a $\lambda - \xi$ curve can easily be obtained):

$$[3\lambda e^{2(\xi_s - \xi)}(e^{2\xi} - 1)/2 - (\xi + 1)](2\xi + 1) = [\lambda e^{2(\xi_s - \xi)} - 1](3e^{2\xi} - 3 - 4\xi) \tag{5.28}$$

Knowing ξ from (5.28) the velocity of the center of the plate by integration of (5.26) is

$$V = [\lambda e^{2(\xi_s - \xi)} - 1]e^{2\xi}(\xi + 1)\tau'/(2\xi + 1) \tag{5.29}$$

The central deflection of the plate at time $t = t_o$ is

$$\delta_o = \frac{mR^2}{12M_o} \int_0^{\tau_o'} V(\tau')d\tau' = \frac{I^2R^2}{6mM_o}[1 - \frac{1}{\lambda e^{2(\xi_s - \xi)}}]\frac{(\xi + 1)}{(2\xi + 1)\lambda e^{2\xi_s}} \tag{5.30}$$

83

Phase 2 is essentially the same as the phase 2 described earlier when it followed a phase 1 deformation according to mechanism 2.

From (5.29),

$$V_o = \frac{2I}{m} \left[1 - \frac{1}{\lambda e^{2(\xi_s - \xi)}} \right] \left(\frac{\xi+1}{2\xi+1} \right)$$

Now set $\zeta = V/V_o$ as was done earlier. Then ζ and $\tau_2 - \tau_1$ (where now $\tau_1 = \tau_o = 2/\lambda e^{2\xi_s}$ because there is no phase 1b) are given by (5.23) and (5.24), and in place of (5.25), the central deflection δ_2 when motion ceases is given by

$$\delta_2 - \delta_1 = \frac{I^2 R^2}{3mM_o} \left[1 - \frac{1}{\lambda e^{2(\xi_s - \xi)}} \right]^2 \left(\frac{\xi+1}{2\xi+1} \right)^2 \int_{\xi_1}^{\xi_2} \frac{(3e^{2\xi} - 4\xi^2 - 6\xi - 3)\zeta^2 \, d\xi}{e^{2\xi}(\xi+1)(4+7\xi+2\xi^2-3e^{2\xi})}$$

(5.31)

In (5.31), $\delta_1 = \delta_o$ (no phase 1b) which is given by formula (5.30). Also, ξ_1 is the solution of Eq. (5.28).

5. Conclusions

Figure 5.10 shows the relationship among the final central deflection δ, the impulse per unit area I and the pressure p_m in nondimensional form for both the clamped and simply supported plates. The curve for the clamped plates is obtainable from formulas (5.17), (5.20) and (5.25) for $\lambda > \lambda_1 \approx 2$ and from formulas (5.30) and (5.31) for $1 < \lambda \leq \lambda_1$. That for the simply supported plates is obtainable from the results in [5.3]. In using Fig. 5.10 it should be noted that $p_s = 6M_o/r_s^2$ for the clamped plates and $p_s = 6M_o/R^2$ for the simply supported plates. The static collapse pressure for the former is 1.875 times that for the latter.

84
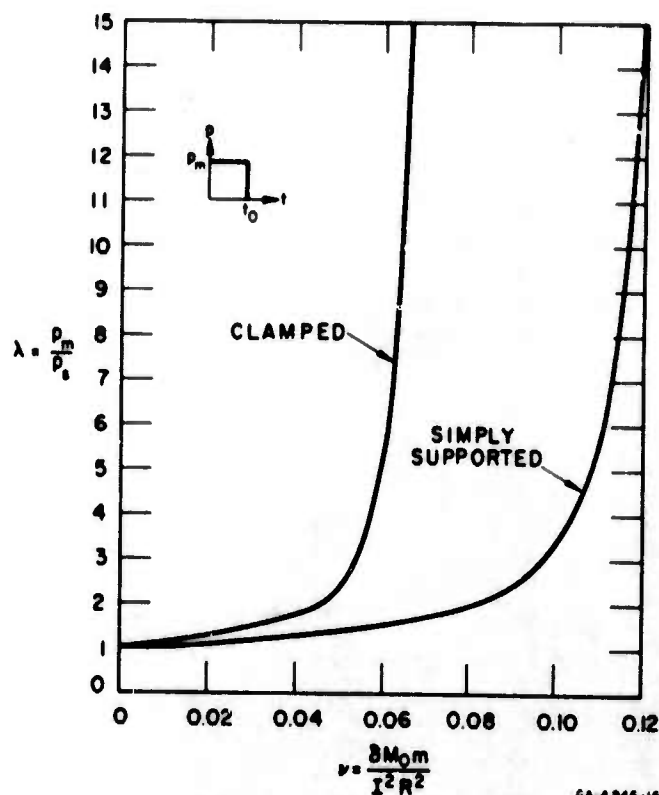
FIG. 5.10 RELATIONSHIP BETWEEN δ, λ AND I

Figure 5.11 shows the relationship that must exist between the pressure and impulse to provide a given central deflection of a clamped plate. (The corresponding curve for a simply supported plate lies almost on top of the shown curve.) In other words, points on the curve define a family of rectangular pulses each member of which produces the same central deflection of a clamped plate. The coordinates of Fig. 5.11 have been rendered nondimensional by using λ and I_i, the latter being the ideal impulse which causes the same central deflection as the rectangular pulses. In fact, $\delta = 0.07\, I_i^2 R^2/mM_o$ [5.1], and $\delta = \nu I^2 R^2/mM_o$ where ν is obtainable from Fig. 5.10 (ν depends on λ).

85
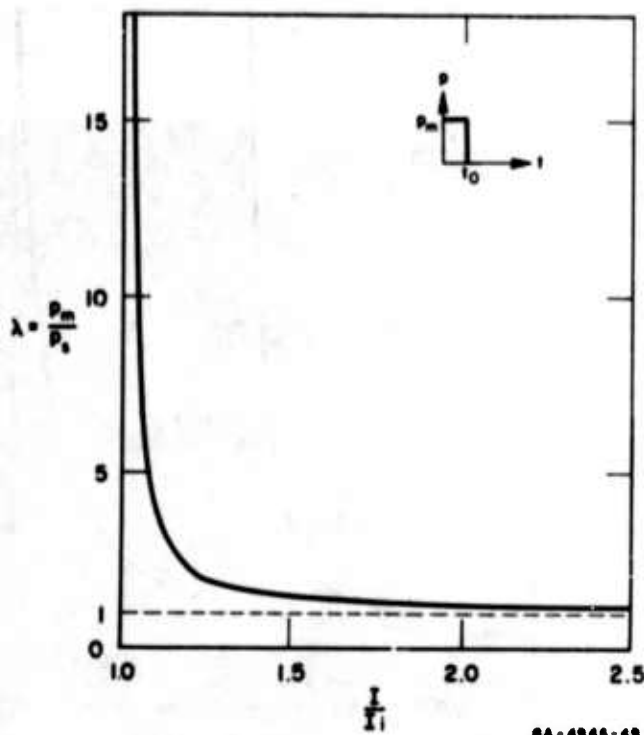
FIG. 5.11 PRESSURE-IMPULSE DIAGRAM

From Figs. 5.10 and 5.11 the following conclusions can be drawn:

1. For a given impulse, the central deflection δ increases with the pressure p_m becoming a maximum when the pressure is infinite, that is, when the given impulse is applied as an ideal impulse. This can be seen in Fig. 5.10 for both clamped and simply supported plates by fixing I, varying λ and observing v.

2. Again for a given impulse, consideration of how δ increases with λ in Fig. 5.10 reveals that for clamped and simply supported plates respectively over 85% and 90% of the maximum central deflection (δ for impulse I_i) are obtained whenever the pressure is greater than six times the static collapse pressure, that is, whenever $\lambda > 6$. Below this value of λ the decrease of δ with λ is quite pronounced.

3. For a given central deflection δ, Fig. 5.11 shows that as the pressure is decreased from infinity to a value corresponding to about $\lambda = 6$ the increase in impulse, over the ideal impulse, necessary to maintain the given deflection δ is less than 7%. $(1 < I/I_i < 1.07$ for $6 < \lambda < \infty)$ A large increase in impulse is required to maintain δ as λ decreases further, especially in the range $1 < \lambda < 2$.

4.   In comparing the effect of the boundary conditions the
static collapse pressure for clamped and simply supported
edges are in the ratio 1.875 : 1 . From the results of
[5.1, 5.2] the ratio of ideal impulses to achieve the same
central deflection is 1.34 : 1 . This latter ratio is the
minimum value for rectangular pulses for all values of
$\lambda > 1$ which implies considerable strengthening due to
clamping the edges.

6.   Description of Experiments

Circular plates of 6061-T651 aluminum and of various thicknesses
ranging from 3/16 inch to 3/8 inch, clamped at either 8 inches or 12
inches diameter, were subjected to the same type of pulse generated
in an oxyacetylene shock tube 32 inches long and having the same
internal diameter as the supports. The experimental arrangement is
shown assembled in Fig. 5.12 and dismantled in Fig. 5.13. Thick
steel annular supports provided clamping against rotation only, a
spacer keeping their distance apart slightly greater than the plate
thickness. Apart from circumferential membrane forces and unavoid-
able frictional effects the plate material was allowed to displace freely
inwards during deformation. To ensure good clamping the overall
diameters of the plates tested were 9 1/2 and 15 inches but to minimize
the build-up of membrane forces they were slotted radilly at 1/2-inch
intervals around the rim. The length of the slots were such that their
ends did not pass over the support circle during deformation. Gas
seals of heavy silicon grease were provided at the junctions of the upper
steel support with both the plate and the shock tube to reduce to rare-
faction of the applied shock wave due to relief of pressure at the junctions.

The pulse, shown in Fig. 2.4, was taken to be that recorded under
a similar configuration by a rod gage and is therefore the pressure
acting on a fixed target. This implies the assumption that the modifi-
cation of the pulse due to plate motion is small. The peak pressure
p_m is obtained from the pressure record of Fig. 2.4 by extrapolating
smoothly the mean pressure curve back to the starting time. This
results in a peak pressure of $p_m = 1440$ lb/in^2. Now the mean pressure
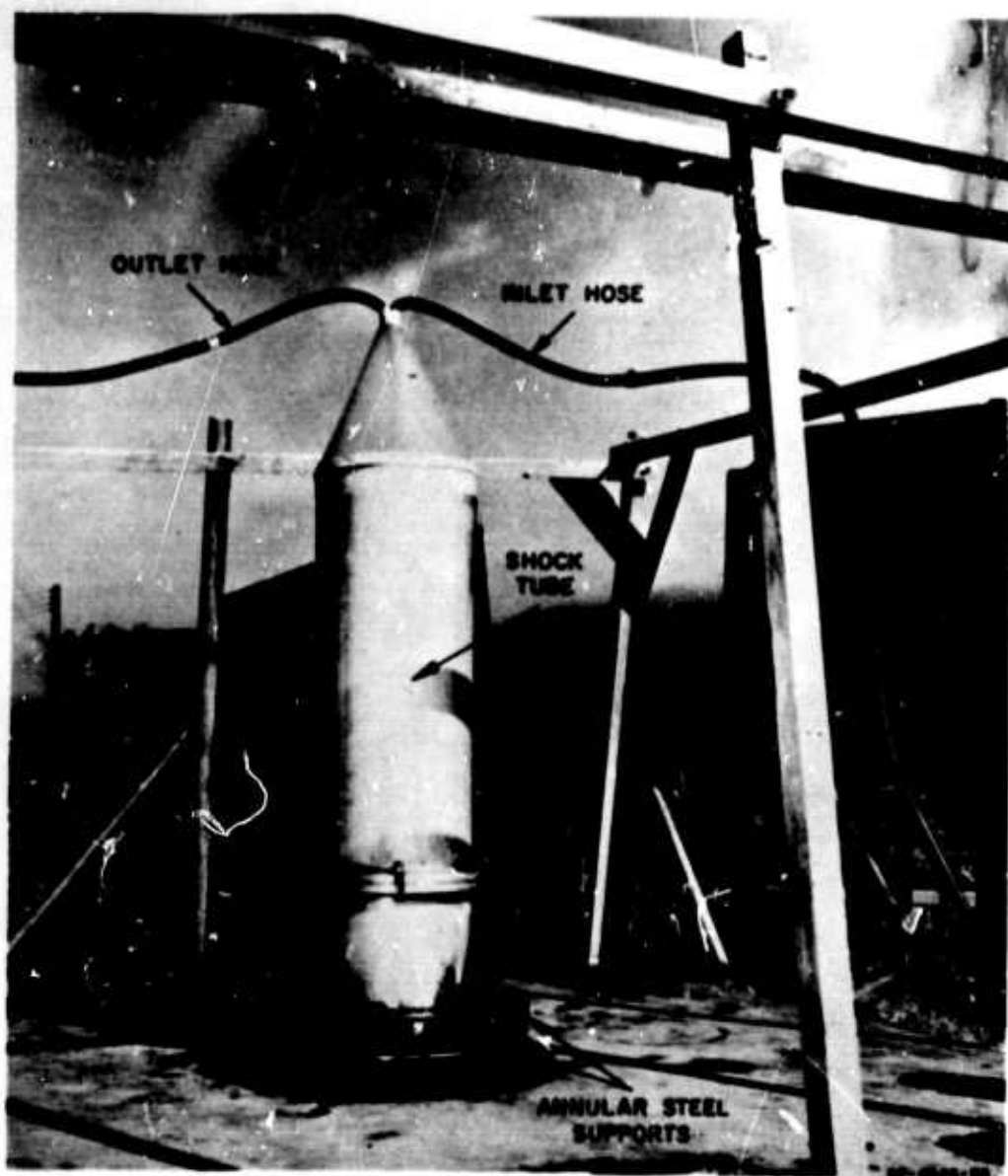
FIG. 5.12 EXPERIMENTAL ARRANGEMENT

curve is fitted by the equation $p = p_m e^{-st}$ to find s. By integration, $I = p_m/s$ and hence the impulse (area under pressure-time curve) is known. The value of the impulse is $I = 0.335$ lb-sec/in^2.
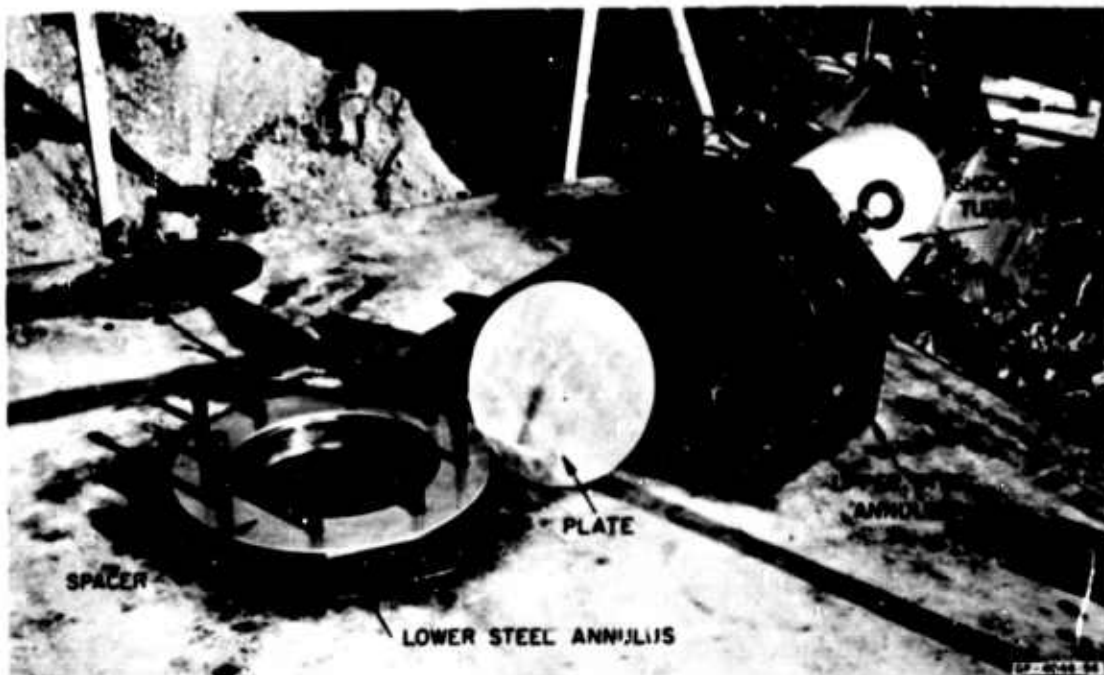
FIG. 5.13 EXPERIMENTAL ARRANGEMENT (DISMANTLED)

Tensile tests performed with the Instron machine on standard ASTM specimens taken with and across the direction of rolling of the plate material provided stress-strain diagrams from which the yield stress was determined. The yield stress is here defined as the stress at the point of intersection of the straight line approximations to the elastic and strain-hardening portions of the stress-strain diagram. An average of the yield stresses obtained from specimens with and across the rolling direction was taken. The plate material, 6061-T651 aluminum, was chosen because it exhibits only slight strain-hardening and is insensitive to strain rate.

After the blast loading tests the permanent central deflections δ_{ex} were measured.

7. Experimental Results and Observations

The results of the experiments described above are presented in Table 5.2 and Fig. 5.14. Correlation with the predictions of the rigid-plastic theory takes place through the ratio δ_{ex}/δ_{th} of the central deflections in Table 5.2 and by means of the λ versus $IR/(12mM_o\delta)^{1/2}$ plot of Fig. 5.14 which is a form of p-I diagram.

The main observation is that the central deflection ratios δ_{ex}/δ_{th}, by ranging from 0.14 to 0.38, show that the theory overestimates the central deflections from the present experiments by factors ranging from about 3 to 7. That the plates are much stronger than predicted is due to the following reasons:

(1)   In the rigid-plastic theory the effects of elastic strain energy and vibrations, strain-hardening, and strain rate are neglected all of which add strength to a structure. However, the material used has little strain-hardening and is fairly insensitive to strain rate.

(2)   If the deflections become large enough membrane forces become significant and the theory considers a bending action only. In general, it can be seen in Table 5.2 that as the ratio δ_{ex}/R increases the ratio δ_{ex}/δ_{th} decreases.

(3)   Frictional and circumferential membrane forces near the plate rim, or rather near the circle passing through the ends of the radial slots, add strength to the plate.

(4)   The experimental pulse was exponential whereas the theoretical pulse was rectangular and for a given peak pressure and impulse the latter predicts larger deformations.

(5)   The applied impulse is probably less than that recorded against a rigid target. In Fig. 5.14 all the experimental points would be moved to the left (in the direction of decreasing impulse) and hence into closer agreement with the theoretical curve.

Table 5.2

EXPERIMENTAL RESULTS

Radius R (inches)	Thickness d (inch)	Yield Stress σ (lb/in²)	Static Collapse Pressure P_s (lb/in²)	$\lambda = \dfrac{P_m}{P_s}$	Central Deflection δ_{ex} (inches)	$\sqrt{\dfrac{IR}{12m M_o \delta_{ex}}}$	$\dfrac{\delta_{ex}}{R}$	$\dfrac{\delta_{ex}}{\delta_{th}}$
6	3/8	43,350	254	5.67	.312	2.72	.052	.18
					.344	2.61	.057	.21
					.344	2.61	.057	.21
	5/16	42,700	174	8.31	.781	2.29	.13	.25
					.688	2.44	.12	.22
	1/4	41,800	109	13.22	1.219	2.59	.20	.19
					1.250	2.56	.21	.19
					1.156	2.66	.19	.18
	3/16	39,300	58	25.05	1.875	2.56	.31	.19
					1.875	2.56	.31	.19
4	3/8	44,550	688	2.10	.1875	2.32	.047	.33
					.219	2.15	.055	.38
	5/16	42,700	391	3.68	.375	2.17	.094	.30
					.375	2.17	.094	.30
	1/4	42,200	248	5.81	.688	2.30	.17	.26
					.688	2.30	.17	.26
	3/16	39,300	129	11.10	1.0312	2.98	.26	.14

Peak pressure	P_m	=	1440 lb/in²
Impulse	I	=	0.335 lb-sec/in²
Mass density	ρ	=	0.000253 lb-sec²/in⁴
Mass	m	=	ρd lb-sec²/in³
Plastic moment	M_o	=	$\sigma_o d^2 / 4$ lb-in/in

Material: 6161-T651 aluminum
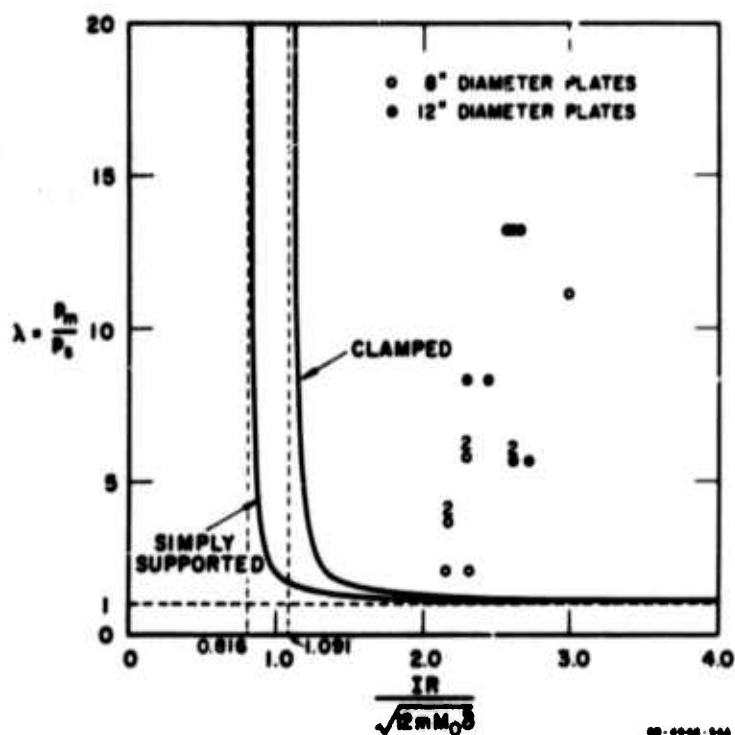
FIG. 5.14 THEORETICAL AND EXPERIMENTAL RESULTS

The duration of the fixed target pulse is about 800 μsec (Fig. 2.3) and much longer than the fundamental response times of quarter periods $T/4$ of the fundamental modes of vibration of the plates (see Table 5.3 below). It is known from the photodiode experiments (Section II) that both the shape and impulse of the rigid-target pulse is affected by the target mobility. An additional complication is that the target mobility varies over the plate. This interaction is important and requires further study.

Table 5.3

RESPONSE TIMES OF FUNDAMENTAL MODES

Radius a (inches)	Thickness d (inch)	Response Time T/4 (μsec)
6	3/8	223
	5/16	268
	1/4	335
	3/16	446
4	3/8	99
	5/16	119
	1/4	149
	3/16	193

NOMENCLATURE

d	plate thickness
I	impulse
I_i	ideal impulse
m	mass per unit area
M, N	components of bending moment
M_o	fully plastic moment
p	pressure
P_1	mechanism pressure bound
P_m	peak pressure
P_s	static collapse pressure
r	radial coordinate
r_o, r_1, r_s	plastic radii of regime boundaries
R	plate radius
t	time
t_o	pulse duration
t_1	time at end of phase 1b
t_2	time at end of phase 2
T	fundamental period of plate vibration
V	velocity of plate center
V_o	$V(t_o)$
w	plate deflection
δ_o	plate central deflection at time t_o
δ_1	plate central deflection at time t_1
δ_2, δ	plate central deflection at time t_2
δ_{ex}	experimental final central deflection
δ_{th}	theoretical final central deflection
ζ	V/V_o
η	$1 - \rho_o/\rho_1$
λ	p/P_s
λ_1	$P_1/P_s = P_m/P_s$

NOMENCLATURE (Continued)

ν	$\delta M_o m / I^2 R^2$
ζ	$\ln(1/\rho_1)$
ζ_s	$\ln(1/\rho_s)$
ζ_1	ζ at time t_1
ζ_2	ζ at time t_2
ρ_o	r_o/R
ρ_1	r_1/R
ρ_s	r_s/R
τ	$12 M_o (t - t_o)/IR^2$
τ_1	$12 M_o (t_1 - t_o)/IR^2$
τ_2	$12 M_o (t_2 - t_o)/IR^2$
τ'	$12 M_o t / mR^2$
τ_o'	$12 M_o t_o / mR^2$
σ	$(\ln R/r_1 + 1)^{-1}$

This page intentionally left blank.

SECTION VI

CLAMPED CIRCULAR RIGID-PLASTIC PLATES
UNDER BLAST LOADING (Partial Loading)

A theoretical study is made of clamped circular plates of rigid-
plastic material subjected to blast loading uniformly distributed over
a central circular area. The dependence of the permanent central
deflection on pressure, impulse and loaded area is obtained when the
blast pulse is taken as a rectangular pulse. Experiments are described
and the permanent central deflections obtained are correlated with the
theoretical predictions.

1.   Introduction

The problem treated is the response of a clamped circular plate
subjected to a suddenly applied pressure uniformly distributed over a
central circular area. The pressure is assumed high enough or held on
the plate long enough to produce moderately large plastic deformations.
Although the governing equations are derived for a general pressure-
time relationship, they are solved only for the simplest case; that of a
pressure held constant for a time and then suddenly released (a rec-
tangular pulse). It is the variation of the permanent central deflection
with pressure, impulse (area under the pressure-time curve) and the
loaded area that constitutes the principal result. Because of interest
in moderately large plastic deformations and in order to simplify the
analysis the plate material is assumed to be rigid-perfectly plastic
obeying the Tresca yield condition and the associated flow rule. Only
the bending action of the plate is taken into account.

Past work on the dynamic response of a rigid-plastic circular
plate concerns blast or impulsive loading uniformly distributed over
the entire area. In Section V a clamped plate subjected to a rectangular
pulse is treated. Wang and Hopkins [5.1] found the response of a
clamped plate to an ideal impulse. A similar method of solution, the
established continuity and jump conditions, and similar nomenclature

97

are employed here as is done in Section V. The responses of a simply
supported plate to an ideal impulse and a rectangular pulse were found
by Wang [5.2] and by Hopkins and Prager [5.3] respectively.

The present problem is quite similar to that of Section V but,
due to the loading covering only a central part of the plate (Fig. 6.1),
two additional mechanisms of deformation can exist. An analogous
situation exists for beams and the two additional mechanisms are 2b
and 3 of Section III.

2.   Mechanisms of Deformation

A blast pulse may be idealized to the form shown in Fig. 6.2
with an instantaneous rise to the peak pressure p_m followed by a
continuous monotonic decay. It is assumed that this form of pulse
allows a steady progress through the various mechanisms of deformation
that will be described.
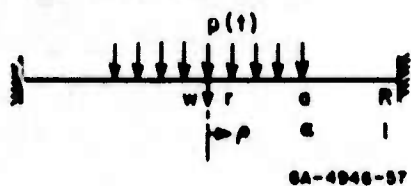
FIG. 6.1 CIRCULAR PLATE PROBLEM   FIG. 6.2 IDEALIZED BLAST PLATE
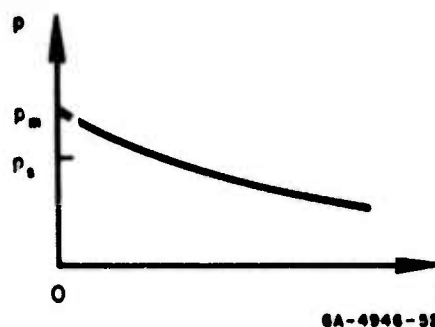
During deformation the plate is divided into annular regions in
each of which exists a certain plastic regime defined by a vertex or
side of the Tresca yield hexagon (Fig. 6.3) relating M and N , the
radial and circumferential components of bending moment (positive
moments cause tension on the underside of the plate). In this problem
only the portion ABC is involved. Associated with these annular regions
are velocity fields which must satisfy the flow rule, boundary conditions,
and the appropriate continuity and discontinuity conditions [5.1].

98
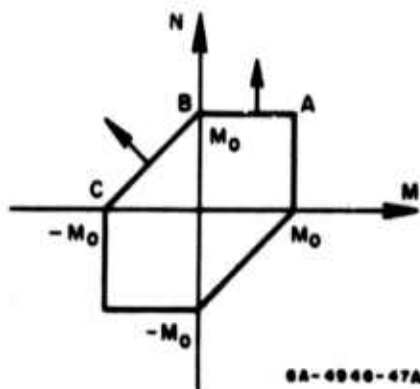
FIG. 6.3 TRESCA YIELD HEXAGON

From the equation of equilibrium, the static collapse pressure p_s, acting on a central circular area of radius $r = a$ of a plate of radius $r = R$, is found by assuming that in the circle $0 \le r \le r_s$, the plastic regime is AB, A being at the plate center and B at radius $r = r_s$, while in the outer annular region $r_s \le r \le R$ the plastic regime is BC, C being at the plate support $r = R$. The result may be expressed in the form [5.4]

$$p_s R^2 \alpha^2 (1 - 2\alpha/3\rho_s)/2M_o = 1 \qquad 0 < \alpha \le \rho_s \qquad (6.1)$$

where ρ_s is the solution of

$$2\alpha(1 + \ln 1/\rho_s)/3\rho_s = 1 \qquad (6.2)$$

and

$$p_s R^2 \rho_s^2/6M_o = 1 \qquad \rho_s \le \alpha \le 1 \qquad (6.3)$$

where now ρ_s is the solution of

$$\rho_s^2(5 + 2\ln 1/\rho_s) = 3\alpha^2(1 + 2\ln 1/\alpha) \qquad (6.4)$$

In Eqs. (6.1), (6.2), (6.3) and (6.4), $\rho_s = r_s/R$, $\alpha = a/R$ and M_o is the fully plastic moment.

For values of the peak pressure in excess of the static collapse pressure the plate deforms initially in one of four mechanisms depending on the parameters $\lambda = p_m/p_s$ and $\alpha = a/R$.

99

(a) **Mechanism 3**

For large values of λ it is assumed that the initial mechanism of deformation consists of a central portion of radius $r_0(t)$ moving at a velocity $V(t)$, an outer annular portion $r_2(t) \leq r \leq R$ at rest, and an annular region between undergoing plastic deformation (Fig. 6.4). At $r = r_0(t)$ and $r = r_2(t)$ $(r_0 < r_2)$ two plastic hinge circles exist and, for blast pulses of the kind shown in Fig. 6.2, the inner radius is assumed to decrease until the center is reached while the outer increases until the support is reached. At the radius $r = r_1(t)$ the plastic regime B exists and the rate of the radial component of curvature changes sign across this circle. The plastic regimes existing elsewhere are shown in Fig. 6.4.
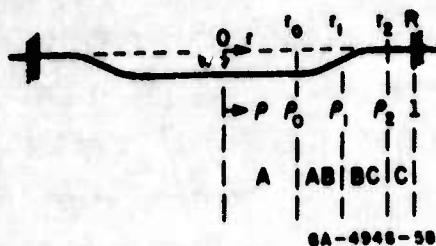
FIG. 6.4 MECHANISM 3

The velocity field meeting the above description, satisfying the flow rule, boundary conditions and the appropriate continuity and discontinuity conditions [5.1] is

$$
w_t = \begin{cases}
V & 0 \leq r \leq r_0(t) \\
V\left[1 - \sigma(r - r_0)/r_1\right] & r_0(t) \leq r \leq r_1(t) \\
V\sigma\ln r_2/r & r_1(t) \leq r \leq r_2(t) \\
0 & r_2(t) \leq r \leq R
\end{cases} \tag{6.5}
$$

where $1/\sigma = \ln r_2/r_1 + 1 - r_0/r_1$.

In (6.5), w is the plate deflection and the subscript t denotes partial differentiation.

Deformation proceeds under another mechanism once one of the hinge circles reaches its terminal position. If the outer hinge

100

circle reaches the support first the ensuing mechanism, called mechanism 2a, is described by the velocity field (6.5) with $r_2 = R$. If the inner hinge circle reaches the center first the ensuing mechanism, called mechanism 2b, is described by (6.5) with $r_o = 0$. The final phase of deformation occurs after both traveling hinge circles have reached their terminal positions and the mechanism, called mechanism 1, is described by (6.5) with both $r_o = 0$ and $r_2 = R$. This last mode is the same as that for static collapse.

(b)   Mechanism 2a

This mechanism given by the velocity field (6.5) with $r_2 = R$ is an initial mechanism for certain ranges of α and λ . In fact, the range of α turns out to be $0.56 \leq \alpha \leq 1$. The range of λ depends on α and is denoted by $\lambda_1 < \lambda \leq \lambda_2$ the numerical values for which are shown in Fig. 6.5.

(c)   Mechanism 2b

This mechanism given by (6.5) with $r_o = 0$ is likewise an initial mechanism for certain ranges of α and λ . The range of α is $0 < \alpha \leq 0.56$ while the range of λ depends on α and is again denoted by $\lambda_1 < \lambda \leq \lambda_2$ the numerical values for which are shown in Fig. 6.5

(d)   Mechanism 1

This mechanism, given by (6.5) with $r_o = 0$ and $r_2 = R$, is an initial mechanism, and hence for blast pulses the only mechanism, for all α and for a certain range of λ depending on α . The range of λ denoted by $1 < \lambda \leq \lambda_1$ is obtainable from Fig. 6.5.

The way in which λ_1 and λ_2 are found is described once the governing equations are derived.

101
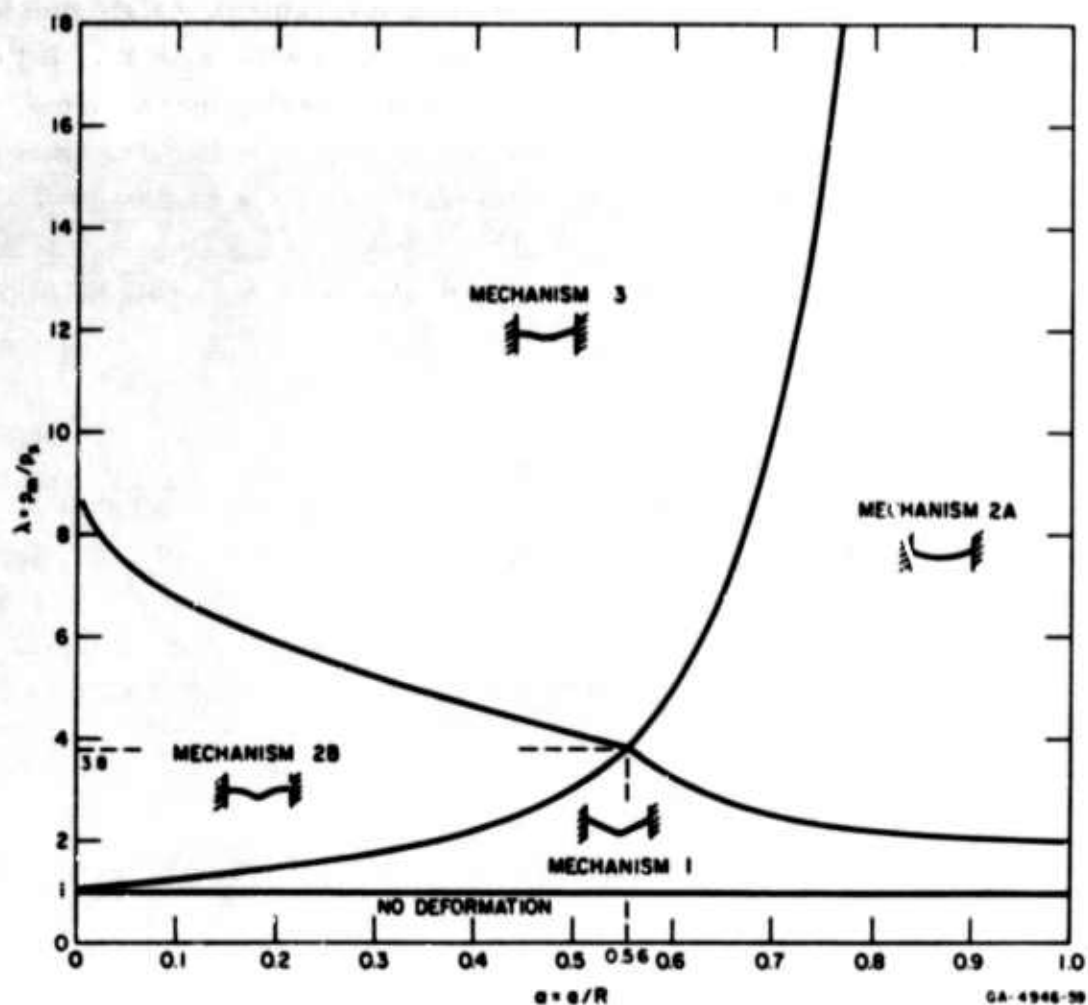
FIG. 6.5 DEFORMATION MECHANISM DIAGRAM

3. Governing Equations

Independent of mechanisms the equation of motion is

$$N - (rM)_r = \int_0^r (p - mw_{tt})r\,dr \qquad (6.6)$$

where the subscripts r and t denote partial differentiation and m is the mass per unit area of plate. Differentiating the velocity (6.5) provides the acceleration to be substituted in (6.6) and the yield condition (Figs. 6.3 and 6.4) allows the circumferential component of

102

bending moment N to be eliminated. Performing the integration in (6.6) and using the properties $M = 0$ in $0 \le r \le r_o$, $M(r_1) = 0$, $M(r_2) = -M_o$ and $M_r(r_2) = 0$ leads to the following four equations governing mechanism 3.

$$V' = \rho R^2/12M_o \tag{6.7}$$

$$V'\eta(\xi_1 - \xi_2 + \eta)[\eta(6-8\eta+3\eta^2) + 2(\xi_1-\xi_2)(3-3\eta+\eta^2)] - V\xi_1'\eta[\eta(1-\eta)(4-3\eta)$$

$$+ (\xi_1-\xi_2)(6-8\eta+3\eta^2)] - V\xi_2'\eta^3(4-3\eta) - V\eta'\eta^2[\eta(4-3\eta) + 2(\xi_1-\xi_2)(3-2\eta)]$$

$$= \begin{cases} [(\rho R^2/6M_o)\left\{3a^2 - 2a^3 e^{\xi_1} - (1-\eta)^3 e^{-2\xi_1}\right\} - 1]e^{2\xi_1}(\xi_1-\xi_2+\eta)^2 & a < \rho_1 \\ [(\rho R^2/6M_o)e^{-2\xi_1}\eta(3-3\eta+\eta^2) - 1]e^{2\xi_1}(\xi_1-\xi_2+\eta)^2 & \rho_1 < a \end{cases}$$

$$\tag{6.8}$$

$$V'(\xi_1-\xi_2+\eta)[3e^{2(\xi_1-\xi_2)} - 3 - 2(\xi_1-\xi_2)(3-3\eta+3\eta^2-\eta^3)] - V\xi_1''[3e^{2(\xi_1-\xi_2)}$$

$$-3-2(\xi_1-\xi_2)\left\{3-\eta^2(1-\eta)(3-2\eta)\right\} - 2(\xi_1-\xi_2)^2(3-6\eta+6\eta^2-2\eta^3)]$$

$$-V\xi_2'[3e^{2(\xi_1-\xi_2)}\left\{\xi_1-\xi_2-(1-\eta)\right\} + (\xi_1-\xi_2)(3-6\eta+6\eta^2-2\eta^3) + 3(1-\eta)]$$

$$-V\eta'[3e^{2(\xi_1-\xi_2)} - 3 - 2(\xi_1-\xi_2)(3-3\eta^2+2\eta^3) - 6(\xi_1-\xi_2)^2(1-\eta)^2]$$

$$= \begin{cases} [\left\{(\rho R^2 a^2/2M_o) - 1\right\}(\xi_1-\xi_2) - 1]e^{2\xi_1}(\xi_1-\xi_2+\eta)^2 & a < \rho_1 \\ [(\rho R^2 a^2/4M_o)\left\{1-2\xi_2+2\ln(1/a)-e^{-2\xi_2}/a^2\right\} - (1+\xi_1-\xi_2)]e^{2\xi_1}(\xi_1-\xi_2+\eta)^2 \\ \qquad\qquad\qquad\qquad\qquad\qquad\qquad\qquad\qquad\qquad \rho_1 < a \end{cases}$$

$$\tag{6.9}$$

$$V'(\xi_1 - \xi_2 + \eta)[3e^{2(\xi_1-\xi_2)} - 3 + 2\eta(3-3\eta+\eta^2)] - V\xi_1'[3e^{2(\xi_1-\xi_2)}$$

$$-3 - 2(\xi_1-\xi_2)(3-6\eta+6\eta^2-2\eta^3) + 2\eta^2(1-\eta)(3-2\eta)] \quad V\xi_2'[3e^{2(\xi_1-\xi_2)}$$

$$\left\{2(\xi_1-\xi_2)-1+2\eta\right\} + 3 - 6\eta + 4\eta^2 - 2\eta^3] - V\eta'[3e^{2(\xi_1-\xi_2)} - 3 - 6(\xi_1-\xi_2)$$

$$(1-\eta)^2 + 2\eta^2(3-2\eta)] - V\xi_2'[3e^{2(\xi_1-\xi_2)}$$

$$= [(pR^2a^2/2M_o) - 1]e^{2\xi_1}(\xi_1-\xi_2+\eta)^2 \qquad 0 < \rho_2 < 1$$

$$(6.10)$$

The new variables that have been introduced in the derivation of (6.8), (6.9) and (6.10) are defined by

$$\xi_1 = \ell n(1/\rho_1) \qquad \xi_2 = \ell n(1/\rho_2) \qquad \eta = 1 - \rho_o/\rho_1$$

$$\rho_o = r_o/R \qquad \rho_1 = r_1/R \qquad \rho_2 = r_2/R$$

Primes over the dependent variables V, ξ_1, ξ_2, and η denote differentiation with respect to the variable τ' where

$$\tau' = 12M_o t/mR^2 \qquad (6.11)$$

The equations governing mechanisms 2a, 2b and 1 are readily obtained from (6.7), (6.8), (6.9) and (6.10) as outlined below.

(a) Mechanism 2a

The outer hinge circle is stationary at radius $r = r_2 = R$ and the properties leading to the governing equations are $M = 0$ in the region $0 \leq r \leq r_o$, $M(r_1) = 0$, and $M(R) = -M_o$. Consequently, the equations are (6.7), (6.8) and (6.9) with $\xi_2 = \xi_2' = 0$.

104

(b)   <u>Mechanism 2b</u>

There is no inner hinge circle and the relevant properties
are $M(r_1) = 0$, $M(r_2) = -M_o$, and $M_r(r_2) = 0$. Thus, the governing
equations are (6.8), (6.9) and (6.10) with $\eta = 1$ and $\eta' = 0$.

(c)   <u>Mechanism 1</u>

The outer hinge circle is stationary at radius $r = r_2 = R$
and there is no inner hinge circle, leaving the two properties $M(r_1) = 0$
and $M(R) = -M_o$, so the governing equations are (6.8) and (6.9) with
$\zeta_2 = \zeta_2' = 0$, $\eta = 1$, and $\eta' = 0$.

Having now the equations governing motion in all four
mechanisms, it is possible to find the functions λ_1 and λ_2 shown in
Fig. 6.5. It is assumed that the hinge circles and the circle $r = r_1$
have zero initial velocities so that $\zeta_1' = \zeta_2' = \eta' = 0$ at $\tau' = 0$. λ_1 is
the upper bound of the values of λ for which mechanism 1 applies and
the initial value of ζ_1, designated $\zeta_1^{(0)}$, for each $\lambda = p_m/p_s$ or
peak pressure p_m of this mechanism is obtained by solving the
following two equations which are the appropriate special cases of
(6.8) and (6.9):

$$
V'(1+2\zeta_1) = \begin{cases} [(p_m R^2/6M_o)\alpha^2(3-2\alpha e^{\zeta_1})-1]e^{2\zeta_1}(1+\zeta_1) & \alpha < \rho_1 \\[2ex] [(p_m R^2/6M_o)e^{-2\zeta_1}-1]e^{2\zeta_1}(1+\zeta_1) & \rho_1 < \alpha \end{cases} \qquad (6.12)
$$

$$
V'(3e^{2\zeta_1} - 4\zeta_1) = \begin{cases} [(p_m R^2\alpha^2/2M_o)\zeta_1-(1+\zeta_1)]e^{2\zeta_1}(1+\zeta_1) & \alpha < \rho_1 \\[2ex] [(p_m R^2\alpha^2/4M_o)\left\{1+2\ln(1/\alpha)-e^{-2\zeta_1}/\alpha^2\right\} \\ -(1+\zeta_1)]e^{2\zeta_1}(1+\zeta_1) & \rho_1 < \alpha \end{cases} \qquad (6.13)
$$

By considering an increasing sequence of λ's the upper bound λ_1 is that value which causes an inflection point in the bending moment diagram for M either at the plate center or at the support. This means that the yield condition will be violated at these places for values of λ infinitesimally larger than λ_1. The conditions $M_{rr}(0,0) = 0$ and $M_{rr}(R,0) = 0$ are expressed by the equations

$$V' = p_m R^2 / 12 M_o \qquad (6.14)$$

$$V'(3e^{2\zeta_1} - 1) = [p_m R^2 \alpha^2 / 2M_o) - 1]e^{2\zeta_1}(1+\zeta_1) \qquad (6.15)$$

and when $\lambda = \lambda_1$ either (6.14) or (6.15) is satisfied by the solutions $V'(0)$ and $\zeta_1^{(0)}$ of (o.12) and (6.13). Computations show that whenever $0 \le \alpha \le 0.56$, λ_1 is determined by the condition $M_{rr}(0,0) = 0$ represented by (6.14), and whenever $0.56 \le \alpha \le 1$, λ_1 is determined by the condition $M_{rr}(R,0) = 0$ represented by (6.15). For further increases in λ_1 the former case indicates that the initial mechanism is 2b whereas for the latter it is 2a. The two portions of the λ_1 curve are shown in Fig. 6.5.

The values of λ_2 are found in a similar way. If the initial mechanism is 2a, the initial values $V'(0)$, $\zeta_1^{(0)}$, and $\eta^{(0)}$ are obtained by solving for each $\lambda(\lambda > \lambda_1)$ or p_m Equations (6.7), (6.8) and (6.9) with the special values $\zeta_1' = \zeta_2' = \eta' = 0$, and $\zeta_2 = 0$. λ_2 is that value of λ which causes an inflection point in the bending moment diagram for M at the support. The condition $M_{rr}(R,0) = 0$ is expressed by the equation

$$V'[3e^{2\zeta_1} - 3 + 2\eta(3 - 3\eta + \eta^2)] = [(p_m R^2 \alpha^2 / 2M_o) - 1]e^{2\zeta_1}(1+\zeta_1) \quad (6.16)$$

and when $\lambda = \lambda_2$, the initial values $V'(0)$, $\zeta_1^{(0)}$ and $\eta^{(0)}$ satisfy (6.16). If the initial mechanism is 2b, the initial values $V'(0)$, $\zeta_1^{(0)}$ and $\zeta_2^{(0)}$ are obtained by solving for each $\lambda (\lambda > \lambda_1)$ or p_m Equations (6.3), (6.9) and (6.10) with the special values $\zeta_1' = \zeta_2' = \eta' = 0$, and

$\eta = 1$. λ_2 is that value of λ which causes an inflection point in the bending moment diagram for M at the plate center. The condition $M_{rr}(0,0) = 0$ is expressed by the equation

$$V' = p_m R^2 / 12 M_o \qquad (6.17)$$

and when $\lambda = \lambda_2$, the initial value $V'(0)$ satisfies (6.17). The two portions of the λ_2 curve are shown in Fig. 6.5.

4.   Solution for Rectangular Pulse

In this section is an outline of the method of solution applicable to rectangular pulses with pressures high enough to cause initial deformation by mechanism 3. For the other initial mechanisms the method is similar and the details simpler.

A solution is obtained if it is assumed that while the constant pressure is being applied the hinge circles and the circle of radius $r = r_1$ remain stationary. This phase of the motion, called phase 1a, involves the solution of Equations (6.7), (6.8), (6.9) and (6.10) with the pressure p a constant $(\lambda > \lambda_2)$ and with the special values $\zeta_1' = \zeta_2' = \eta' = 0$. The solutions are denoted by $\zeta_1^{(0)}$, $\zeta_2^{(0)}$, and $\eta^{(0)}$. V' is given explicitly by (6.7). Corresponding to these values some initial values of the radii ρ_o, ρ_1, and ρ_2 are listed in Table 6.1 for two values of α. Note that as λ increases they tend to the radius α of the loading.

Let the pulse end at time $t = t_o$, or when $\tau' = \tau_o'$, and let the velocity and deflection of the plate center at this time be V_o and δ_o. Then from Equation (6.7) alone, successive integrations give

$$V_o = I/m \qquad (6.18)$$

and

$$\delta_o = I^2 / 2mp \qquad (6.19)$$

where $I = pt_o$ is the impulse applied per unit area.

107

Table 6.1

INITIAL VALUES OF ρ_0, ρ_1, AND ρ_2

λ	$\alpha = 0.438$				$\alpha = 0.656$			
	$\rho_0^{(0)}$	$\rho_1^{(0)}$	$\rho_2^{(0)}$	Initial Mechanism	$\rho_0^{(0)}$	$\rho_1^{(0)}$	$\rho_2^{(0)}$	Initial Mechanism
1.05	0.	.492	1.0	1	0.	.635	1.0	1
1.1	0.	.487	1.0	1	0.	.636	1.0	1
1.2	0.	.480	1.0	1	0.	.637	1.0	1
1.5	0.	.460	1.0	1	0.	.639	1.0	1
2.	0.	.438	1.0	1	0.	.643	1.0	1
2.5	0.	.423	.987	2b	0.	.645	1.0	1
3.	0.	.419	.906	2b	.039	.648	1.0	2a
4.	0.	.418	.816	2b	.143	.649	1.0	2a
5.	0.	.420	.766	2b	.200	.648	1.0	2a
6.					.238	.646	1.0	2a
7.	0.	.424	.709	2b	.265	.643	1.0	2a
8.					.292	.643	.983	3
10.	.186	.428	.662	3	.337	.646	.947	3
15.	.239	.431	.619	3	.402	.649	.892	3
50.	.335	.436	.536	3	.523	.654	.784	3
100.	.366	.437	.507	3	.564	.655	.747	3

When $t > t_o$, no pressure acts on the plate and, according to (6.7), the velocity of the plate center or rather the central region $0 \le r \le r_o$ is constant during this phase of motion, called phase 1b. It is evident from (6.8), (6.9) and (6.10) with $V' = p = 0$ that ζ_1, ζ_2, and η can no longer be treated as constants.

In Equations (6.8), (6.9) and (6.10) set $V' = 0$, $V = V_o$ and, for convenience, introduce the nondimensional time variable τ defined by

$$t = mR^2 \tau'/12M_o = mR^2 V_o \tau/12M_o \qquad (6.20)$$

The resulting equations, in indicial notation, may be written in the form

$$\zeta_i' A_{ij} = B_j \qquad i, j = 1, 2, 3 \qquad (6.21)$$

in which the derivatives are with respect to τ, and, for notational purposes only, $\zeta_3 = \eta$.

The chosen numerical scheme for the solution of (6.21) commences by solving for the derivatives ζ_i' (Equations (6.21) are linear in the derivatives) to give

$$\zeta_i' = f_i(\zeta_1, \zeta_2, \zeta_3) \qquad i = 1, 2, 3 \qquad (6.22)$$

From (6.21) the variable τ can be eliminated resulting in the two equations

$$d\zeta_1/d\zeta_3 = g(\zeta_1, \zeta_2, \zeta_3) \text{ and } d\zeta_2/d\zeta_3 = h(\zeta_1, \zeta_2, \zeta_3) \qquad (6.23)$$

The initial values determined in phase 1a are $\zeta_i^{(0)}$. From its initial value an incremental change is made in one of the variables here chosen to be ζ_3 so that its new value is $\zeta_3^{(1)} = \zeta_3^{(0)} + \Delta\zeta_3$. Then,

from (6.23), the corresponding new values of ζ_1 and ζ_2 are

$$\zeta_1^{(1)} = \zeta_1^{(0)} + g^{(0)} \Delta \zeta_3$$

$$\zeta_2^{(1)} = \zeta_2^{(0)} + h^{(0)} \Delta \zeta_3$$

where $g^{(0)} = g(\zeta_1^{(0)}, \zeta_2^{(0)}, \zeta_3^{(0)})$ and $h^{(0)} = h(\zeta_1^{(0)}, \zeta_2^{(0)}, \zeta_3^{(0)})$. With the values $\zeta_i^{(1)}$ the new values $g^{(1)}$ and $h^{(1)}$ can be determined and hence $\zeta_i^{(2)}$ can be calculated with the next increment $\Delta \zeta_3 = \zeta_3^{(2)} - \zeta_3^{(1)}$. This procedure is continued until either $\zeta_3 = \eta = 1$ or $\zeta_2 = 0$. In the former case the deformation continues by mechanism 2b whereas in the latter case it continues by mechanism 2a. To find the value of τ_1 of τ at the end of phase 1b all the time increments are summed. The first of such increments is

$$\Delta \tau = \tau^{(1)} - \tau^{(0)} = (\zeta_3^{(1)} - \zeta_3^{(0)})/\zeta_3'^{(0)}$$

in which $\zeta_3'^{(0)} = f_3^{(0)}$ by (6.22).

Finally the deflection δ_1 of the plate center at the end of phase 1b is given by

$$\delta_1 - \delta_0 = V_0(t_1 - t_0) = I^2 R^2 (\tau_1 - \tau_0)/12mM_0 \tag{6.24}$$

in which δ_0 is determined by formula (6.19) and $\tau_0 = 12M_0/R^2 p$.

As mentioned above the next phase of motion, called phase 1c, can take one of two forms depending on which hinge circle reaches its terminal position first. Only the case of the inner hinge circle of radius $r_0(t)$ reaching the center first will be described since the other case is covered by the description of phase 1b in the problem of Section V the only difference being in the initial values ζ_1 and η. (In Section V ζ plays the role of ζ_1.) Numerical calculations show that $r_0(t) = 0$ before $r_2(t) = R$ whenever $0 \leq \alpha \leq 0.56$. The equations governing phase 1c for deformation by mechanism 2b are (6.8), (6.9)

110

and (6.10) with the special values $p = 0$, $\eta' = 0$ and $\eta = 1$. For brevity, the indicial notation is used to express these equations in the form

$$\xi_i' C_{ij} = D_j \qquad i, j = 1, 2, 3 \tag{6.25}$$

In (6.25), derivatives are with respect to the time variable τ defined by (6.20) and, for notational purposes, $\xi_3 = \gamma = V/V_o$.

The numerical procedure is the same as that in phase 1b except that increments $\Delta\xi_2$ are used (instead of $\Delta\xi_3$) and the initial values are the final values of phase 1b. The procedure is halted at $\xi_2 = 0$ ($\rho_2 = 1$) when phase 1c ends. Let the central deflection and the time at the end of phase 1c be δ_2 and t_2 ($\tau = \tau_2$). Then

$$\tau_2 - \tau_1 = \sum_{n=1}^{N} \Delta\tau^{(n)}$$

where

$$\Delta\tau^{(n)} = (\xi_2^{(n)} - \xi_2^{(n-1)})/\xi_2'^{(n-1)}$$

Also

$$\delta_2 - \delta_1 = \int_{t_1}^{t_2} V dt = \frac{I^2 R^2}{12 m M_o} \int_{\tau_1}^{\tau_2} \gamma(\tau) d\tau$$

which, by the numerical procedure adopted above, is replaced by the summation

$$\delta_2 - \delta_1 = \frac{I^2 R^2}{12 m M_o} \sum_{n=1}^{N} \gamma^{(n)} \Delta\tau^{(n)} \tag{6.26}$$

In the final phase of motion, called phase 2, deformation is by mechanism 1 with the governing Equations (6.8) and (6.9) having the special values $\xi_2' = \eta' = \xi_2 = p = 0$, and $\eta = 1$. So that the analysis of this phase conforms to those of Section V and Reference [5.1], the variable τ is retained and the variable $\zeta = V/V_2$ is introduced where

111

$V_2 = V(\tau_2)$. Then, the initial and final values of ζ are unity and zero. Also, the governing equations become

$$\zeta'(\xi_1+1)(2\xi_1+1) - \zeta \xi_1'\xi_1 = -(\xi_1+1)^2 e^{2\xi_1}/\gamma_2 \qquad (6.27)$$

$$\zeta'(\xi_1+1)(3e^{2\xi_1}-3-4\xi_1) - \zeta\xi_1'(3e^{2\xi_1}-3-6\xi_1-2\xi_1^2) = -(\xi_1+1)^3 e^{2\xi_1}/\gamma_2 \qquad (6.28)$$

in which differentiation is with respect to τ and $\gamma_2 = V_2/V_o$ (this is the value of γ at the end of phase 1c). Eliminating τ from (6.27) and (6.28) leads to a linear differential equation with the solution

$$\zeta = \left[\frac{\xi_1+1}{\xi_1(\tau_2)+1} \right] \exp\left[- \int_{\xi_1(\tau_2)}^{\xi_1} \frac{(1-\xi)d\xi}{4+7\xi+2\xi^2-3e^{2\xi}} \right] \qquad (6.29)$$

Motion ceases when $\zeta = 0$ and this occurs when $\xi_1 \approx 0.478$ which is the solution of the equation

$$4 + 7\xi + 2\xi^2 - 3e^{2\xi} = 0$$

Let $\tau = \tau_3$ when motion ceases. Then

$$\tau_3 - \tau_2 = \int_{\xi_1(\tau_2)}^{\xi_1(\tau_3)} \frac{d\xi}{\xi'} = \gamma_2 \int_{\xi_1(\tau_2)}^{\xi_1(\tau_3)} \frac{(3e^{2\xi}-4\xi^2-6\xi-3)\zeta d\xi}{e^{2\xi}(\xi+1)(4+7\xi+2\xi^2-3e^{2\xi})} \qquad (6.30)$$

Finally, let the central deflection when $\tau = \tau_3$ ($t = t_3$) be δ_3. Then

$$\delta_3 - \delta_2 = \frac{IR^2}{12M_o} \int_{\tau_2}^{\tau_3} V d\tau = \frac{I^2R^2}{12mM_o} \gamma_2^2 \int_{\xi_1(\tau_2)}^{\xi_1(\tau_3)} \frac{(3e^{2\xi}-4\xi^2-6\xi-3)^2\zeta^2 d\xi}{e^{2\xi}(\xi+1)(4+7\xi+2\xi^2-3e^{2\xi})} \qquad (6.31)$$

In Figs. 6.6 and 6.7 are shown the paths ABCD followed by the point (ξ_1, ξ_2, η) for values of α equal to 0.438 and 0.656 respectively,

112
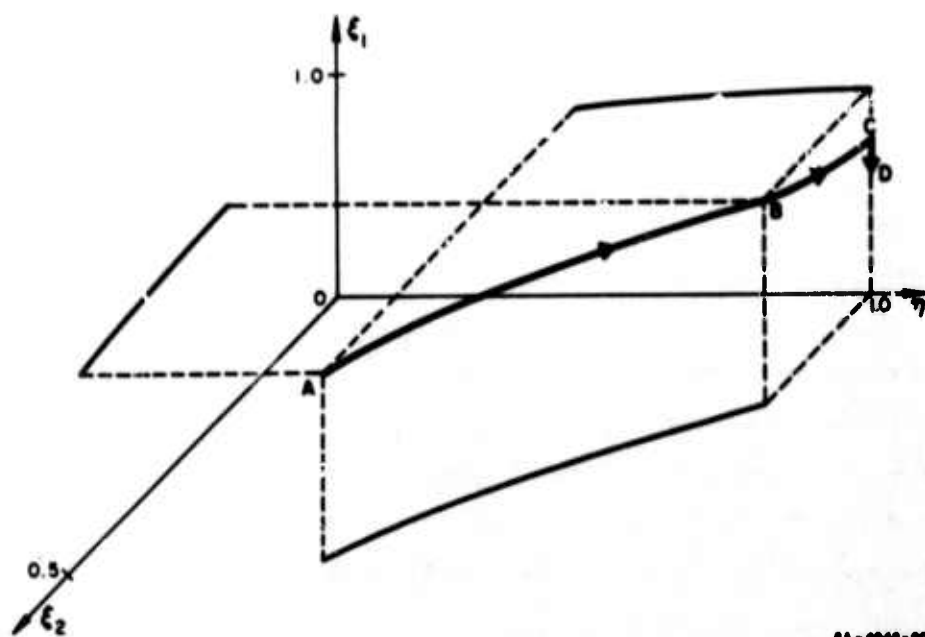
FIG. 6.6 TRAJECTORY OF (ξ_1, ξ_2, η) FOR $\alpha = 0.438$ AND $\lambda = 15$
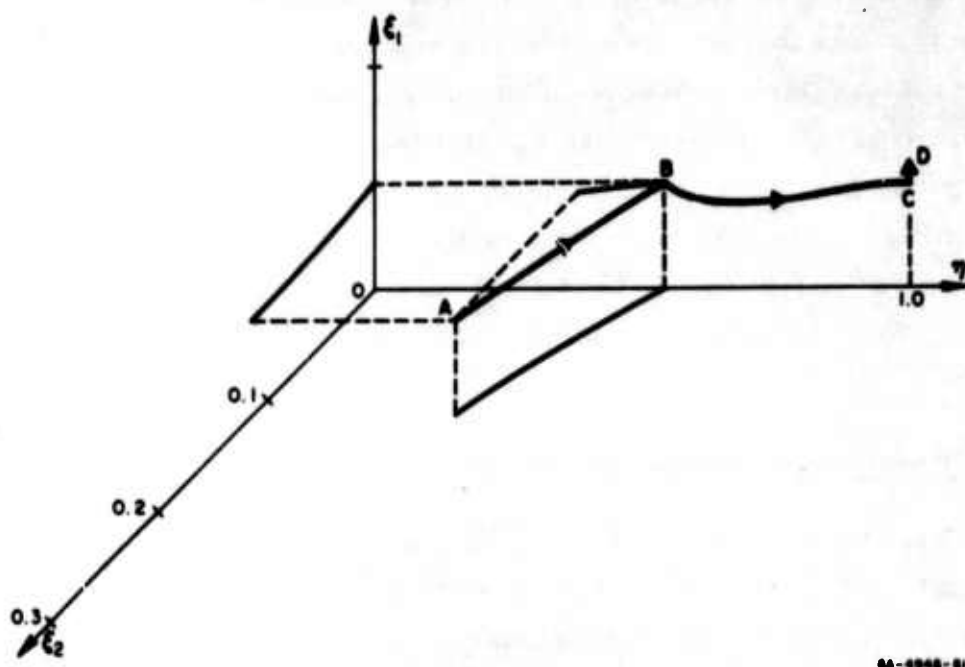
FIG. 6.7 TRAJECTORY OF (ξ_1, ξ_2, η) FOR $\alpha = 0.656$ AND $\lambda = 15$

113

both for $\lambda = 15$ which starts motion by mechanism 3 (see Fig. 6.5 or Table 6.1). In the case of the smaller value of α Fig. 6.6 shows the trajectory starting at A and intersecting the plane $\eta = 1$ at B which corresponds to the value $\rho_0 = 0$. At this point of intersection the inner hinge circle has reached the center and the trajectory continues along BC in the plane $\eta = 1$ which corresponds to mechanism 2b. It next intersects the plane $\xi_2 = 0$ at C which corresponds to the value $\rho_2 = 0$. At this point of intersection the outer hinge circle has reached the support and the trajectory continues along CD, the line of intersection of the planes $\xi_2 = 0$ and $\eta = 1$, corresponding to motion by mechanism 1. Figure 6.7 for $\alpha = 0.656$ can be interpreted in a similar manner. Figures 6.8 and 6.9 show the trajectories ABCD in ρ_0, ρ_1, ρ_2 space.

Figures 6.10 and 6.11 show the variation of ρ_0, ρ_1, and ρ_2 with τ in all phases for values of α equal to 0.438 and 0.656 respectively, both for $\lambda = 15$. In each case the starting values of ρ_1 are close to the loading radius α with ρ_0 and ρ_1 almost equally spaced on either side (see Table 6.1). The three radii are constant during phase 1a. The magnitudes of the average velocities in phase 1b are comparable. During phase 1b and, in Fig. 6.11, during phase 1c the values of ρ_0' are almost constant. During phase 2, ρ_0 is almost constant in Fig. 6.11 for $\alpha = 0.656$ unlike that in Fig. 6.10 but like that in Fig. 6.12 which has been included to allow a comparison with the case $\alpha = 1$ ($\lambda = 15.7$). The final value of τ, i.e., τ_3, increases with α which is to be expected because the work input increases with α.

5. Results and Conclusions

For three values of α Fig. 6.13 shows the relationship among the final central deflection δ, the impulse per unit area I, and the pressure p_m in the nondimensional form of λ versus $mM_o\delta/I^2R^2 = \nu$.
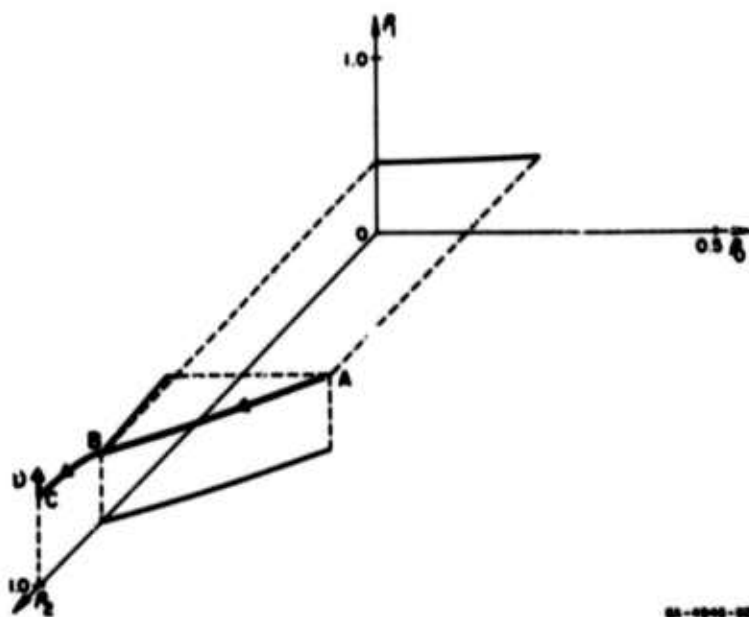
FIG. 6.8   TRAJECTORY OF (ρ_0, ρ_1, ρ_2) FOR $\alpha = 0.438$ AND $\lambda = 15$
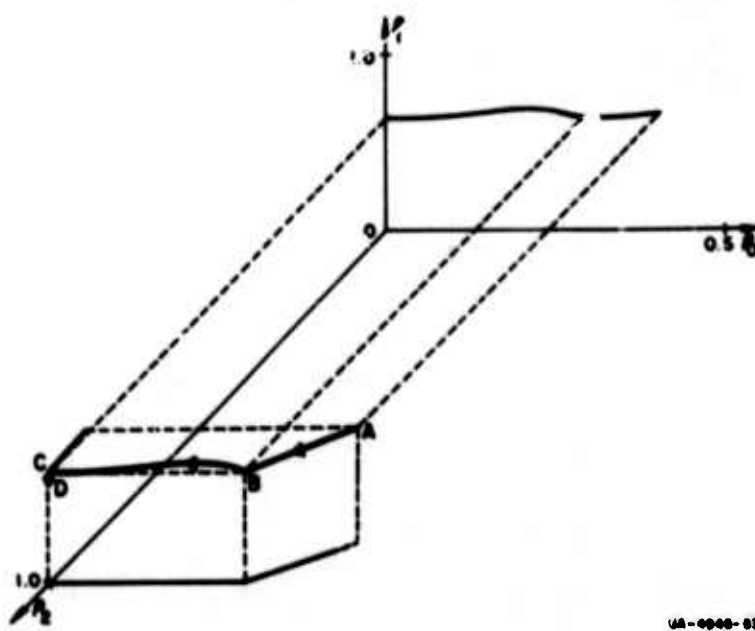
FIG. 6.9   TRAJECTORY OF (ρ_0, ρ_1, ρ_2) FOR $\alpha = 0.656$ AND $\lambda = 15$

115
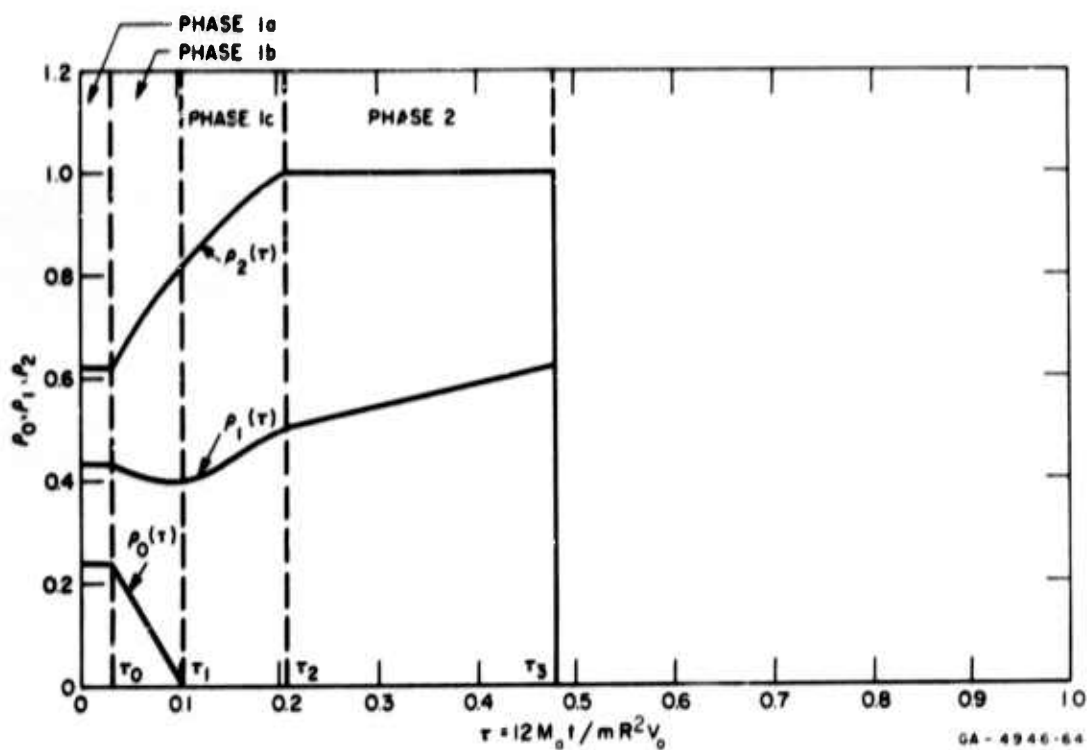
FIG. 6.10 VARIATION OF ρ_0, ρ_1, AND ρ_2 WITH τ FOR $\alpha = 0.438$ AND $\lambda = 15$
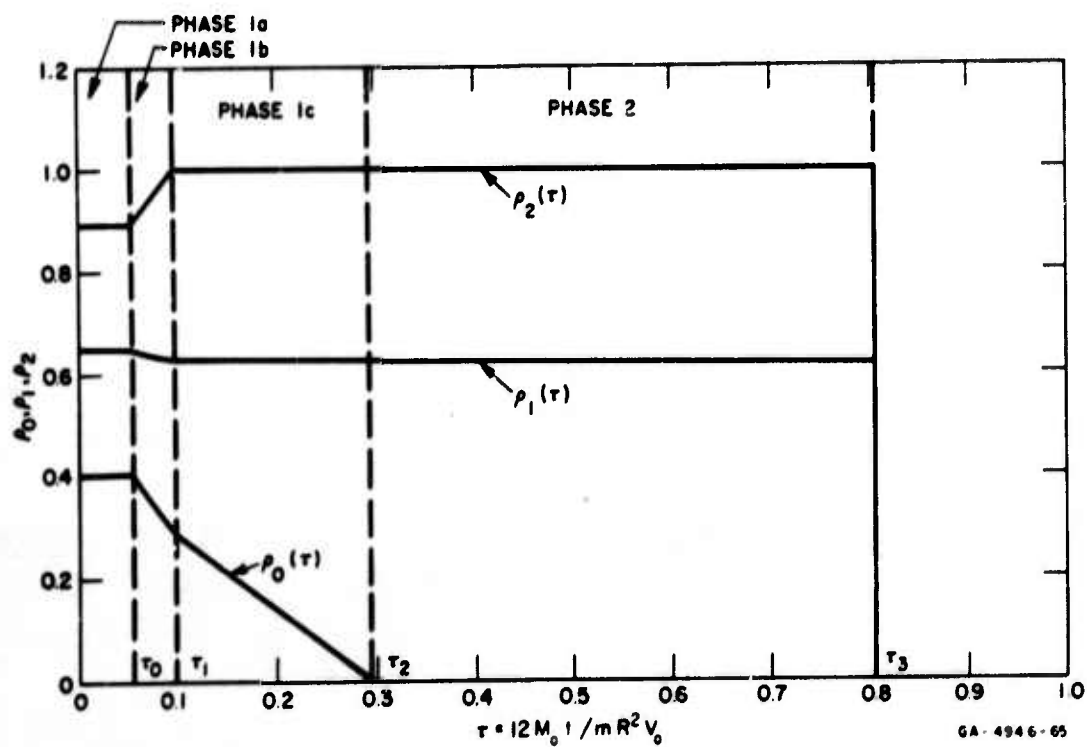
FIG. 6.11 VARIATION OF ρ_0, ρ_1, AND ρ_2 WITH τ FOR $\alpha = 0.656$ AND $\lambda = 15$

116
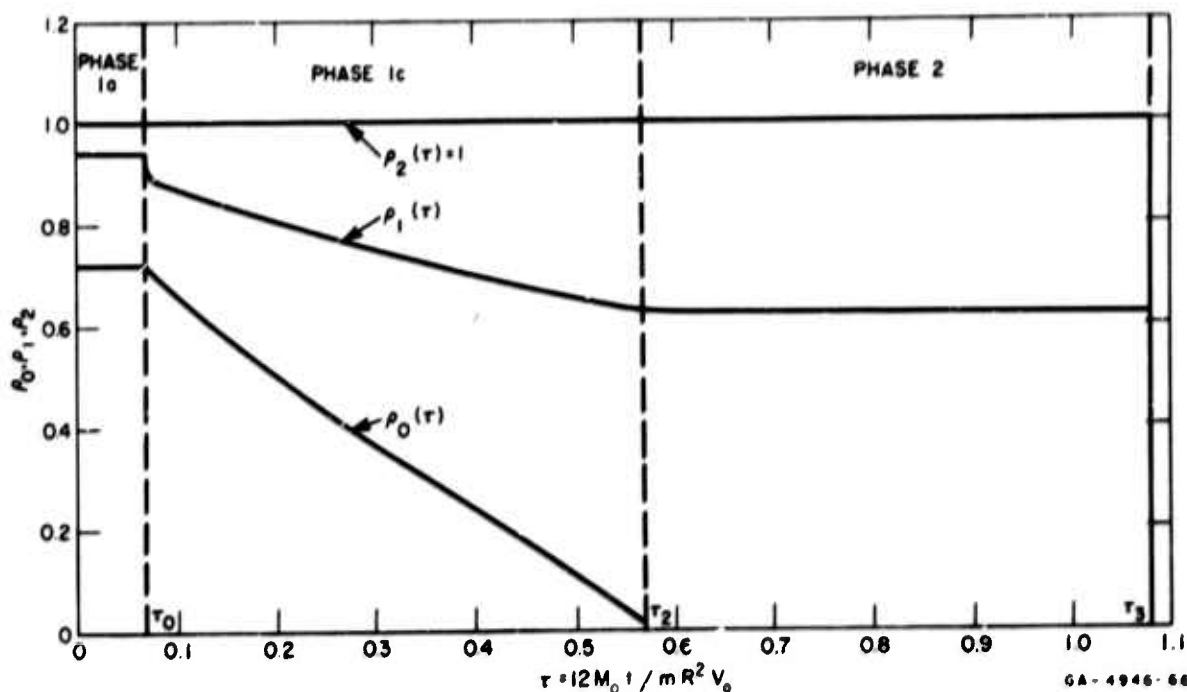
FIG. 6.12 VARIATION OF ρ_0, ρ_1, AND ρ_2 WITH τ FOR $\alpha = 1$ AND $\lambda = 15.7$

The curve for $\alpha = 1.0$ was obtained from the results of Section V. The three curves are alike. They start from the value $\lambda = 1$ where $\delta = 0$ and without curvature change tend monotonically toward vertical asymptotes. The location of these asymptotes have not been found for $\alpha = 0.438$ and $\alpha = 0.656$ but would be determined by considering the case of an ideal impulse ($\lambda = \infty$). However, judging by the case $\alpha = 1.0$ for which the asymptote is known, the value of ν when $\lambda = 100$ is sufficiently close. These values are 0.0212 and 0.0456 for α equal to 0.438 and 0.656 respectively. Figure 6.14 is another way of representing the same information and is essentially a pressure-impulse diagram.

Figure 6.15 is a nondimensional plot relating the pressure to the loaded area considering as a parameter ν which is proportional to the ratio δ/I^2. By treating both impulse and permanent central deflection as fixed quantities the curves show how the pressure must be increased as the loaded area decreases in order to maintain δ.

117
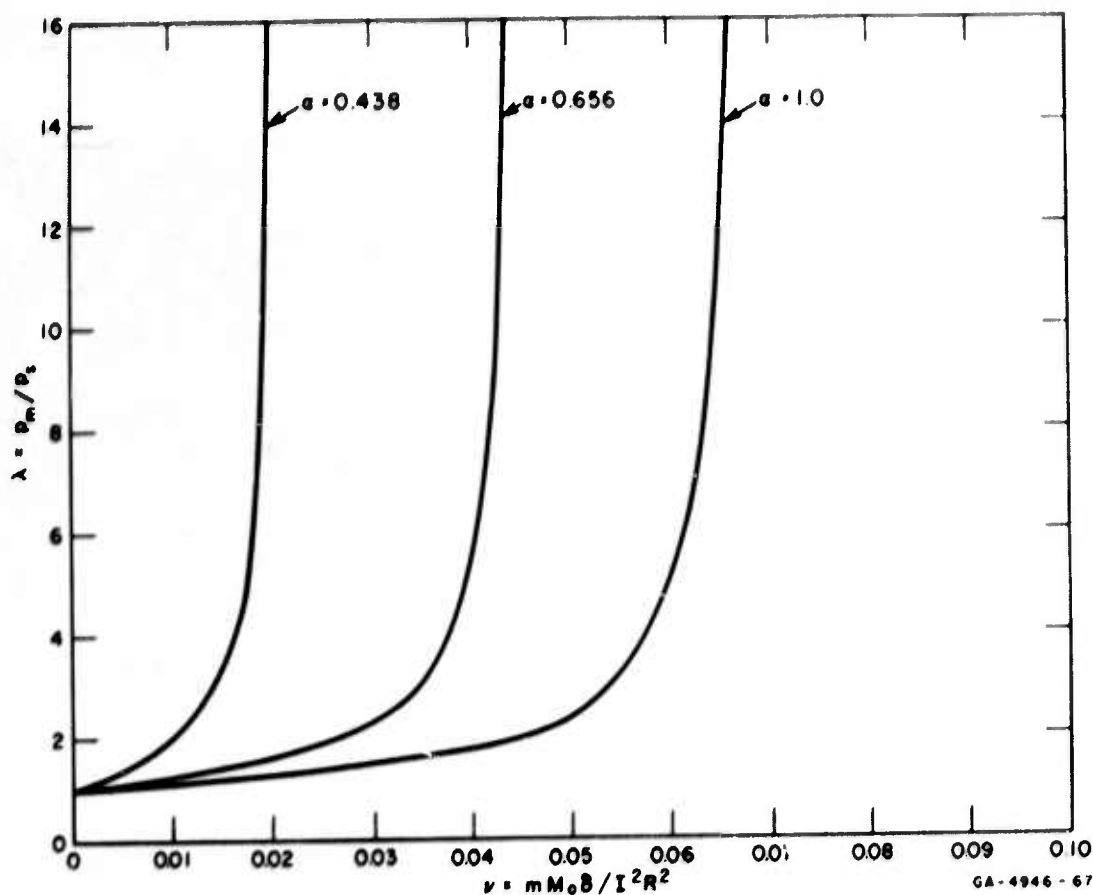
FIG. 6.13   RELATIONSHIP AMONG δ, λ AND I

From Figs. 6. 13, 6. 14 and 6. 15 the following conclusions can
be drawn:

(1)   For a given impulse, the central deflection δ increases
       monotonically with the pressure p_m becoming a maximum
       when the pressure is infinite, that is, when the given
       impulse is applied as an ideal impulse.

(2)   Again for a given impulse, consideration of how δ increases
       with λ in Fig. 6. 13 reveals that for $\alpha > 0.438$ the central
       deflections are greater than 85 percent of that due to an ideal
       impulse for pressures about seven times the corresponding
       static collapse pressure, that is, whenever $\lambda > 7$. Below
       this value of λ the decrease of λ with δ is quite pronounced.

118

(3) For a given central deflection δ , Fig. 6.14 shows that
for $\lambda > 7$ ($\alpha > 0.438$) the increase in impulse, over the
ideal impulse, necessary to maintain the given deflection
is less than 7 percent. A large increase in impulse is
required to maintain δ as λ decreases further, especially
in the range $1 < \lambda < 3$.

(4) For a given permanent central deflection δ and a given
impulse I Fig. 6.15 shows that the pressure required to
maintain δ increases rapidly as the loaded area decreases,
especially for $\alpha < 0.6$ (for the values of ν shown).
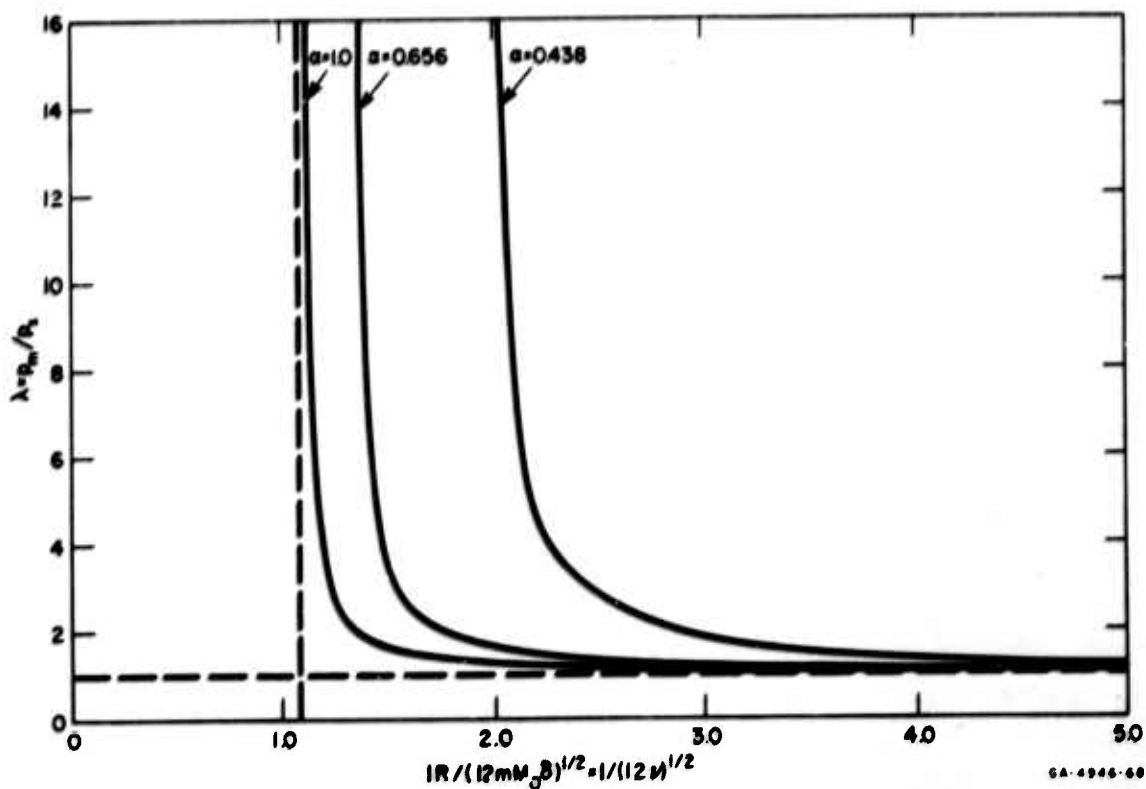
FIG. 6.14 PRESSURE-IMPULSE DIAGRAM

6. Description of Experiments

Circular plates of 6061-T651 aluminum with thicknesses of 1/8,
3/16 and 1/4 inch, clamped at either 8-inches or 12-inches diameter,

119
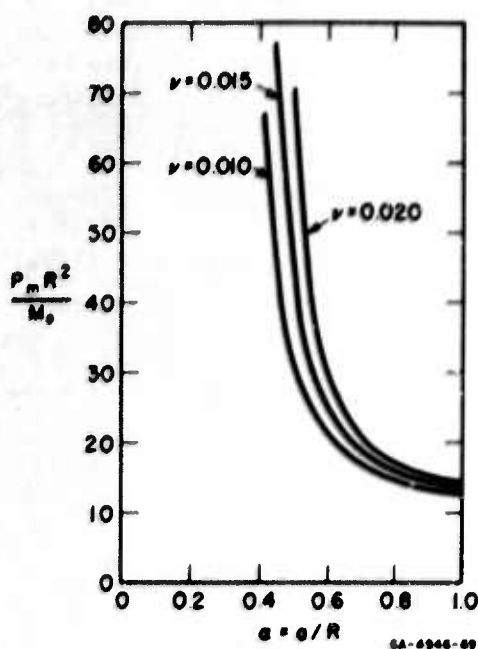
FIG. 6.15 VARIATION OF PRESSURE
WITH LOADED AREA

were subjected to pulses generated
in an oxyacetylene shock tube having
a spring-mass system against each
plate. The experimental arrange-
ment is shown in Fig. 6.16. Thick
steel annular supports provided
clamping against rotation only, a
ring spacer keeping their distances
apart slightly greater than the plate
thickness. Apart from circumferen-
tial membrane forces and unavoid-
able frictional effects the plate
material was allowed to displace
freely inwards during deformation.
To ensure good clamping the overall
diameters of the plates tested vere
9 1/2 and 15 inches but to minimize
the build-up of membrane forces
they were slotted radially at about 1/2-inch intervals around the rim.
The lengths of the slots were such that their ends did not pass over the
support circle during deformation. Figure 6.17 shows two plates of
different diameter after deformation.

Two types of pulse were used and their shapes were taken to be
those recorded under a similar configuration by a rod gage. They are
therefore the pressures acting on a fixed target and they imply the assump-
tion that the modification of the pulse due to plate motion is small. The
first pulse is that of Fig. 2.8(d) with a peak pressure p_m = 865 lb/in^2
and an impulse (area under pressure-time curve) I = 0.363 lb-sec/in^2.
The diagram and table shown opposite the pressure record gives the
configuration. The second pulse used in the experiments is that of
Fig. 2.9(e) with a peak pressure p_m = 485 lb/in^2 and an impulse
I = 0.209 lb-sec/in^2.

120

FIG. 6.16   EXPERIMENTAL ARRANGEMENT

Tensile tests performed with the Instron machine on standard ASTM specimens taken with and across the direction of rolling of the plate material provided stress-strain diagrams from which the yield stress was determined.   The yield stress is here defined as the stress
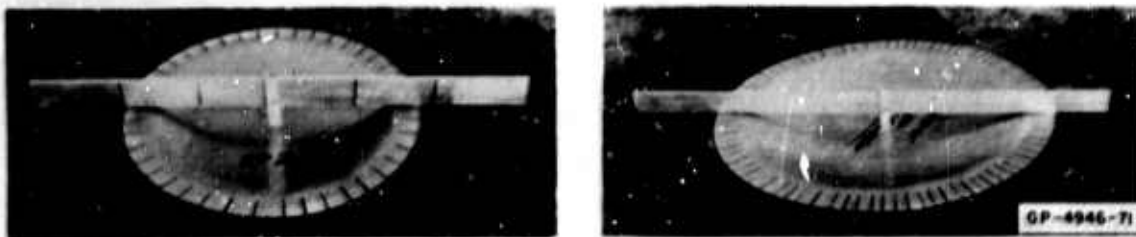
FIG. 6.17 TWO PLATES AFTER DEFORMATION

at the point of intersection of the straight line approximations to the
elastic and strain-hardening portions of the stress-strain diagram.
An average was taken of the yield stresses obtained from specimens
with and across the rolling direction.

After the blast-loading tests, the permanent central deflections
δ_{ex} were measured.

7.   Experimental Results and Observations

The results of the experiments described above are presented
in Table 6.2 and Fig. 6.18. Correlation with the predictions of the
rigid-plastic theory takes place through the ratio δ_{ex}/δ_{th} of the
central deflections in Table 6.2 and by means of the λ versus
$IR/(12mM_o\delta)^{1/2}$ plot of Fig. 6.18 which is a form of p-I diagram.

The main observation is that the central deflection ratios
δ_{ex}/δ_{th}, by ranging from 0.041 to 0.416, show that the theory over-
estimates the central deflections from the present experiments by
factors ranging from about 2 1/2 to 24. The plates are much stronger
than predicted for the following reasons:

(1)   In the rigid-plastic theory the effects of elastic strain-
       energy and vibrations, strain-hardening, and strain-rate
       are neglected, all of which add strength to a structure.
       Among these effects it is probably the elastic strain-
       energy and vibrations that are dominant in the present
       experiments. The plate material, 6061-T651 aluminum,
       was chosen because it shows little strain-hardening and
       is insensitive to strain-rate.

122

(2) If the deflections become large enough membrane forces become significant and the theory considers a bending action only. However, in Table 6.1 it can be seen that the final values of δ_{ex}/R are not large enough to allow considerable build-up of membrane forces [1.15].

(3) Frictional and circumferential membrane forces at the support give the plate added strength.

(4) The experimental pulse is not rectangular (see Figs. 2.8(d) and 2.9(e)). For a given impulse a rectangular pulse inflicts the greatest damage among blast pulses. This has not been proved in general but is true in all known solutions, for example, in the clamped beam problem of Section 3.

(5) The applied impulse is probably less than that recorded against a rigid target. Comparison of fixed target impulses obtained from rod-gage records and completely free or unrestrained target impulse from photodiode velocity measurements indicate considerable falling off of impulse due to the mobility of the target (see Section 2). It is also probable that the pulse shape changes with the mobility of the target.

Among the above reasons for the unsatisfactory correlation, the mobility of the target is considered the most important. This means that the impulse imparted is less than that assumed and that the deflection is proportional to the square of the impulse. For ideal impulses on simply-supported plates of 6061-T651 aluminum the correlation in the range of δ_{ex}/R used here is $\delta_{ex}/\delta_{th} \approx 0.6$ [1.15] whereas the best value in Table 6.2 is 0.42. In Table 6.2 it can be seen that for a given plate radius and assumed pulse the correlation worsens as the plate becomes thinner. This observation points to the effect of target mobility.

The interaction of the elastic vibration modes with the applied pressure mechanisms is probably also very important, especially since the pulse times (see Figs. 2.8(d) and 2.9(e)) are greater than the response time or quarter period $T/4$ of the fundamental symmetric mode of vibration for each plate. For the plates listed in Table 6.2 the response times are listed in Table 6.3.

Table 6.2
EXPERIMENTAL RESULTS

Radius R (inches)	Thickness d (inch)	$\alpha = \frac{a}{R}$	Yield Stress σ_o (lb/in²)	Static Collapse Pressure P_s (lb/in²)	Peak Pressure P_m (lb/in²)	$\lambda = \frac{P_m}{P_s}$	Impulse I (lb-sec/in²)	Central Deflection δ_{ex} (inch)	$\frac{IR}{\sqrt{12mM_o}\,\delta_{ex}}$	$\frac{\delta_{ex}}{R}$	$\frac{\delta_{ex}}{th}$
6	1/4	.438	41,800	460	865	1.88	.363	.26 / .25	6.07 / 6.18	.043 / .042	.245 / .236
	3/16	"	39,300	243	"	3.56	"	.44 / .44	7.43 / 7.43	.073 / .073	.098 / .098
	1/8	"	41,400	114	"	7.59	"	.71 / .71	10.48 / 10.48	.118 / .118	.041 / .041
	3/16	"	39,300	243	485	1.99	.209	.16 / .24	7.33 / 5.99	.027 / .040	.155 / .233
	1/8	"	41,400	114	"	4.25	"	.34 / .33	9.00 / 9.13	.057 / .055	.063 / .061
4	1/4	.656	41,800	608	865	1.42	.363	.33 / .33	3.59 / 3.59	.083 / .083	.416 / .416
	3/16	"	39,300	322	"	2.69	"	.41 / .42	5.12 / 5.06	.103 / .105	.096 / .099
	1/8	"	41,400	151	"	5.72	"	.74 / .74 / .70	6.82 / 6.82 / 7.02	.185 / .185 / .175	.045 / .045 / .042
	3/16	"	39,300	322	485	1.51	.209	.24 / .24 / .24	3.84 / 3.84 / 3.84	.06 / .06 / .06	.313 / .313 / .313
	1/8	"	41,400	151	"	3.21	"	.41 / .42	5.28 / 5.21	.103 / .105	.08? / .087

Radius of loading   a   =   2 5/8 inches

Mass density ρ =   0.000253 lb-sec²/in⁴

Mass   m   = ρd lb-sec²/in³

Plastic moment M_o = $\sigma_o d^2/4$ lb-in/in

124
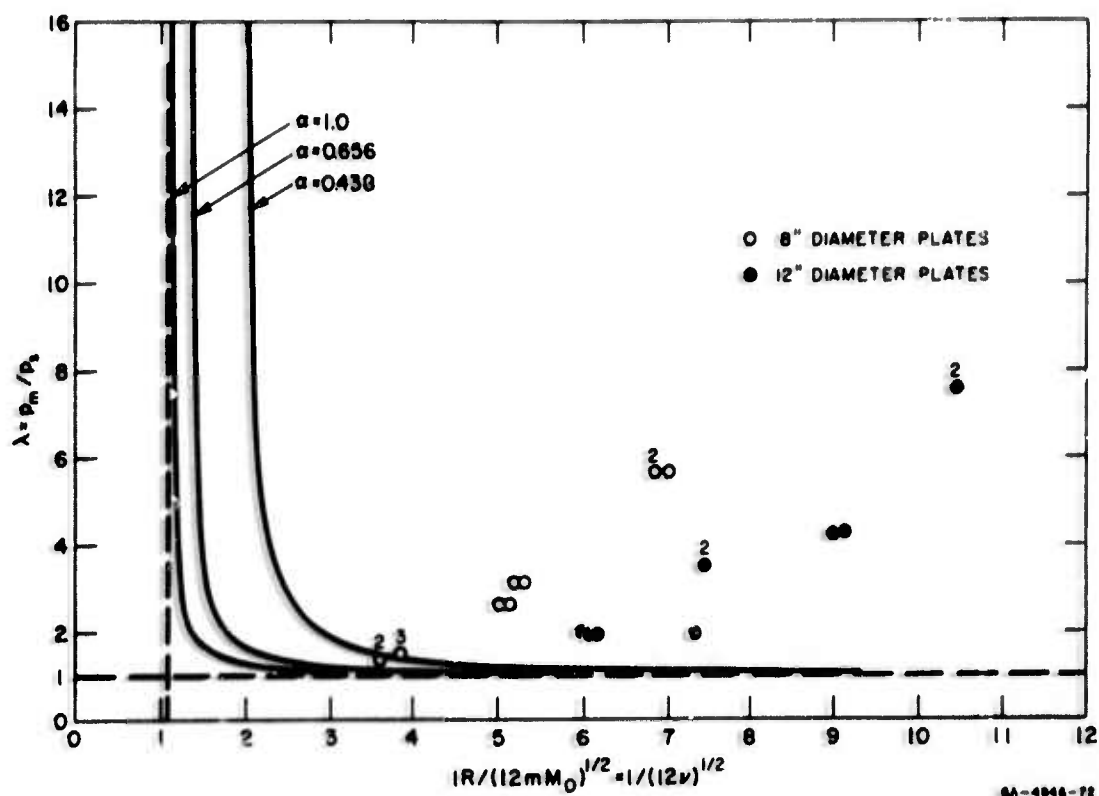
FIG. 6.18 THEORETICAL CURVES AND EXPERIMENTAL POINTS

Table 6.3

RESPONSE TIMES OF THE FUNDAMENTAL MODES

Radius a (inches)	Thickness d (inch)	Response Times T/4 (μsec)
6	1/4	335
	3/16	446
	1/8	669
4	1/4	149
	3/16	198
	1/8	297

125

NOMENCLATURE

a	loading radius
d	plate thickness
I	impulse
m	mass per unit area
M, N	radial and circumferential components of moment
M_o	fully plastic moment $\sigma_o d^2/4$
p	pressure
p_m	peak pressure
p_s	static collapse pressure
r	radial coordinate
r_s	radius of plastic regime boundary (static solution)
r_o, r_1, r_2	radii of plastic regime boundaries (dynamic solution)
R	plate radius
t	time
t_o	pulse duration
t_1	time at end of phase 1b
t_2	time at end of phase 1c
t_3	time at end of phase 2 (motion ceases)
T	fundamental period of plate vibration
V	velocity of plate center
V_o	$V(t_o)$
w	plate deflection
α	a/R
$\delta, \delta_3, \delta_{th}$	$w(o, t_2)$, plate central deflection at time $t = t_2$ (final deflection)
δ_o	$w(o, t_o)$, plate central deflection at time $t = t_o$
δ_1	$w(o, t_1)$, plate central deflection at time $t = t_1$
δ_2	$w(o, t_2)$, plate central deflection at time $t = t_2$
δ_{ex}	experimental final central deflection

126

NOMENCLATURE (Continued)

η $\qquad\qquad\qquad\qquad$ $1 - \rho_o/\rho_1$

λ $\qquad\qquad\qquad\qquad$ P_m/P_s

λ_1, λ_2 $\qquad\qquad\qquad$ mechanism bounds on λ

ν $\qquad\qquad\qquad\qquad$ $mM_o \delta/I^2 R^2$

ξ_1 $\qquad\qquad\qquad\qquad$ $\ell n(1/\rho_1)$

ξ_2 $\qquad\qquad\qquad\qquad$ $\ell n(1/\rho_2)$

ξ_3 $\qquad\qquad\qquad\qquad$ η

ρ $\qquad\qquad\qquad\qquad$ r/R

ρ_o, ρ_1, ρ_2 $\qquad\qquad$ r_o/R, r_1/R, r_2/R

$\rho_o^{(0)}, \rho_1^{(0)}, \rho_2^{(0)}$ $\qquad$ initial values of ρ_o, ρ_1, ρ_2

ρ_s $\qquad\qquad\qquad\qquad$ static collapse pressure

σ $\qquad\qquad\qquad\qquad$ $\left[\ell n(r_2/r_1) + 1 - r_o/r_1 \right]^{-1}$

σ_o $\qquad\qquad\qquad\qquad$ yield stress

τ $\qquad\qquad\qquad\qquad$ $12M_o t/mR^2 V_o$

$\tau_o, \tau_1, \tau_2, \tau_3$ $\qquad$ $12M_o t_o/mR^2 V_o$, $12M_o t_1/mR^2 V_o$, $12M_o t_2/mR^2 V_o$, $12M_o t_3/mR^2 V_o$

τ' $\qquad\qquad\qquad\qquad$ $12M_o t/mR^2$

τ_o' $\qquad\qquad\qquad\qquad$ $12M_o t_o/mR^2$

This page intentionally left blank.

SECTION VII

MATHEMATICAL MODEL OF SPRING-MASS SYSTEM

1. Introduction

In this section is described a simple mathematical model of the layered media used in the shock-tube experiments of Section 2. The experimental configurations and corresponding pressure-time records are shown in Figs. 2.5 to 2.9. Among these, the records of Figs. 2.9(a), (d), and (3) have been chosen for comparison with the predictions of the mathematical model. In the photodiode experiments the configuration of Fig. 2.9(e) was used against a free aluminum disk and the (x, t) plot of the disk, shown in Fig. 2.16, is compared with the predictions of the model.

2. Spring-Mass System

Instead of attempting the solution of the complicated problem of finite amplitude wave propagation through the layered media, a very simple model is considered. This consists of a spring-mass system as illustrated in Fig. 7.1. The mass of foam and Mylar are assumed to be concentrated at the ends of each massless spring. The spring constants are based on the stress-strain relationship of polyurethane foam (5 lb/ft^3) shown in Fig. 7.2. This stress-strain curve is itself approximate since it was obtained from a compression test on an unconfined specimen.
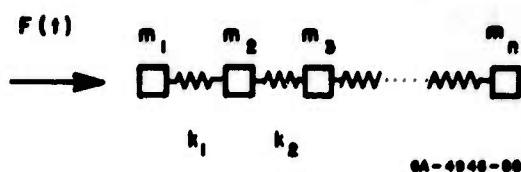
FIG. 7.1 SPRING-MASS-SYSTEM

As a simplification this stress-strain curve is approximated by two straight lines or a straight line and a cubic curve as shown in Fig. 7.3. The foam is assumed to compress to B or E under negligible
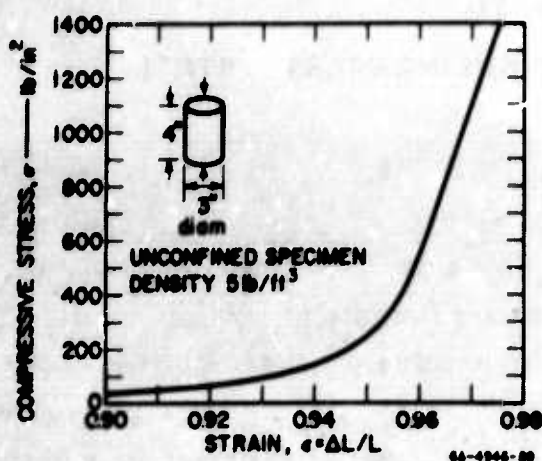
FIG. 7.2 STRESS–STRAIN DIAGRAM
FOR POLYURETHANE FOAM
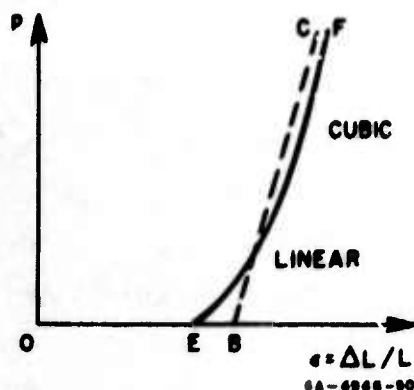
FIG. 7.3 POLYURETHANE SPRING
PROPERTIES

pressure and under further compression behave like a linear (BC) or
cubic (EF) spring.

If the displacements of the masses m_1, m_2, ... are x_1,
x_2, ... the equations of motion are

$$m_n \ddot{x}_n - f_{n-1} + f_n = \begin{cases} F(t) & n = 1 \\ 0 & n \neq 0 \end{cases} \qquad (7.1)$$

in which

$$f_n = \begin{cases} k_n(x_n - x_{n+1}) & \text{linear spring} \\ \bar{k}_n(x_n - x_{n+1})^3 & \text{cubic spring} \end{cases}$$

and

$$f_o \equiv 0$$

The dots in (7.1) denote differentiation with respect to time. If there
are N springs and N masses attached to a rigid target (an infinite
N + 1 th mass) the final equation in the set (7.1) consisting of N
equations requires

$$f_n = \begin{cases} k_N x_N & \text{linear spring} \\ \bar{k}_N x_N^3 & \text{cubic spring} \end{cases}$$

130

If there are N springs and $N+1$ masses, the last being the relatively heavy aluminum disk of the photodiode experiments the final equation in the set (7.1) consisting of $N+1$ equations requires

$$f_{n+1} = 0$$

3. Solution of the Differential Equations

In the set of Equations (7.1) the masses m_n are obtained from the densities and dimensions of the styrofoam, polyurethane foam and Mylar (and aluminum disk when used). The spring constant k or $\bar{k}$ depends on the choice made for B or E in Fig. 7.4 when fitting the experimental curve in Fig. 7.2. It also depends on the length of each foam layer.

The force applied to the mass m_1 is taken in the form

$$F(t) = F_m e^{-\alpha t} \tag{7.2}$$

The numerical value of F_m and α are based on the pressure caused by a shock wave from an oxyacetylene gas acting on a rigid wall and were obtained by fitting curves to rod-gage records similar to that shown in Fig. 2.3. The experimental arrangement for these measurements is that of Fig. 2.1.

The initial conditions are $x_n(o) = \dot{x}_n(o) = 0$.

For the solution of Equations (7.1) the predictor and corrected method of numerical integration has been used. In particular the method devised by Clippinger [7.1] and Hamming [7.2] has been used with the B5500 computer [7.2, 7.4]. The stability of the methods are discussed in References [7.3] and [7.5].

131
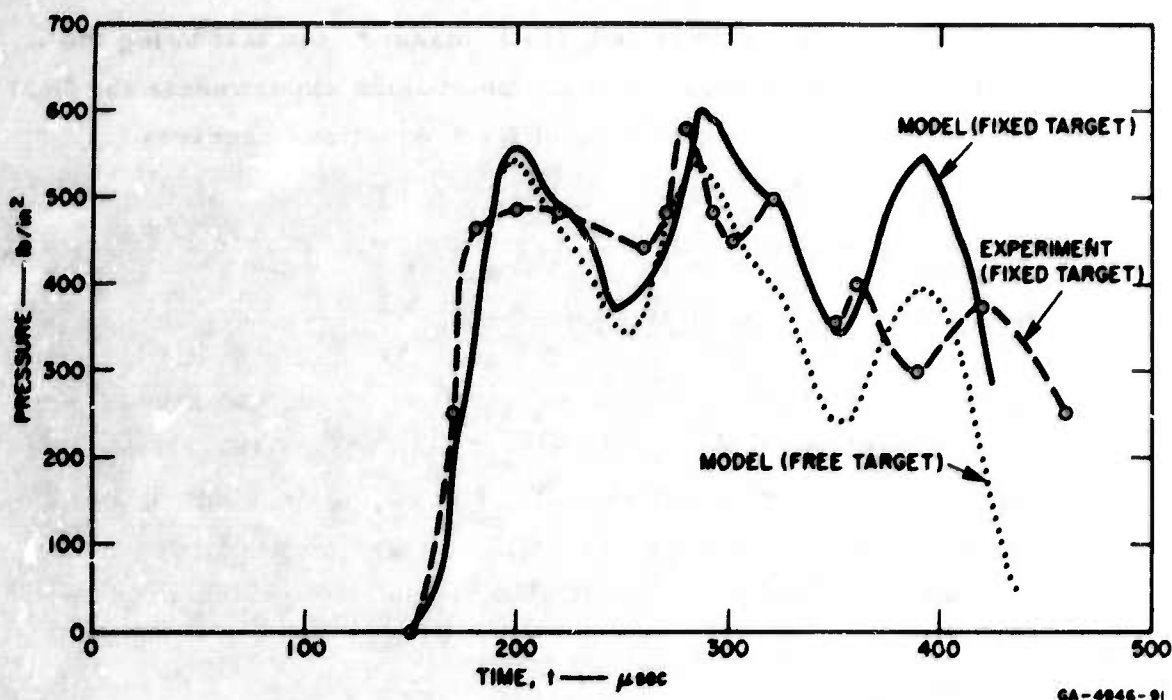
FIG. 7.4 EXPERIMENTAL AND MODEL PULSES — CONFIGURATIONS OF FIG. 2.9(e)

4. Numerical Results and Comparisons with Experiment

The first comparison to be made is with the pressure record of Fig. 2.9(e). Corresponding to the layered media of the experiment the mathematical model had 10 masses (and an eleventh infinite mass) and 10 springs. Counting from the loaded end, the first 7 springs were considered cubic with $\bar{k} = 26.6 \times 10^6$ lb/in^3 and the last 3 springs were considered linear with $k = 0.014 \times 10^6$ lb/in, the latter value being taken from a fit of the lower part of the stress-strain curve of Fig. 7.2 because the pressures are lower in this region. An attenuation factor (reduction of the peak pressure of the loading) was used to take account of the plastic nature of the styrofoam piston.

Figure 7.4 shows a comparison of the pressure record of Fig. 2.9(e) with the pressure (on the fixed plane to which the tenth spring was attached) obtained from the model. Bearing in mind the simplicity of the model the agreement is quite good, at least for times up to 250 μsec from the arrival time of the pressure wave. After this

132

time agreement deteriorates. Certain parameters, such as the value of $\bar{k}$ or k and the chosen drop in pressure to simulate the effect of the styrofoam, called above an attenuation factor, were adjusted to aid agreement of experiment and theory.

A similar comparison to the pulses of Figs. 2.9(a) and (d) can be seen in Figs. 7.5 and 7.6 and again agreement is quite good up to 250 μsec from the arrival time of the wave.

In the photodiode experiments the configuration of Fig. 2.9(e) was used against an unrestrained disk. By means of the photodiode technique described in Section II the (x, t) plot of the disk was obtained and is shown in Fig. 2.16 as the curve labeled "experiment". The (x, t) plot obtained from the mathematical model is also shown in Fig. 2.16. Since the transit time of the wave was shorter in the case of the model the "experimental" and "mathematical model" curves were positioned by giving them a point in common at x = 0.0025 inch and t = 50 μsec. The higher transit time observed in the experiments is probably mainly due to the friction between the styrofoam piston and the cylinder wall as the styrofoam deforms plastically. Once again it can be seen that the agreement is quite good. In Fig. 7.4 is shown the pressure acting on the disk and hence the predicted effect of the mobility of the target. The two curves labeled "model (fixed target)" and "model (free target)" clearly exhibit a divergence, that is, the pressure difference increases with time during the period between t = 200 μsec and t = 400 μsec.

It is concluded that the simple mathematical model gives a reasonable account of the behavior of the layered media used in the experimental technique for pulse shaping. The various adjustments of parametric values used to achieve agreement would largely become unnecessary if a less simple but more accurate model were constructed to account for such effects as wave propagation and dissipation.
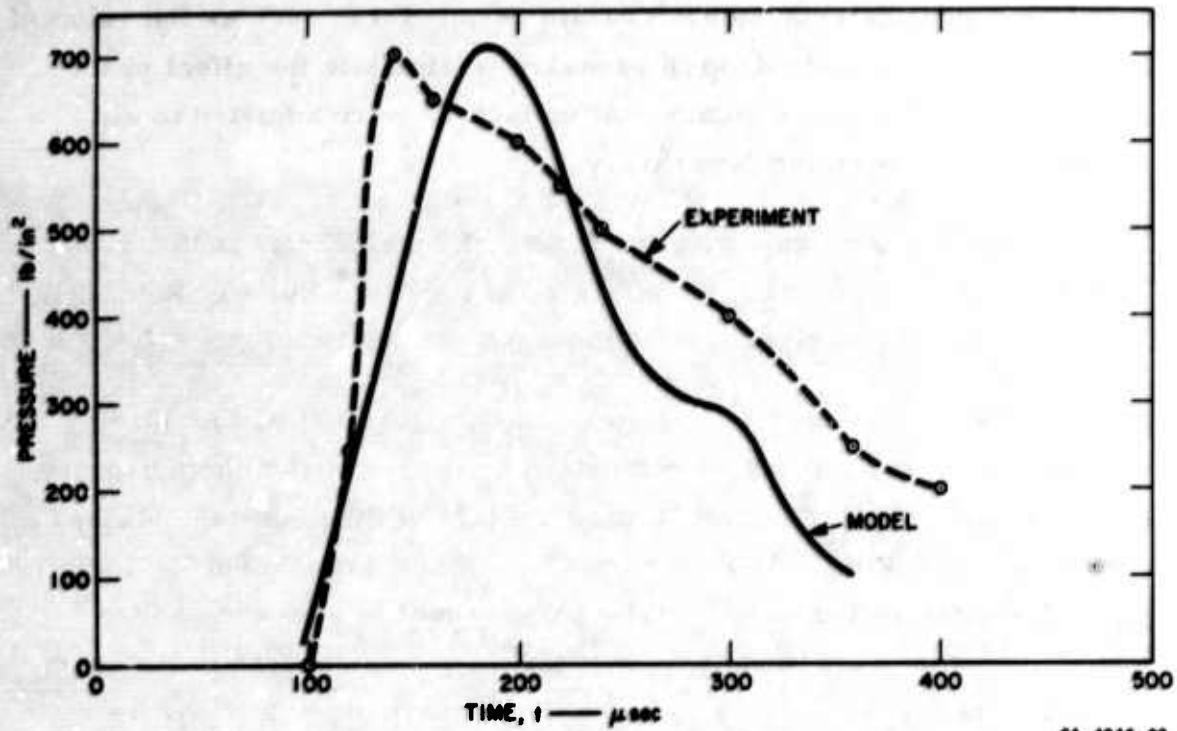
FIG. 7.5 EXPERIMENTAL AND MODEL PULSES — CONFIGURATIONS OF FIG. 2.9(a)
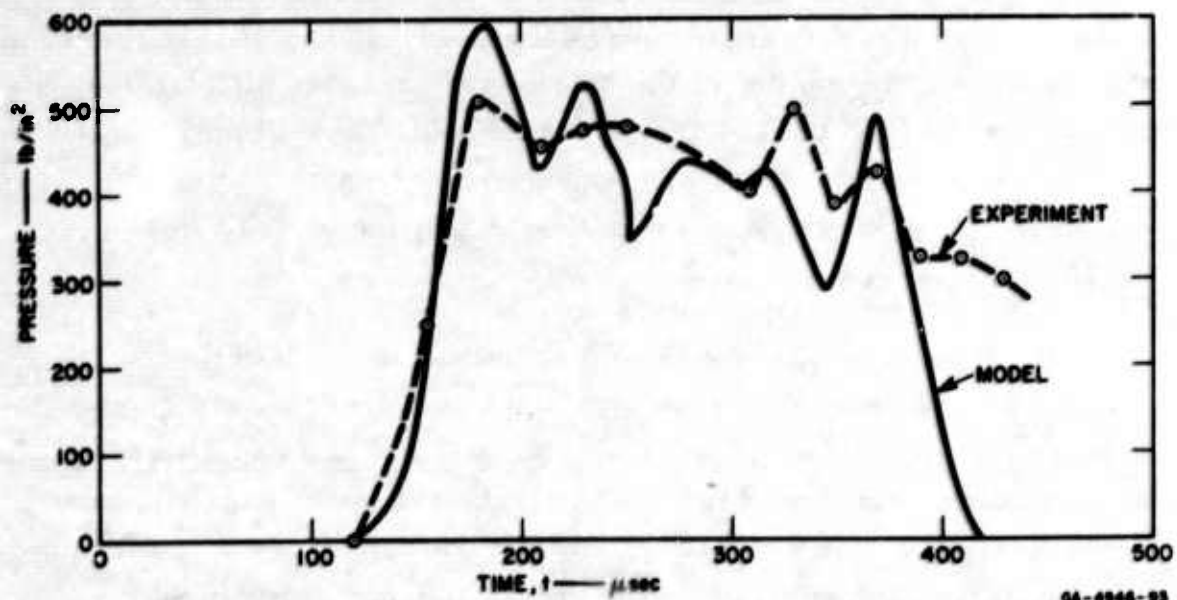
FIG. 7.6 EXPERIMENTAL AND MODEL PULSES — CONFIGURATIONS OF FIG. 2.9(d)

NOMENCLATURE

$F(t)$	force applied to mass m_1
F_m	peak force
k_1 , k_2	spring constants
m_1 , m_2	lumped masses
p	pressure
t	time
x_1 , x_2	mass displacements
ϵ	strain

AFWL-TR-65-81

This page intentionally left blank.

136

SECTION VIII

DEPENDENCE OF DAMAGE ON PULSE SHAPES

1. Introduction

In this section a comparison is made of the permanent deformations of simple rigid-plastic structures caused by pulses of equal peak pressure and impulse. It is proved that for a class of simple rigid-plastic structures the rectangular pulse causes the greatest damage (defined as maximum permanent deformation). Some illustrative examples are given.

2. Simplest Rigid-Plastic System

The dependence on the pulse shape of the maximum displacement in the following system will be found. Consider a pulse $p(t)$ acting on a mass m per unit area having a constant resisting pressure p_s (Fig. 8.1). Whenever $p(t)$ becomes larger than p_s the mass is set in motion, this motion being governed by the equation

$$p(t) - p_s = m\ddot{x} \qquad (8.1)$$

where x is the displacement from the initial at rest position. Dots denote differentiation with respect to time.
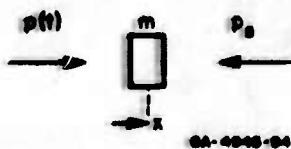
FIG. 8.1 SIMPLEST RIGID-PLASTIC SYSTEM

137

With the initial conditions $x(0) = \dot{x}(0) = 0$ successive integrations of (8.1) yield

$$I(t) - p_s t = m\dot{x} \tag{8.2}$$

$$A(t) - p_s t^2/2 = mx \tag{8.3}$$

In (8.2), $I(t)$ is the impulse at time t (area under pressure-time diagram at time t) and in (8.3), $A(t)$ is the area under the impulse-time diagram at time t. Although it is not necessary, it is convenient to consider pulses with an initial value greater than p_s, i.e., $p(0) > p_s$.

Let the mass come to rest at time $t = t_f$. Then, (8.2) with $\dot{x}(t_f) = 0$ gives $t_f = I_f/p_s$ where $I_f = I(t_f)$. Substituting this value of t_f in (8.3) gives the final displacement in the form

$$mx_f = A_f - p_s t_f^2/2 = A_f - I_f t_f/2 \tag{8.4}$$

in which $A_f = A(t_f)$.

By means of expression (8.4) the values of x_f from pulses of equal peak pressure p_m and impulse I_o are compared to that from a rectangular pulse of pressure p_m and impulse I_o. To clarify the difference between I_o and I_f, they are defined by

$$I_o = \int_0^\infty p(t)dt \quad \text{and} \quad I_f = \int_0^{t_f} p(t)dt$$

Two cases immediately arise depending on whether $I_o = I_f$ or $I_o > I_f$.

(1)   Case 1 $I_o = I_f$

In this case the whole of the pulse is applied before motion ceases. If the pulse ends at time $t = t_o$, then $t_o < t_f$. Since

138

$t_f = I_f/p_s = I_o/p_s$, the duration of motion is the same for all pulses. It also follows that the term $I_f t_f/2 = I_o^2/2p_s$ ($I_f t_f/2$ appears in (8.4)) is the same for all pulses. It therefore remains to study A_f in (8.4). Let t_o' be the duration of a rectangular pulse so that $t_o' = I_o/p_m$. Now

$$I(t) = \int_0^{t < t_o'} p(\tau)d\tau \leq p_m t \quad \text{(equality for rectangular pulse only)}$$

so that

$$A(t) = \int_0^{t < t_o'} I(\tau)d\tau \leq p_m t^2/2 \quad \text{(equality for rectangular pulse only)}$$

Also

$$I(t) = \int_0^{t > t_o'} p(\tau)d\tau \leq I_o$$

so that

$$A(t) = \int_0^{t > t_o'} I(\tau)d\tau = \int_0^{t_o'} I(\tau)d\tau + \int_{t_o}^{t > t_o'} I(\tau)d\tau \leq p_m t_o'^2/2 + I_o(t-t_o')$$

(8.5)

or

$$A(t) \leq I_o t_o'/2 + I_o(t - t_o')$$

The equality in (8.5) holds only for a rectangular pulse and therefore A_f is a maximum for a rectangular pulse. It was shown earlier that the term $I_f t_f/2$ is the same for all pulses of this case. Hence, from (8.4) the maximum permanent displacement occurs when the pulse is rectangular.
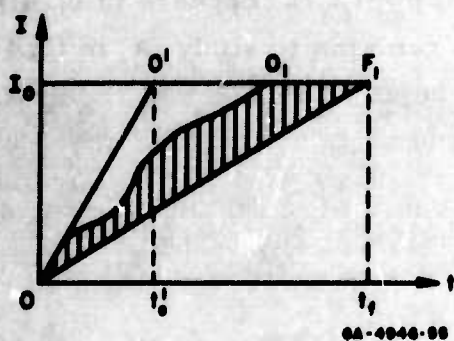
FIG. 8.2 IMPULSE-TIME DIAGRAM —
CASE 1

This result may be illustrated in the impulse-time plane of Fig. 8.2. A_f for a rectangular pulse is the area under $O U' F_1$ whereas for all other pulses A_f is the area under the curve OO_1 and line $O_1 F_1$. The triangular area under OF_1 is $I_f t_f/2$. Thus the final displacement x_f is proportional to the difference of these areas and is shown shaded in Fig. 8.2. The maximum slope of the curve OO_1 is that of OO', i.e., p_m , and OO_1 lies wholly in the triangle $OO'F_1$ the area of which represents x_f when the pulse is rectangular. Note that the slope of OF_1 is p_s . If the curve OO_1 intersects OF_1 the mass comes to rest (see case 2 below).

(2)   <u>Case 2</u> $I_f < I_o$

In this case pressure is still being applied when motion ceases. Since $t_f = I_f/p_s < I_o/p_s$, the values of t_f , unlike case 1, depend on the pulse and are all less than the value of t_f in case 1. However, the reasoning of case 1 applies leading to the rectangular pulse giving the maximum displacement. Expression (8.5) becomes an inequality for $I_f < I_o$ and $A_f - p_s t_f^2/2$ in (8.3) is less than the value corresponding to a rectangular pulse at the same time $t = t_f$.

An illustration of this result can be seen in the impulse-time diagram of Fig. 8.3. Since $I_f/t_f = p_s$ the point F_2 lies on the line OF_1 of Fig. 8.2. The area under the curve OF_2 is A_f and the triangular area under the straight line OF_2 is $I_f t_f/2$. Their difference, shown shaded in Fig. 8.3, is proportional to the displacement x_f . The shaded area is less than the area of triangle $OO'F_1$ which is proportional to the displacement x_f from a rectangular pulse.

140
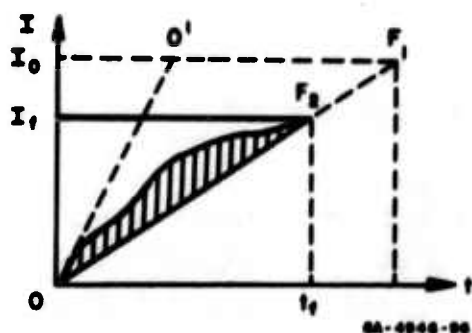
FIG. 8.3 IMPULSE-TIME DIAGRAM —
CASE 2

From the above, the following theorem may be stated. **Theorem:** Among all pulses of equal peak pressures and impulse the rectangular pulse causes the maximum permanent deformation of a rigid-plastic structure that is representable by a mass with a constant resisting force.

The above proof can readily be modified to include certain pathological pulses such as double pulses. It is believed that the theorem can be generalized to include rigid-plastic structures with more complicated representations or modes of deformation. This is illustrated later for the case of a beam subjected to uniform blast loading.

A few examples illustrating the applicability of the above theorem follow immediately.

3.   **Rigid-Plastic Cylinder**

Assuming that the cylinder remains stable [1.9] the equation of motion when a pulse p(t) is applied uniformly around the circumference is

$$p(t) - \sigma_o h/a = m\ddot{w} \tag{8.6}$$

where σ_o is the yield stress, m the mass per unit length of circumference, h the thickness, a the radius, and w is the inward displacement. Dots denote differentiation with respect to time. The static collapse pressure is $p_s = \sigma_o h/a$ and is regarded as the constant resisting pressure, so (8.7) may be written in the form

$$p(t) - p_s = m\ddot{w} \tag{8.7}$$

141

Two integrations of (8. 7) then give

$$mw_f = A_f - p_s t_f^2/2 \qquad (8.8)$$

and (8. 8) is the same result as (8. 3).

Consequently, the maximum permanent deformation occurs when the pulse is rectangular.

4. Simply Supported Circular Plate

A simply supported circular plate of radius R is subjected to a pulse p(t) uniformly distributed over a central circular area of radius a . This is the problem of Section IV and from Eq. (4. 10) the final central deflection is given by

$$mw_f = (12M_0/p_s R^2)(A_f - p_s t_f^2/2) \qquad (8.9)$$

Equation (8. 9) is the same as (8. 3) so that the rectangular pulse causes the greatest central deflection (p_s is given by (4. 6)).

5. Rigid-Plastic Beams

Consider the clamped beam problem of Section III in which a blast pulse is applied uniformly over a central part of the span. The equation of motion governing deformation by mechanism 1 is

$$m\ddot{y}_0 = 3\xi_0(1 - \xi_0/2)[p(t) - p_s] \qquad (8.10)$$

in which y_0 is the central deflection, $\xi_0 = a/\ell$, where a is the loaded length of the half-span ℓ (see Fig. 3. 1), m is the mass per unit length, and p_s is the static collapse pressure given by formula (3. 4), and the dots denote differentiation with respect to time.

142

Two integrations of (8.10) give the final central deflection in the form

$$my_f = 3\xi_o(1 - \xi_o/2)(A_f - p_s t_f^2/2) \tag{8.11}$$

Equations (8.10) and (8.11) are similar to (8.1) and (8.3), and by applying the theorem it can be stated that a rectangular pulse causes the greatest damage. This result is confirmed by the results of Section III in which the central deformations due to a rectangular, triangular, and exponential pulses are compared.

6. Rigid-Plastic Beam with Moving Hinges

As an example of a structure which does not quite have the representation or action called for in the theorem, a simply supported beam subjected to a blast pulse uniformly distributed along the entire span is considered. It is shown that among all pulses with the same peak pressure and impulse the rectangular pulse causes the greatest damage. This is an indication that the theorem can be generalized.

The deformations for this problem have been found by Symonds [8.1] and when not derived the required results will be extracted from this reference.

For peak pressures (assumed to occur immediately at time $t = 0$ (Fig. 5.1)) greater than some value p_1 to be determined, the beam deforms by mechanism 2 in which two hinges form immediately and travel towards midspan. From the equation of motion and the continuity of velocity condition it can be shown that the location of the moving hinges is given by

$$z_o^2 = 6M_o t/I \tag{8.12}$$

where $z_o = L - x_o$ (Fig. 8.4), M_o is the fully plastic moment, and I is the impulse per unit length at time t.

143
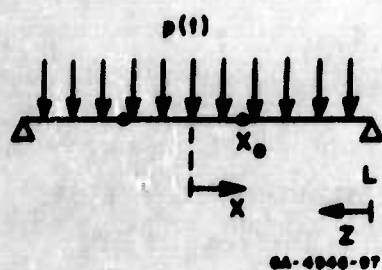
From (8.12) the initial position of the hinge in $0 \leq x \leq L$ is given by

$$z_o^2(o) = 6M_o/p_m \qquad (8.13)$$

From (8.13) the smallest value of p_m for which traveling hinges occur is obtained by setting $z_o(o) = L$. Let this lower bound of p_m be p_1. Then

$$p_1 = 6M_o/L^2 = 3p_s \qquad (8.14)$$

where p_s is the static collapse pressure.

FIG. 8.4 BEAM PROBLEM

Whenever $p_m \leq p_1$ the beam deforms in mechanism 1 with a stationary hinge at the center and the theorem can be applied directly. Consideration is given here to the cases $p_m > p_1$ because the theorem cannot be applied directly.

Let the moving hinges meet at midspan at time $t = t_1$. Then from (8.12) and (8.14)

$$t_1 = I/p_1 \qquad (8.15)$$

Two cases are now considered. In the first the pulse ends at a time $t = t_o$ which is less than the time $t = t_1$, that is, the whole of the pulse has been delivered in phase 1, while the beam is deforming by mechanism 2. In the second the pulse extends into phase 2. This second case may be subdivided into two cases depending on whether or not the pulse has been delivered before motion ceases.

(1) Case 1: Pulse ending in phase 1, $t_o < t_1$

In this case the central deflection and central velocity at time $t = t_1$ are

$$y_o(t_1) = A_1/m \quad \text{and} \quad \dot{y}_o(t_1) = I_o/m$$

144

where I_o is the total impulse and A_1 is the area under the impulse-time diagram at time $t = t_1$. Since I_o is the same for all pulses and A_1 is a maximum for rectangular pulses (see proof of theorem) phase 2 has with the same initial velocity for all pulses but has a maximum initial deflection when the pulse is rectangular. Hence the rectangular pulse gives the maximum final deflection.

The expression giving the final displacement is readily found to be

$$my_o(t_2) = (3A_2 - A_1)/2 - I_o(3t_2 - t_1)/4 \qquad (8.16)$$

where $t_2 = 3I_o/p_1 = 3t_1$ is the time when motion ceases.

(2)   Case 2a: Pulse ending in phase 2, $t_1 < t_o < t_2$

During the time $t_1 < t < t_o$ the equation of motion is

$$m\ddot{y}_o = (3p - p_1)/2 = 3(p - p_s)/2 \qquad (8.17)$$

Noting that $m\dot{y}_o(t_1) = I_1$ and $t_1 = I_1/p$ from (8.15) one integration of (8.17) gives

$$m\dot{y}_o = (3I - p_1 t)/2 \qquad t_1 < t < t_o \qquad (8.18)$$

Noting that $my_o(t_1) = A_1$ a further integration gives

$$my_o = (3A - A_1)/2 - p_1(t^2 - t_1^2)/4 \qquad t_1 < t < t_o \qquad (8.19)$$

During the time $t_o < t < t_2$ (t_2 is the time when motion ceases) the equation of motion is

$$m\ddot{y}_o = -p_1/2 \qquad (8.20)$$

145

Making use of the continuity of velocity and displacement at time $t = t_0$ and hence making use of (8.18) and (8.19) successive integrations of (8.20) yield

$$m\dot{y}_0 = (3I_0 - p_1 t)/2 \qquad\qquad t_0 < t < t_2 \qquad (8.21)$$

$$my_0 = (3A - A_1)/2 - p_1(t^2 - t_1^2)/4 \qquad t_0 < t < t_2 \qquad (8.22)$$

From (8.21) motion ceases at time $t = t_2$ given by

$$t_2 = 3I_0/p_1 \qquad\qquad (8.23)$$

and from (8.22) and (8.23) the displacement at time $t = t_2$ is given by

$$my_0(t_2) = (3A_2 - A_1)/2 - (3I_0 t_2 - I_1 t_1)/4 \qquad (8.24)$$

Before discussing expressions (8.16) and (8.24) that for case 2b will be derived.

(3)   <u>Case 2b</u>: Pulse ending after motion ceases, $t_2 < t_0$

During the whole of phase 2 the equation of motion is (8.17) and the initial displacement and velocity are those of case 2a. Hence the expression for the final deflection is, from (8.19)

$$my_0 = (3A_2 - A_1)/2 - p_1(t_2^2 - t_1^2)/4 \qquad (8.25)$$

where, from (8.18),

$$t_2 = 3I_2/p_1 \qquad\qquad (8.26)$$

Using the result (8.26) for t_2 , (8.26) may be written in the form

$$my_0 = (3A_2 - A_1)/2 - (3I_2 t_2 - I_1 t_1)/4 \qquad (8.27)$$

A comparison is now made of expressions (8.16), (8.24) and (8.27) by means of geometrical considerations in the impulse-time

146

planes of Fig. 8.5(a), (b) and (c). For this purpose it is convenient to rearrange (8.16), (8.24) and (8.27) into the forms

$$my_o(t_2) = (A_2 - I_o t_2/2) + [(A_2 - I_o t_2/2) - (A_1 - I_o t_1/2)]/2 \qquad (8.16)$$

$$my_o(t_2) = (A_2 - I_o t_2/2) + [(A_2 - I_o t_2/2) - (A_1 - I_1 t_1/2)]/2 \qquad (8.24)$$

$$my_o(t_2) = (A_2 - I_2 t_2/2) + [(A_2 - I_2 t_2/2) - (A_1 - I_1 t_1/2)]/2 \qquad (8.27)$$
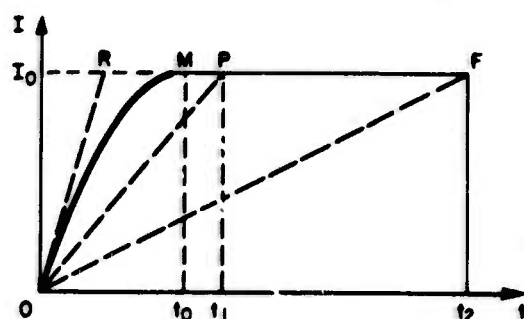
(a) CASE 1

(b) CASE 2

(c) CASE 3

FIG. 8.5 IMPULSE-TIME DIAGRAMS
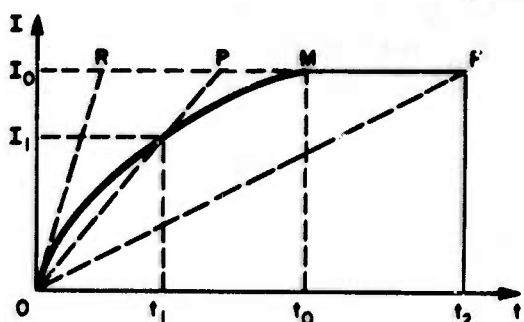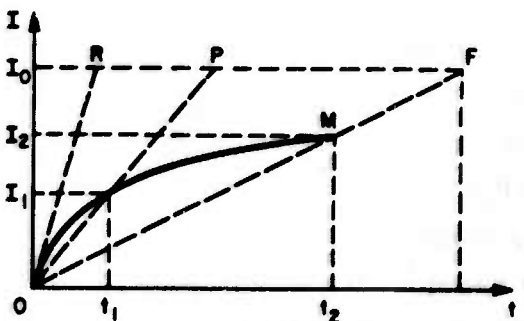
One important feature of the diagrams is that the lines OR, OP, and OF are the same in each. OR is the path that is taken by a rectangular pulse and has a slope equal to the pressure p_m. OP has a slope $p_1 = 6M_o/L^2$ and OF has a slope $p_s = 2M_o/L^2 = p_1/3$. Three typical pulse paths OM are shown, one in each of cases 1, 2a, and 2b.

By algebraically adding the areas represented by the individual terms in each of (8.16), (8.24), and (8.27), it can be seen that each sum is bounded by that for a rectangular pulse, this sum being the triangle ORF plus one-half of triangle OPF. Thus the rectangular pulse causes the greatest deflection.

147

NOMENCLATURE

a	radius of cylinder, half load length on beam
A	area under impulse-time curve
A_1, A_2, A_f	$A(t_1)$, $A(t_2)$, $A(t_f)$
h	thickness of cylinder
$I(t)$	impulse (area under pressure-time curve)
I_o	total impulse
I_1, I_2, I_f	$I(t_1)$, $I(t_2)$, $I(t_f)$
ℓ, L	half span of beam
m	mass
M_o	fully plastic moment
p	pressure
p_m	peak pressure
p_s	static collapse pressure
p_1	mechanism bound on p_m for beams
R	radius of plate
t	time
t_o	pulse duration
t_1	time at end of phase 1
t_2	time at end of phase 2
t_f	time when motion ceases
t_o'	duration of rectangular pulse
w	displacement of cylinder or plate
w_f	displacement at time $t = t_f$, $w(t_f)$
x	displacement of mass
x_f	final displacement $x(t_f)$
x_o	coordinate of moving hinge
y_o	central deflection of beam
y_f	final central deflection of beam $y_o(t_f)$
z_o	$L - x_o$
ζ_o	a/ℓ (a is half load length on beam)
σ_o	yield stress

148

APPENDIX A

FORMULAS FOR THE CENTRAL DEFLECTION OF A CLAMPED BEAM DUE TO RECTANGULAR, TRIANGULAR AND EXPONENTIAL PULSES

In the following, the central deflection δ is in nondimensional form and denoted by ν where $\nu = \delta m M_o / I_1^2 \ell^2$. The notation is that of Section III.

A. **Rectangular Pulse**

    (1) **Mechanism 1**

$$\nu = 3\xi_o^2 (2 - \xi_o)^2 (\lambda - 1)/16\lambda$$

    (2) **Mechanism 2a and 3a**

$$\nu = \xi_o (2 - \xi_o)(2\lambda - 1)/8\lambda - 1/12$$

    (3) **Mechanism 2b**

$$\nu = (\xi_o^2/6)[(2 - \xi_o)/(2 - \xi_o - \xi_o\lambda) + 2\ell n\left\{(2\lambda/3)/(2 - \xi_o - \xi_o\lambda)\right\} + 2]$$

    (4) **Mechanism 3b**

$$\nu = (\xi_o^2/12)[5 - 4\ell n(2\xi_o) - 3(2 - \xi_o)/2\lambda\xi_o]$$

B. **Triangular Pulse**

    (1) $1 \leq \lambda \leq 2$ $0 \leq \xi_o \leq 1$

$$\nu = \xi_o^2 (2 - \xi_o)^2 (\lambda - 1)^3/\lambda^4$$

    (2) $2 \leq \lambda \leq \lambda_1$ $0 \leq \xi_o \leq 1$

$$\nu = \xi_o^2 (2 - \xi_o)^2 (3\lambda - 4)/16\lambda$$

149

(3) $\quad \lambda_1 \leq \lambda \leq 2\lambda_1 \qquad \xi_0 \geq 1/2$

$$\nu = \xi_0^2 (2 - \xi_0)^2 (3\lambda - 4)/16\lambda$$

$$+ (2 - \xi_0)(2 + 3\xi_0^2 - 6\xi_0)(\xi_0/3\lambda)[1 - 3\xi_0(2 - \xi_0)/(6\xi_0 - 3\xi_0^2 - 2)]^3$$

(4) $\quad \lambda \geq 2\lambda_1 \qquad \xi_0 \geq 1/2$

$$\nu = \xi_0(2 - \xi_0)(3\lambda - 2)/12\lambda - 1/2$$

(5) $\quad \lambda \geq 2\lambda_2 \qquad \xi_0 \leq 1/2$

$$\nu = (\xi_0^2/12)[5 - 4 \ln(2\xi_0)] - \xi_0(2 - \xi_0)/6\lambda$$

For the other regions of the failure mechanism diagram
the function Φ is introduced.

$$\Phi = c_1 \sum_{i=1}^{3} a_i (b_2^i - b_1^i) + 64 c_1 c_2 \ln(b_1/b_2)$$

where

$$a_1 = 32[6 + \xi_0\lambda/(2 - \xi_0)]$$

$$a_2 = -12 - \xi_0\lambda/(2 - \xi_0)$$

$$a_3 = 1/3$$

$$b_1 = 8 + \xi_0\lambda(2 - \tau_2)/(2 - \xi_0)$$

$$b_2 = 8 + \xi_0\lambda(2 - \tau_1)/(2 - \xi_0)$$

$$c_1 = (8/3\xi_0^2)[(2 - \xi_0)/\lambda]^4$$

$$c_2 = 8 + 2\xi_0\lambda/(2 - \xi_0)$$

150

(6) $\quad \lambda_1 \le \lambda \le 2\lambda_1 \qquad 0 \le \xi_0 \le 2/5$

$\quad\quad\quad \lambda_1 \le \lambda \le \lambda_2 \qquad 2/5 \le \xi_0 \le 1/2$

$$\nu = \Phi + \xi_0^2 (2 - \xi_0)^2 (3\lambda - 4)/16\lambda - \tau_1^2 \xi_0^2 (2 - \xi_0)^2 (3\lambda - 3 - \tau_1\lambda)/4\lambda^2$$

where

$$\tau_1 = 2[1 - 3(2 - \xi_0)/\lambda(2 - 3\xi_0)]$$

$$\tau_2 = 0$$

(7) $\quad 2\lambda_1 \le \lambda \le \lambda_2 \qquad \xi_0 \le 2/5$

$$\nu = \Phi + \xi_0^2/3 + (\xi_0^2/3)\ln[2\lambda/(12 - 6\xi_0 + 3\xi_0\lambda)]$$

$$\tau_1 = 1$$

$$\tau_2 = 0$$

(8) $\quad \lambda_2 \le \lambda \le 2\lambda_2 \qquad 0 \le \xi_0 \le 2/5$

$\quad\quad\quad 2\lambda_1 \le \lambda \le 2\lambda_2 \qquad 2/5 \le \xi_0 \le 1/2$

$$\nu = \Phi + (\xi_0^2/3)\ln[2\lambda/(12 - 6\xi_0 + 3\xi_0\lambda)]$$
$$+ \xi_0\tau_2^2 (2 - \xi_0)(3 - \tau_2)/6\lambda + 3\xi_0^2 (2 - \xi_0)^2/16$$
$$- 3\tau_1\xi_0^2 (2 - \xi_0)^2 (\lambda - \tau_1)/4\lambda^2$$

where

$$\tau_1 = \lambda(2 - 3\xi_0)/6(2 - \xi_0)$$

$$\tau_2 = 2[1 - 3(2 - \xi_0)/\xi_0\lambda]$$

(9) $\quad \lambda_2 \le \lambda \le 2\lambda_2 \qquad 2/5 \le \xi_0 \le 1/2$

$$\nu = \Phi + \xi_0\tau_2^2 (2 - \xi_0)(3 - \tau_2)/6\lambda + \xi_0^2 (2 - \xi_0)^2 (3\lambda - 2)/8\lambda$$
$$- \xi_0^2 \tau_1^2 (2 - \xi_0)^2 (3 - \tau_1)/4\lambda - 3\xi_0^2 (2 - \xi_0)^2 (\lambda^2 - 4\tau_1^2)/16\lambda^2$$

where

$$\tau_1 = 2[1 - 3(2 - \xi_0)/\lambda(2 - 3\xi_0)]$$

$$\tau_2 = 2[1 - 3(2 - \xi_0)/\xi_0\lambda]$$

C. **Exponential Pulse**

    (1) **Mechanism 1**

$$\nu = (2 - \xi_o)^2 (3\xi_o^2/16\lambda^2)[2\lambda(\tau_f + e^{-\tau_f} - 1) - \tau_f^2]$$

where

$$\tau_f = \lambda(1 - e^{-\tau_f})$$

    (2) **Mechanism 2a and 3a**

$$\nu = (2 - \xi_o)(\xi_o/4\lambda)(\tau_1 + e^{-\tau_1} - 1)$$
$$+ (2 - \xi_o)^2 (3\xi_o^2/16\lambda^2)[2\lambda(\tau_f + e^{-\tau_f} - \tau_1 - e^{-\tau_1}) - \tau_f^2 + \tau_1^2]$$

where τ_f is that of mechanism 1 and

$$\tau_1 = \lambda(6\xi_o - 3\xi_o^2 - 2)(1 - e^{-\tau_1})/3\xi_o(2 - \xi_o)$$

    (3) **Mechanism 2b**

$$\nu = (2 - \xi_o)^2 (\xi_o^3/3) \int_0^{\tau_1} \frac{(1 - e^{-\tau})^2 d\tau}{\xi_o(2 - \xi_o)\tau + \xi_o^2 \lambda(1 - e^{-\tau})}$$
$$+ (2 - \xi_o)^2 (3\xi_o^2/16\lambda^2)[2\lambda(\tau_f + e^{-\tau_f} - \tau_1 - e^{-\tau_1}) - \tau_f^2 + \tau_1^2]$$

where τ_f is that of mechanism 1 and

$$\tau_1 = \lambda(2 - 3\xi_o)(1 - e^{-\tau_1})/3(2 - \xi_o)$$

    (4) **Mechanism 3b**

$$\nu = (2 - \xi_o)(\xi_o^3/3) \int_0^{\tau_1} \frac{(1 - e^{-\tau})^2 d\tau}{\xi_o(2 - \xi_o)\tau + \xi_o^2 \lambda(1 - e^{-\tau})}$$
$$+ \xi_o(2 - \xi_o)(\tau_2 + e^{-\tau_2} - 1)/4\lambda + (2 - \xi_o)^2 (3\xi_o^2/16\lambda^2)[2\lambda(\tau_f + e^{-\tau_f}$$
$$- \tau_1 - e^{-\tau_1}) - \tau_f^2 + \tau_1^2]$$

where τ_f is that of mechanism 1, τ_1 is that of mechanism 2b and

$$\tau_2 = \xi_0 \lambda (1 - e^{-\tau_2})/3 (2 - \xi_0)$$

This page intentionally left blank.

APPENDIX B

FORMULAS FOR THE FINAL DEFORMED SHAPE OF A CLAMPED BEAM DUE TO A RECTANGULAR PULSE

In the following, the deflection y is in nondimensional form and denoted by w where $w = ymM_o/I_1^2 \ell^2$ and $\zeta = x/\ell$. The notation is that of Section III.

A.   Mechanism 1

$$w = 3\zeta_o^2(1 - \zeta)(2 - \zeta_o)^2(\lambda - 1)/16\lambda$$

B.   Mechanism 2a

$$w = (1 - \zeta)(2 + \zeta)/12 - (1 - \zeta_o)^2/4 - \zeta_o(2 - \zeta_o)/8\lambda \qquad 0 \leq \zeta \leq \zeta_2$$

$$w = (1 - \zeta)[(\zeta_o/8\lambda)(2 - \zeta_o)/(1 - \zeta_2) + \zeta_2/6 + 1/12] \qquad \zeta_2 \leq \zeta \leq 1$$

where ζ_2 is given by

$$(1 - \zeta_2)^2 = 3\zeta_o(2 - \zeta_o)/\lambda + 3(1 - \zeta_o)^2$$

C.   Mechanism 2b

$$w = (\zeta_o^2/3\zeta_1)(\zeta_1 - \zeta)[3(2 - \zeta_o)/4\lambda\zeta_1 + 1] - (\zeta_o^2/3)\ell n\zeta \qquad 0 \leq \zeta \leq \zeta_1$$

$$w = (\zeta_o^2/3)\ell n(1/\zeta) \qquad \zeta_1 \leq \zeta \leq 1$$

where

$$\zeta_1 = 3\zeta_o/2 + 3(2 - \zeta_o)/2\lambda$$

D. **Mechanism 3a**

$$w = (1-\xi)(2+\xi)/12 - (1-\xi_0)^2/4 - \xi_0(2-\xi_0)/8\lambda \qquad 0 \le \xi \le \bar{\xi}_2$$

$$w = (1-\xi)(4\xi_0-1)/12 + (\xi_0-\xi)(2-3\xi_0+\xi)/24$$
$$\quad + (1-\xi_0)^2/24 + \xi_0(2-\xi_0)/8\lambda \qquad \bar{\xi}_2 \le \xi \le \xi_2$$

$$w = (\xi_0/8\lambda)(2-\xi_0)(\xi_2-\xi)/(\xi_1-\xi_2)$$
$$\quad + (1-\xi)(4\xi_0-\xi_1)/12 + (1-\xi_0)(1-\xi_1)/8 \qquad \xi_2 \le \xi \le \xi_1$$

$$w = (1-\xi)(8\xi_0-\xi-1)/24 \qquad \xi_1 \le \xi \le 1$$

where

$$\xi_1 = \xi_0 + [3\xi_0(2-\xi_0)/\lambda]^{\frac{1}{2}}$$

$$\xi_2 = \xi_0 - [3\xi_0(2-\xi_0)/\lambda]^{\frac{1}{2}}$$

$$\bar{\xi}_2 = 2\xi_0 - 1$$

E. **Mechanism 3b**

$$w = (\xi_0^2/12)[5 - 3)(2-\xi_0)/2\xi_0\lambda - \ln(2\xi_0)]$$
$$\quad - \xi(2\xi_0-\xi)/12 \qquad 0 \le \xi \le \xi_2$$

$$w = (\xi_0/8\lambda)(2-\xi_0)(\xi_2-\xi)/(\xi_1-\xi_2) + (\xi_0^2/24)[9 - 8\ln(2\xi_0)$$
$$\quad + 2\xi_1/\xi_0] - \xi(\xi_2+2\xi_0)/12 \qquad \xi_2 \le \xi \le \xi_1$$

$$w = (\xi_0-\xi)(7\xi_0-\xi)/24 + (\xi_0^2/24)[5 - 8\ln(2\xi_0)] \qquad \xi_1 \le \xi \le \bar{\xi}_1$$

$$w = (\xi_0^2/3)\ln(1/\xi) \qquad \bar{\xi}_1 \le \xi \le 1$$

where ξ_1 and ξ_2 are those of mechanism 3a and $\bar{\xi}_1 = 2\xi_0$.

156

REFERENCES

1.1 Abrahamson, G. R., "Structural Response of Re-Entry Vehicles to Impulsive Loads (U)," Stanford Research Institute Final Report, AFSWC-TR-61-44, Contract AF 29(601)-2791, 9 June 1961, (SRD).

1.2 Lindberg, H. E., "Impulse Response of an Early A3X Polaris Re-Entry Structure (U)," Stanford Research Institute Final Report, Contract LMSC P.O. 18-10338 Under NOrd-17017, November 1, 1962, (SRD).

1.3 Florence, A. L., "Structural Response of the Mark 6 Re-Entry Vehicle to Impulsive Loads (U)," Stanford Research Institute Final Report, TDR 63-3117, Contract AF 29(601)-5858, November 29, 1963, (SRD).

1.4 Firth, R. D., "Structural Response of Agena B Satellite to Impulsive Loading (U)," Stanford Research Institute Supplementary Report, Contract AF 29(601)-4329, January 31, 1964 (S).

1.5 Abrahamson, G. R. and A. L. Florence, "Investigation of Response of Simplified ICBM-Type Structures to Impulsive Loading," Stanford Research Institute Technical Report No. 1, Vol. II, Contract AF 29(601)-4329, August 21, 1962.

1.6 Abrahamson, G. R., A. L. Florence and H. E. Lindberg, "Investigation of Response of Simplified ICBM-Type Structures to Impulsive Loading," Stanford Research Institute Final Report, Technical Report No. 2, Contract AF 29(601)-4329, February 1964.

1.7 Abrahamson, G. R. and H. E. Lindberg, "Estimated Bounds on Suddenly Applied Surface Loads Required to Destroy Reentry Vehicles (U)," Journal of Missile Defense Research, Limited Distribution Supplement to Vol. 2, No. 1, JMDR-64-2S, Summer 1964 (SRD).

1.8 Lindberg, H. E. and L. V. Parker, "Impulse Response of Stiffened Shell Structures (U)," Stanford Research Institute Final Report, AEC Project Agreement 41 under AT(04-3)-115, November 15, 1964, (FRD).

1.9   Abrahamson, G. R. and J. N. Goodier, "Dynamic Plastic
        Flow Buckling of a Cylindrical Shell from Uniform Radial
        Impulse,"Proceedings of 4th U.S. Natl. Congress of Applied
        Mechanics, University of California, Berkeley, June 18, 1962.

1.10   Lindberg, H. E., "Buckling of a Very Thin Cylindrical Shell
        Due to an Impulsive Pressure," J. Appl. Mech., Vol. 31, No. 2,
        June 1964, p 267-272.

1.11   Lindberg, H. E., "Impact Buckling of a Thin Bar," J. Appl.
        Mech. Paper No. 64-APM-44.

1.12   Lindberg, H. E., "Dynamic Plastic Buckling of a Thin Cylindri-
        cal Shell Containing an Elastic Core," Poulter Research Labora-
        tories Technical Report 003-64, Stanford Research Institute,
        1964.

1.13   Payton, R. G., "Dynamic Membrane Stresses in a Circular
        Elastic Shell," J. Appl. Mech., September 1961, p 417-420.

1.14   Florence, A. L. and R. D. Firth, "Rigid-Plastic Beams under
        Uniformly Distributed Impulses," to be published in Journal of
        Applied Mechanics (to be presented at the Summer Conference,
        June 7-9, 1965, Catholic University, Washington, D.C.).

1.15   Florence, A. L., "Circular Plates under Uniformly Distributed
        Impulses," submitted to International Journal of Solids and
        Structures, February 1, 1965.

1.16   Florence, A. L., "Annular Plate under a Transverse Line
        Impulse," to be published in AIAA Journal.

1.17   Florence, A. L. and M. Kanninen, "Traveling Force on a
        String and Membrane," to be published.

1.18   Florence, A. L., "Traveling Force on a Timoshenko Beam",
        J. Appl. Mech., June 1965 (Paper No. 64-WA/APM-26).

1.19   Abrahamson, G. R., "Procedures for Testing Structures with
        Simulated X-Ray Induced Impulses (U)," Stanford Research
        Institute Semiannual Technical Summary Report No. 2,
        Contract AF 29(601)-4745, January 7, 1964, (S).

1.20   Lindberg, H. E. and R. W. Gates, "Simulation and Structural
        Effects of Sharp Pulses (U)," Stanford Research Institute
        Final Report (Vol. 1), Contract LMSC P.O. 18-11572 Under
        NOw 63-0050, October 30, 1964, (SRD).

1.21   Lindberg, H. E., R. W. Gates and M. J. Baer, "Simulation
        and Structural Effects of Sharp Pulses," Stanford Research
        Institute Final Report (Vol 2), Contract LMSC P.O. 18-11572
        Under NOw 63-0050, June 15, 1964.

1.22   Atkins, M. C. and C. M. Gillespie, "Re-Entry Vehicle Com-
        posites (U)," Air Force Special Weapons Center Project Officer's
        Report - Project 834, POR-1453, July 22, 1964, (SRD).

1.23   Hoffman, P. R., "Vulnerability of Air Force ICBM Reentry
        Vehicles to a High-Altitude Nuclear Weapons Effect (U)," Air
        Force Special Weapons Center Technical Documentary Report
        No. AFSWC-TDR-61-64, May 1962, (SRD).

1.24   Abrahamson, G. R. and W. Stuiver, "Effects of Pulse-Spreading
        Countermeasures on Structural Response of Re-Entry Vehicles
        (U)," Stanford Research Institute Final Report, Contract AF 29
        (601)-4745, January 1964, (SRD).

1.25   Bade, W. L., et al, "Analytical Prediction of X-Ray Effects,"
        AVCO Semiannual Technical Report No. 2, Contract AF 29(601)-
        4525, 1 July 1961 to 1 January 1962.

1.26   Hoffman, A. J. and S. N. Mills, Jr., "Air Blast Measurements
        About Explosive Charges at Side-On and Normal Incidence,"
        Dept. of Army Project No. 5B-03-04-002 and 5B-05-016,
        Ordnance Research and Development Project No. TB 3-0112
        and TB 3-0238, Report No. 988, July 1956.

1.27   Goodman, H. J., "Compiled Free-Air Blast Data on Bare
        Spherical Pentolite,"Dept of the Army Project No. 5B-03-04-
        002, Ordnance Management Structure Code 5010.11.815,
        Report No. 1092, February 1960.

1.28   Burns, J. J., Jr., C. H. Popelar, and R. F. Foral, "Buckling
        of Missile Shell Structures Under Transient Pressure,"Martin
        Company, IR-62-17, May 1962.

1.29   Schuman, W. J., Jr., "The Response of Cylindrical Shells to
        External Blast Loading," BRL Memo Report No. 1461,
        March 1963.

2.1   Farrand, W. B., "Piezoelectric Pressure Sensing Devices,"
        Poulter Research Laboratories Technical Report 010-60,
        Stanford Research Institute. July 29, 1960.

3.1   Conroy, M. R., "The Plastic Deformation of Built-In Beams
        Due to Distributed Dynamic Loading," J. Appl. Mech, Paper
        No. 64-APM-17.

4.1   Hodge, P.G., Jr., Plastic Analysis of Structures, McGraw-Hill, Inc., N.Y., 1959, Chap. 10.

4.2   Hodge, P. G., Jr., Limit Analysis of Rotationally Symmetric Plates and Shells, Prentice-Hall, Inc., N.J., 1963, Chap. 4.

5.1   Wang, A. J. and H. G. Hopkins, "On the Plastic Deformation of Built-In Circular Plates Under Impulsive Loading,"Journal of Mechanics and Physics of Solids, Vol. 3, 1954, p 22-37.

5.2   Wang, A. J., The Permanent Deflection of a Plate Under Blast Loading," J. Appl. Mech., Vol. 22, No. 3, 1955, p 375-376.

5.3   Hopkins, H. G. and W. Prager, "On the Dynamics of Plastic Circular Plates,"J. Appl. Math. and Phys., Vol. V. 1954, p 317-330.

5.4   Hopkins, H. G. and W. Prager, "The Load Carrying Capacities of Circular Plates,"Journal of Mechanics and Physics of Solids, Vol. 2, 1953, p 1-13.

7.1   Kunz, K., Numerical Analysis, McGraw-Hill, Inc., N.Y., 1957.

7.2   Hamming, R. W., Numerical Methods for Scientists and Engineers, McGraw-Hill, Inc., N.Y., 1962

7.3   Macek, Anne G., "A B-5000 Program Based on Clippinger and Dimsdale Method," MRS 127 Technical Bulletin, Burroughs Corporation, Detroit, Michigan, 1964.

7.4   Pixley, A. F. and A. C. Macek, "A B-5000 Program for the Solution of First Order Ordinary Differential Equations (Hamming Method)," MRS 126 Technical Bulletin, Burroughs Corporation, Detroit, Michigan, 1964.

7.5   Hamming, R. W., "Stable Predictor-Corrector Methods for Ordinary Differential Equations," J. Assoc. Comp. Machinery 6, 1959, p 37-47.

8.1   Symonds, P. S., "Large Plastic Deformations of Beams under Blast-Type Loading," Proceedings of 2nd U.S. Natl. Congress of Applied Mechanics, 1954.

DISTRIBUTION

No. cys

HEADQUARTERS USAF

1   Hq USAF (AFRSTG), Wash, DC   20330

MAJOR AIR COMMANDS

1   AFSC (SCTR), Andrews AFB, Wash, DC   20331

AFSC ORGANIZATIONS

1   AFSC Scientific and Technical Liaison Office, Research and Technology Division, AFUPO, Los Angeles, Calif   90045

1   FTD (TDBTL), Wright-Patterson AFB, Ohio   4543`

1   AF Materials Laboratory, Wright-Patterson AFB, Ohio   45433

1   AF Flight Dynamics Laboratory, Wright-Patterson AFB, Ohio   45433

      RTD, Bolling AFB, Wash, DC   20332

1   (RTTW)

1   (RTS)

1   BSD (BSYDV), Norton AFB, Calif   92409

KIRTLAND AFB ORGANIZATIONS

1   AFSWC (SWEH), Kirtland AFB, NM   87117

      AFWL, Kirtland AFB, NM   87117

10   (WLIL)

2   (WLRP)

OTHER AIR FORCE AGENCIES

1   Director, USAF Project RAND, via: Air Force Liaison Office, The RAND Corporation (RAND Library), 1700 Main Street, Santa Monica, Calif   90406

ARMY ACTIVITIES

1   Commanding Officer, Ballistic Research Laboratories, Aberdeen Proving Ground, Md   21005

1   Commanding Officer, Picatinny Arsenal (SMUPA-VC1, Samuel Feltman Research Laboratories), Dover, NJ   07801

2   Director, US Army Engineer Research and Development Laboratories, ATTN: STINFO Branch, Ft Belvoir, Va   20260

NAVY ACTIVITIES

1   Director, Special Projects Office (SP-272), Department of the Navy, Wash, DC   20360

DOCUMENT CONTROL DATA · R&D

(Security classification of title, body of abstract and indexing annotation must be entered when the overall report is classified)

1. ORIGINATING ACTIVITY (Corporate author)	2a. REPORT SECURITY CLASSIFICATION
Stanford Research Institute Menlo Park, California	Unclassified
	2b. GROUP

3. REPORT TITLE

DEVELOPMENT OF LONG-DURATION EXPLOSIVE LOADING TECHNIQUES AND RESPONSE OF SIMPLE STRUCTURES TO PULSE LOADS

4. DESCRIPTIVE NOTES (Type of report and inclusive dates)

Final Report   16 March 1964 to 30 June 1965

5. AUTHOR(S) (Last name, first name, initial)

Florence, A. L.

6. REPORT DATE	7a. TOTAL NO. OF PAGES	7b. NO. OF REFS
November 1966	174	43

8a. CONTRACT OR GRANT NO. AF29(601)-6364 b. PROJECT NO. 8814 c. d.	9a. ORIGINATOR'S REPORT NUMBER(S) AFWL-TR-65-81 9b. OTHER REPORT NO(S) (Any other numbers that may be assigned this report) SRI Project GRU-4946

10. AVAILABILITY/LIMITATION NOTICES This document is subject to special export controls and each transmittal to foreign governments or foreign nationals may be made only with prior approval of AFWL (WLRP), Kirtland AFB, N.M. Distribution of this document is limited because of the technology discussed.

11. SUPPLEMENTARY NOTES	12. SPONSORING MILITARY ACTIVITY Air Force Weapons Laboratory (WLRP) Kirtland Air Force Base, New Mexico 87117

13. ABSTRACT Described is an experimental technique for providing long-duration pulses which can be applied to a part or all of a simple structure such as a beam, plate or cylinder. The technique employs essentially the familiar shock tube except that the detonation front of a gaseous explosive provides the shock wave. Many pulse shapes can be produced by placing in the tube and against the target, layers of different materials such as styrofoam, polyurethane, and Mylar, and by sending the explosively-induced shock wave through them to the target. The search for pulse shapes was mainly confined to those of the blast type by the generation of other types is equally feasible. Outlines of the theoretical treatments of four problems are given. They concern the responses of (a) a clamped beam to a blast pulse uniformly distributed over a central length, (b) a simply supported circular plate to a blast pulse uniformly distributed over a central circular area, (c) a clamped circular plate to a rectangular pulse uniformly distributed over the whole plate, and (d) a clamped circular plate to a rectangular pulse uniformly distributed over a central circular area. Analytical treatments employ the rigid-plastic theory because of interest in moderately large permanent deformations and relative simplicity of analysis.

14.		LINK A		LINK B		LINK C	
	KEY WORDS	ROLE	WT	ROLE	WT	ROLE	WT
long duration pulses shock tube structural response							

INSTRUCTIONS

I. ORIGINATING ACTIVITY: Enter the name and address of the contractor, subcontractor, grantee, Department of Defense activity or other organization (corporate author) issuing the report.

2a. REPORT SECURITY CLASSIFICATION: Enter the overall security classification of the report. Indicate whether "Restricted Data" is included. Marking is to be in accordance with appropriate security regulations.

2b. GROUP: Automatic downgrading is specified in DoD Directive 5200.10 and Armed Forces Industrial Manual. Enter the group number. Also, when applicable, show that optional markings have been used for Group 3 and Group 4 as authorized.

3. REPORT TITLE: Enter the complete report title in all capital letters. Titles in all cases should be unclassified. If a meaningful title cannot be selected without classification, show title classification in all capitals in parenthesis immediately following the title.

4. DESCRIPTIVE NOTES: If appropriate, enter the type of report, e.g., interim, progress, summary, annual, or final. Give the inclusive dates when a specific reporting period is covered.

5. AUTHOR(S): Enter the name(s) of author(s) as shown on or in the report. Enter last name, first name, middle initial. If military, show rank and branch of service. The name of the principal author is an absolute minimum requirement.

6. REPORT DATE: Enter the date of the report as day, month, year; or month, year. If more than one date appears on the report, use date of publication.

7a. TOTAL NUMBER OF PAGES: The total page count should follow normal pagination procedures, i.e., enter the number of pages containing information.

7b. NUMBER OF REFERENCES: Enter the total number of references cited in the report.

8a. CONTRACT OR GRANT NUMBER: If appropriate, enter the applicable number of the contract or grant under which the report was written.

8b, 8c, & 8d. PROJECT NUMBER: Enter the appropriate military department identification, such as project number, subproject number, system numbers, task number, etc.

9a. ORIGINATOR'S REPORT NUMBER(S): Enter the official report number by which the document will be identified and controlled by the originating activity. This number must be unique to this report.

9b. OTHER REPORT NUMBER(S): If the report has been assigned any other report numbers (either by the originator or by the sponsor), also enter this number(s).

10. AVAILABILITY/LIMITATION NOTICES: Enter any limitations on further dissemination of the report, other than those

imposed by security classification, using standard statements such as:

(1) "Qualified requesters may obtain copies of this report from DDC."

(2) "Foreign announcement and dissemination of this report by DDC is not authorized."

(3) "U. S. Government agencies may obtain copies of this report directly from DDC. Other qualified DDC users shall request through

_____."

(4) "U. S. military agencies may obtain copies of this report directly from DDC. Other qualified users shall request through

_____."

(5) "All distribution of this report is controlled. Qualified DDC users shall request through

_____."

If the report has been furnished to the Office of Technical Services, Department of Commerce, for sale to the public, indicate this fact and enter the price, if known.

11. SUPPLEMENTARY NOTES: Use for additional explanatory notes.

12. SPONSORING MILITARY ACTIVITY: Enter the name of the departmental project office or laboratory sponsoring (paying for) the research and development. Include address.

13. ABSTRACT: Enter an abstract giving a brief and factual summary of the document indicative of the report, even though it may also appear elsewhere in the body of the technical report. If additional space is required, a continuation sheet shall be attached.

It is highly desirable that the abstract of classified reports be unclassified. Each paragraph of the abstract shall end with an indication of the military security classification of the information in the paragraph, represented as (TS), (S), (C), or (U).

There is no limitation on the length of the abstract. However, the suggested length is from 150 to 225 words.

14. KEY WORDS: Key words are technically meaningful terms or short phrases that characterize a report and may be used as index entries for cataloging the report. Key words must be selected so that no security classification is required. Identifiers, such as equipment model designation, trade name, military project code name, geographic location, may be used as key words but will be followed by an indication of technical context. The assignment of links, rules, and weights is optional.

AFSC (KAFB NM)